AN EXPERIMENTAL STUDY OF A FIBER ABSORBER-SUPPRESSOR MODIFIED TROMBE WALL

Prepared for
U.S. Department of Energy
Appropriate Technology Program
Grant No. DE-FG44-80R410155

21-0011

By

Dipankar Choudhury
Graduate Research Assistant

Dr. Richard C. Birkebak
Professor of Mechanical Engineering

University of Kentucky
Lexington, Kentucky

December 1982

High Temperature and Thermal Radiation Laboratory Technical Report No. HTTL-TR-32

DISCLAIMER

AN EXPERIMENTAL STUDY OF A FIBER ABSORBER-SUPPRESSOR MODIFIED TROMBE WALL

ABSTRACT

An experimental study has been conducted to ascertain the effects of introducing fiber bed absorbers on Trombe wall passive solar collectors. Two identical, Trombe wall passive solar units were constructed that incorporate the basic components of masonry collector-storage walls: glazings, masonry and thermal insulation. Both units were extensively instrumented with thermocouples and heat flux transducers. Ambient temperature, relative humidity, wind speed and insolation are also measured. In the first part of the study the two Trombe wall units were tested with a single glass cover. The thermal performance of both units were found to be virtually identical.

In the second part of the study a single cover Trombe wall unit was compared with a double cover unit and the latter was found to have higher air gap and masonry wall temperatures and heat fluxes. In the final phase of the experiment, an absorbing, scattering and emitting fiberglass-like material was placed in the air gap of the single glazed wall. Tests were conducted to compare the solar-thermal performance, heat loss and gain characteristics between the units with and without the fiber absorber-suppressor. This experiment showed that the fiber bed served to decouple the wall at night from its exterior environment and to reduce the heat losses. The modified Trombe wall with the fiber absorber-suppressor outperformed the double glazed Trombe wall system by approximately ten percent gain in useable thermal energy. Also, the fiber bed eliminates one glazing thereby reducing system cost as well.

Acknowledgements

The authors wish to thank the following agencies for their finiancial support: the Department of Mechanical Engineering, University of Kentucky, Appropriate Technology Program, U.S. Department of Energy, Grant No. DE-FG44-80R410155 and the North Atlantic Treaty Organization, Grant No. 1872. This report was prepared with the support of the U.S. Department of Energy, Grant No. DE-FG44-80R410155. However, any opinions, findings, conclusions or recommendations expressed herein are those of the author(s) and do not necessarily reflect the views of the DOE.

TABLE OF CONTENTS

LIST OF TABLES

LIST OF FIGURES

LIST OF SYMBOLS

C	correction factor
g	acceleration due to gravity (9.81 m/s^2)
G	gain factor
h	heat transfer coefficient (W/m^2 K)
H	thickness of fiber batt (cm)
I_c	insolation (W/m^2)
k	thermal conductivity (W/mK), heat flux sensor multiplication factor ($W/m^2/mV$)
L	Trombe wall air gap width (m)
M	multiplication factor of sensor
Nmax	number of data in sample
Nu	Nusselt number defined by Eq. (C3)
Pr	Prandtl number
q	heat flux (W/m^2)
*q	dimensionless heat flux defined in Eq. (2)
Q	energy gain per square meter of collector area (J/m^2)
R	thermal resistance ($m^2°K/W$)
Ra	Rayleigh number defined by Eq. (C5)
S	solar energy absorbed per square meter of collector area (J/m^2)
t	time (hours)
$\bar{t}$	test period (hours)
T	absolute temperature (°K)
U_t	top loss coefficient (W/m^2K)
V	wind velocity (m/s), voltage
x	reading of sensor in millivolts
Z	heat flux sensor temperature correction factor

Subscripts

a	air
avg	average
A	air gap related
AR	air gap related reduced data
b	absorber surface related
bf	fiber bed free surface related
c	convection related, cover related
CD	copper plate differential thermopile related
cond	conduction
CP	copper plate thermopile related
CPR	copper plate thermopile related reduced data
CR	cover related reduced data
e	environment
E	exterior wall surface related
ER	exterior wall surface related reduced data
HF	heat flux sensor related
I	interior wall surface related
IR	interior wall surface related reduced data
m	mean
o	bounded surface related
OR	copper plate outlet reduced data
p	copper plate connector related
py	pyranometer related
r	radiative
s	free surface related
t	top, total

T	thermocouple related
TR	thermocouple related reduced data

Greek Aphabet

α	thermal diffusivity (m^2/s)
β	collector tilt angle, extinction coefficient
β'	volumetric coefficient of expansion
Δ	difference
ε	emissivity
θ	dimensionless temperature
ν	kinematic viscosity (m^2/s)
ρ	reflectivity
σ	Stefan-Boltzmann constant
$\overline{\sigma}$	scattering parameter
τ	transmissivity
ω	albedo

CHAPTER 1

INTRODUCTION

The ever growing need for cheap, clean and renewable energy sources is the cause of a great deal of interest being shown in the use of solar energy for the purpose of heating dwellings. At this point in time many designs exist in different configurations as reported by Shurchliffe (1975).

These designs can be divided into two broad classes; the so-called "active" and "passive" designs. Active designs use relatively sophisticated equipment to absorb, transfer, release and/or store the energy and they tend to be expensive to install. Passive designs tend to be as simple as possible because the energy collection and storage functions are combined into a single, independent unit.

Examples of passive solar heating designs can be found in the dwellings of some American Indian Tribes in Southwest America. Balcomb (1979) mentions instances of structures constructed during the period 1100-1400 A.D. Cliff dwellers built under overhanging cliffs in canyons - an immediate benefit would be that the low winter sun would penetrate the overhanging caves and heat the thermal mass created by the building walls and the surrounding rock. The high summer sun would be shaded by the overhanging cliffs and energy loss by night radiation would maintain lower-than-ambient temperature. Some Pueblo Indian structures were designed with thick walls and cupped to face the south so as to provide some element of natural solar collection. Bahadori (1979) provides details on sophisticated techniques of natural building cooling which evolved in Iran.

Passive systems utilize natural heating based on the principle of the green house effect: the solar radiation which has a spectral distribution in the visible and near infra-red range of wavelengths between 0.3 and 3 μm can pass through a layer of glass or other suitable transparent materials and is absorbed by an opaque surface.

The heated receiving surface emits energy in the infra-red range, above 4 μm. This radiation is stopped almost completely by the glass cover which is substantially opaque in this range. Consequently, the temperature of the glass increases and it radiates towards the receiving surface as well as the exterior and also loses some heat by convection. A substantial amount of thermal energy is trapped between the cover and the receiving surface. The amount of heat trapped can be increased by interposing a second glass cover.

The ideal receiving surface is, of course, black. However, a surface of rough concrete provides good absorptivity. Hence, the receiving surface may be a concrete wall. In this case, the received solar energy is transferred partly to the circulating air between the glass partition and the wall, and partly to the wall which warms up and serves as large thermal mass with a large time constant to average diurnal temperature variations as well as a heat source for nocturnal heating.

1.1 The Trombe Wall

An effective utilization of this concept was in the Centre Nationale de la Recherche Scientifique (C.N.R.S.) solar houses in the village of Odeillo-Font-Romeu in the Pyrenees Mountains of Southern France. Felix Trombe perfected and popularized this passive system concept that is known as a Trombe or Trombe-Michel system and the collector-storage wall

as a Trombe Wall. In this system, the south facing vertical surfaces are used as solar collectors as in Figure 1.

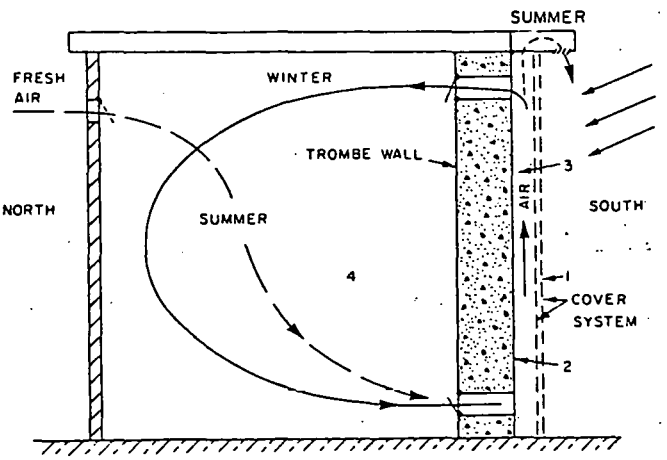

Figure 1. The working priciple of Trombe system.

The Trombe wall is erected directly behind a large expanse of double window glazing. It is a massive floor-to-ceiling wall, usually of concrete, painted black or at least a dark color. It usually has a overhang to keep out the summer sun. The wall intercepts most of the sunlight before it can come into the living area. By the end of the day the wall can be tens of degrees above the room temperature with the near surface providing indirect heat to compensate for the thermal losses of the structure.

If the Trombe wall is too thin, less than 0.2 m thick or too thick - over about 0.5 m - the phaselag for propagation of heat to the interior is not optimal. If it is too thin, the wall heats up rapidly, increasing heat losses to the ambient and causing premature heating inside. The reverse is true if the wall is too thick.

Vents provided at the top and bottom of the Trombe wall allow natural convection to speed the heat transfer to the living space from the front of the wall. The vents have to be closed at night to prevent a reverse thermosyphon effect from cooling the room.

1.2 Survey of Related Research

A substantial quantity of experimental and analytical results have been produced to date relating to the Trombe wall passive solar system. A large part of the work has been done by groups of researchers at the C.N.R.S. in Odeillo, France, and at the Los Alamos Scientific Lab (LASL) in Los Alamos, New Mexico.

Experimental data for specific test facilities in climate specific conditions exist for the thermal performance of Trombe wall systems as listed in the bibliography. These are quite useful from the design point of view - however, they are limited to specific building and weather conditions. In the literature reviewed there does not exist any instance where tests have been made on units with different glass covers and absorber surfaces, under the same weather conditions.

Trombe and his co-workers (1976) made the first effective utilization of the collector-storage wall concept in the C.N.R.S. solar houses in Odeillo, France. The wall thickness, however, was 0.60 m in the prototype houses and was found to be too much to allow the temperature at the inner wall surface to peak when energy demand would be maximum. The phase difference was found to be from 14 to 16 hours. The performance of the C.N.R.S. buildings have been monitored for a long period of time and their performance is well-known. Coarse estimates of free convection thermal energy delivery have been made using bulk velocity and temperature measurements in the wall inlet and outlet ducts.

Casperson and Hocevar (1979) have conducted tests on a variable geometry Trombe wall system to investigate thermocirculation performance characteristics. They obtained velocity and temperature profiles for various air-gap widths. The Trombe wall system performance was

characterized by collector efficiency curves similar to those commonly used for flat-plate solar collectors. The instantaneous efficiency data was calculated based on experimentally determined convective heat transfer rates in the air gap, conductive heat fluxes in the masonry wall, and the insolation rates.

Balcomb et al (1978) have obtained experimental data and have developed approximate design procedures at the Los Alamos Scientific Laboratory. Their procedure gives estimates of long-term solar heating fractions for a specific nominal design. This design method (often called the Solar Load Ratio method) is not general in nature and different correlations have to be used for each configuration and for each variation of a parameter. Corrections have to be estimated on the basis of parametric studies. The Solar Load Ratio method and the results of simulation studies cannot be used to evaluate short-term thermal behavior.

The information available in the literature regarding analytical models of Trombe wall performance is limited - mainly because a truly representative mathematical model is complex. Several studies on thermal network models for the analysis of passively heated buildings exist. Though the models agree with specific test results they do not appear to be sophisticated enough to be generally applicable. Bilgen and Jeldres (1978) took a different approach by writing the energy equation for the glass covers, air gap and wall and used a semi-implicit finite difference method to obtain temperature profiles in the wall as a function of time. They were able to optimise the thickness of the wall for the conditions of the C.N.R.S. dwellings in Odeillo, France. The optimum wall thickness obtained was 0.40 m.

Akbari and Borgers (1979) have performed analytical development work related specifically to the thermocirculation phenomena in the Trombe wall air gap. They have made a mathematical formulation of the fluid mechanics and heat transfer processes in the air gap and have solved the governing differential equations numerically using finite difference techniques. Preliminary comparisons of laminar flow regimes with the data of Casperson and Hocevar (1979) appear to be satisfactory.

1.3 Project Research

The performance of the Trombe wall systems now in use suffer because of thermal radiation emitted by the outer wall which is lost to the cool night environment and also because of convection energy exchange in the space between the wall and the glass cover which is also eventually lost to the environment.

The research reported here tests a new concept to reduce the outer wall heat transfer to the environment. This method involves the use of fibrous materials as both the solar collecting surface and free convection and infra-red radiative suppression systems.

The insulating and thermal radiation properties of fibrous materials have been studied both theoretically and experimentally in references cited in the bibliography. In general, an insulation material can serve to decouple a system from its environment. A fibrous insulating material is generally considered as a collection of fibers of various orientations with the void spaces filled with a gas (usually air).

The fiber bed or batt is usually treated as being bounded by two impermeable boundaries separated by a bed thickness H, which, is usually

much smaller than the length and width of the bed. Since the bed is thin, heat transfer is one-dimensional in nature. A more general case, as represented by the application of fiber batts in this project, is a batt with a free or unbounded surface exposed to the environment. The mechanism of heat transfer in fibrous materials is quite complicated since it involves the combined modes of solid and gas conduction, radiation and convection. In addition, with the introduction of a free surface, the radiation exchange of the fibers within the bed and convection within the bed and the environment must be taken into account.

Most existing studies, analytical or experimental, have been primarily concerned with bounded fibrous beds. In this case, energy transfer is normal to the plane of the bounding surface. Davis (1972) has noted that the relative importance of the different modes of heat transfer depends on such factors as fiber geometry in the bed, fiber dimensions, void ratio and the temperature field within the bed. It is generally agreed that the solid fiber material serves to suppress radiation and convection. Studies by Davis (1972) and Davis and Birkebak (1972) indicate that the free convection and solid conduction are negligible and gas conduction is the dominant mechanism of heat transfer in fibrous insulating materials. Radiation is treated as a correction term on the gas conductivity at low and moderate temperatures.

For batts with one free surface, the environmental radiation and air temperatures significantly affect the temperature distribution within the bed and the surface temperature as well. Birkebak et al. (1982) have presented experimental and theoretical results based on the analysis of Davis and Birkebak (1974), Özil (1976), Özil and Birkebak (1977) and

the experimental results of Chen (1979). The radiative and total heat fluxes through and in a fiber batt are functions of the solid material and surrounding gas thermal properties, the fiber orientation, the bounded surface, air and surrounding radiative temperature. The important dimensionless temperatures are

$$\theta = \frac{T}{T_o}, \quad \theta_s = \frac{T_s}{T_o}, \quad \theta_a = \frac{T_a}{T_o}, \quad \theta_e = \frac{T_e}{T_o} \tag{1}$$

and the dimensionless heat fluxes are

$$q_r^* = \frac{q_r}{\sigma T_o^4} \quad \text{and} \quad q_t^* = \frac{q_t}{\sigma T_o^4} . \tag{2}$$

In the above quantities T represents the absolute temperature in degrees Kelvin and the heat transfer per unit area is designated by q. Subscripts, o, s, a, e, r and t represent bounded surface, free surface, air, environment, radiative and total quantities, respectively.

The experimental results presented by Birkebak et al. (1982) are compared using the model of Özil (1976) and the extended model given in a paper by Birkebak et al. (1982). Details of the development of the Özil method are found in the literature: Özil (1976), Birkebak et al. (1982) and Enoch et al. (1982). Agreement between the theoretical model and the experimental results is quite good. Shown in Figure 2 are the effects of environmental radiation temperature and air temperature on the free surface temperatures of a fiber batt. The extinction coefficient, β, of the sample is 8 cm^{-1} and the albedo, ω, is plotted 0.0, 0.5 and 0.6. The free surface temperature in fiber batts with one free surface is very near the environmental temperature. The results seem

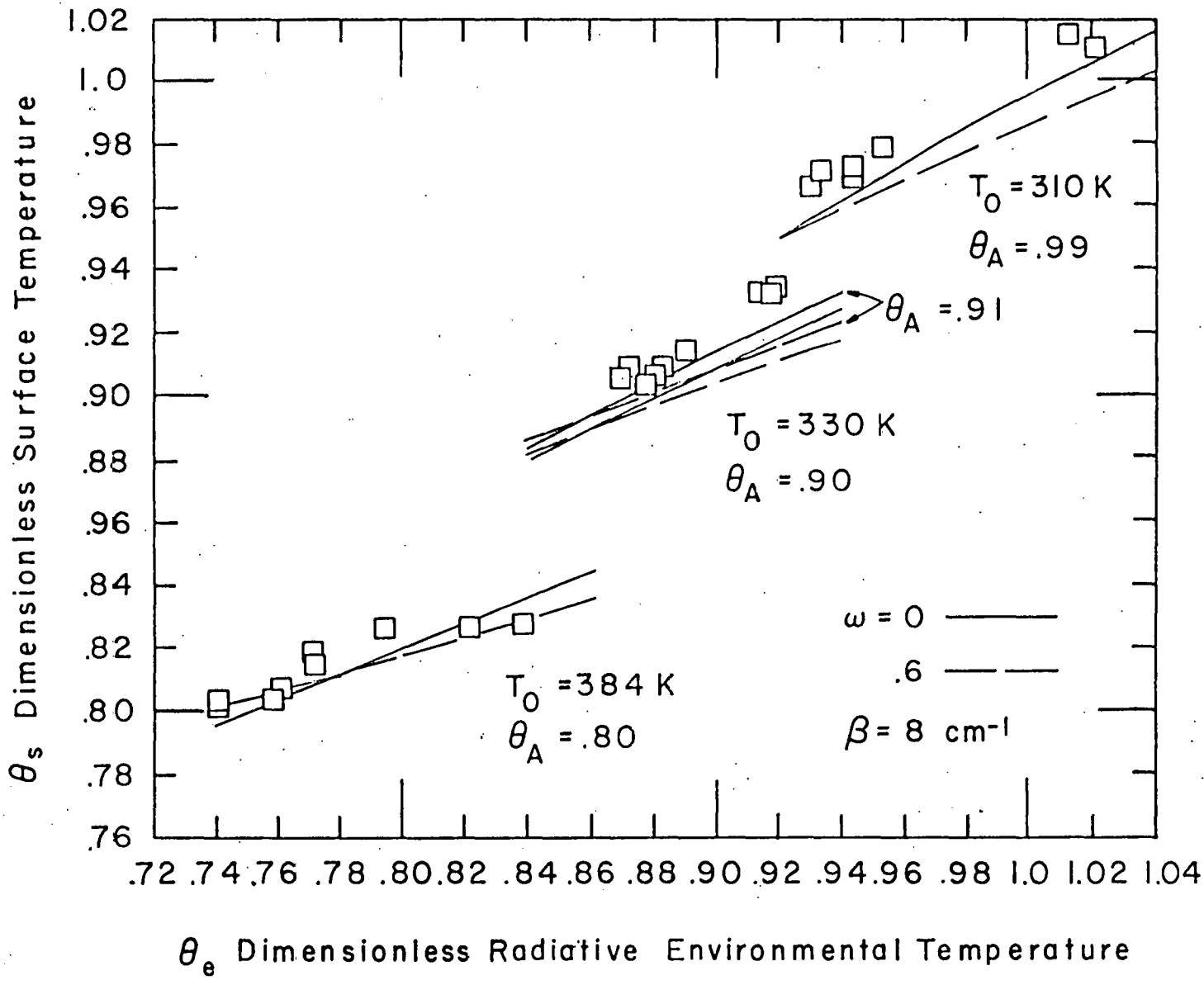

Fig. 2 Effect of θ_e and θ_a on θ_s

to indicate that fibrous materials are a good free convection suppression system (for a 2.84 cm thick fiberglass building insulation batt, a wall temperature of 330 K and an air environmental temperature of 255 K, the batt free surface temperature is 264 K, a temperature difference of only 9 K compared to 65 K without the batts). A fiber batt interfaced in the air gap between a Trombe wall and glazing system would result in the surface temperature of the batt being near the glazing temperature and environment temperature and therefore the free convection heat transfer would be greatly reduced. Figure 3 shows that the net thermal radiative flux is substantially affected by air and environmental radiation temperatures. It is obvious from the figure that a fibrous surface is a good radiation suppression system. The total energy leaving (or entering) the fibrous bed will be made up of the radiative and convective heat transferred:

$$q_t^* = q_r^* + q_c^* \tag{3}$$

The effects of ambient temperature and air temperature on the total heat flux q_t^* is seen in Figure 4. In addition to the theoretical argument for the use of fiber-batts as absorber surfaces, an experimental study by Özil and Birkebak (1979) seems to indicate that flat plate air-type collectors with fiber bed absorbers are as efficient as collectors with conventional, solid absorber surfaces.

1.4 Objective of the Present Study

The primary aim of the present study is to provide experimental data needed to establish if the performance of Trombe wall passive solar systems can be improved by using fibrous materials as:

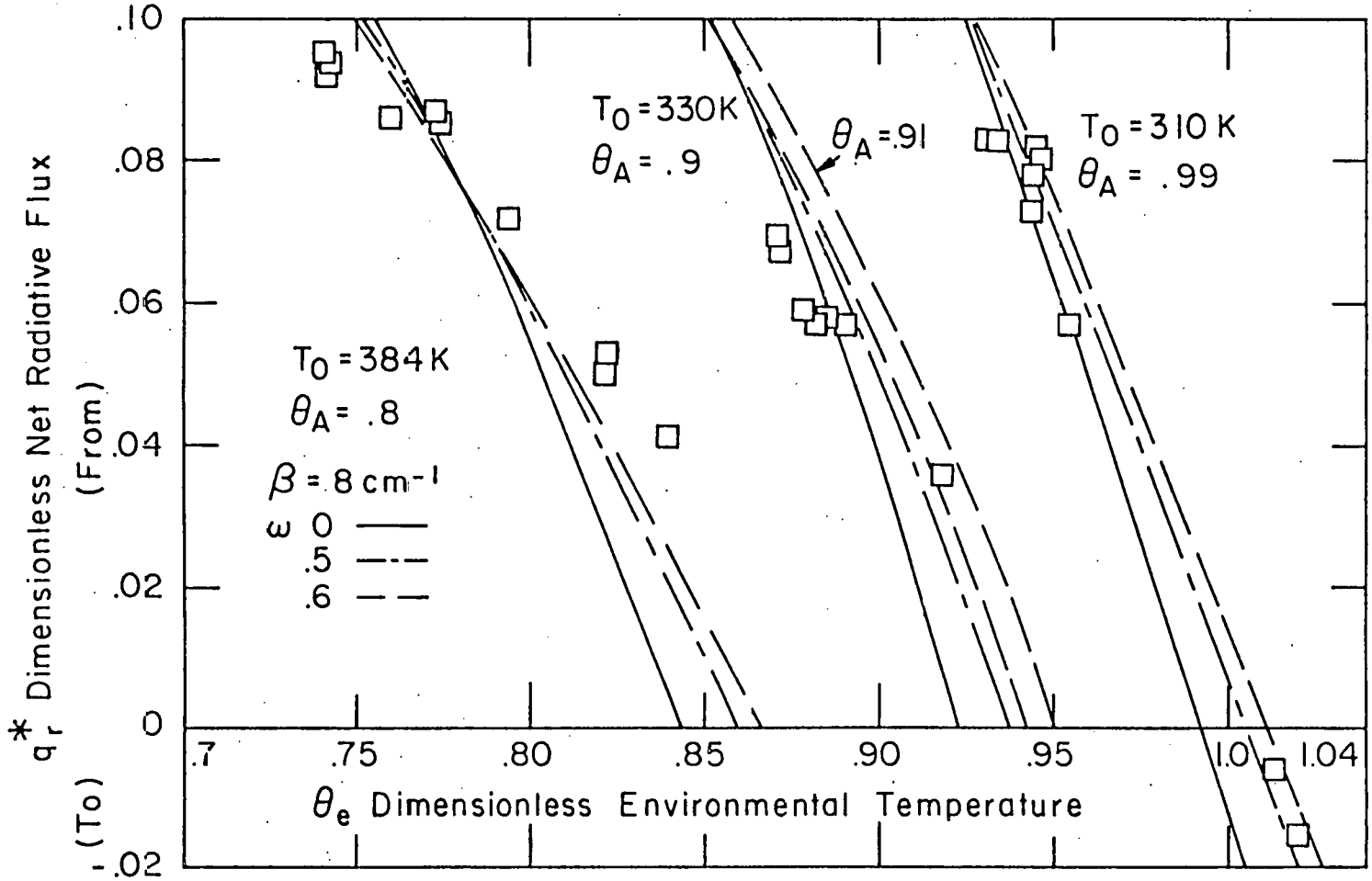

Fig. 3 Effect of θ_e and θ_a on q_r^*

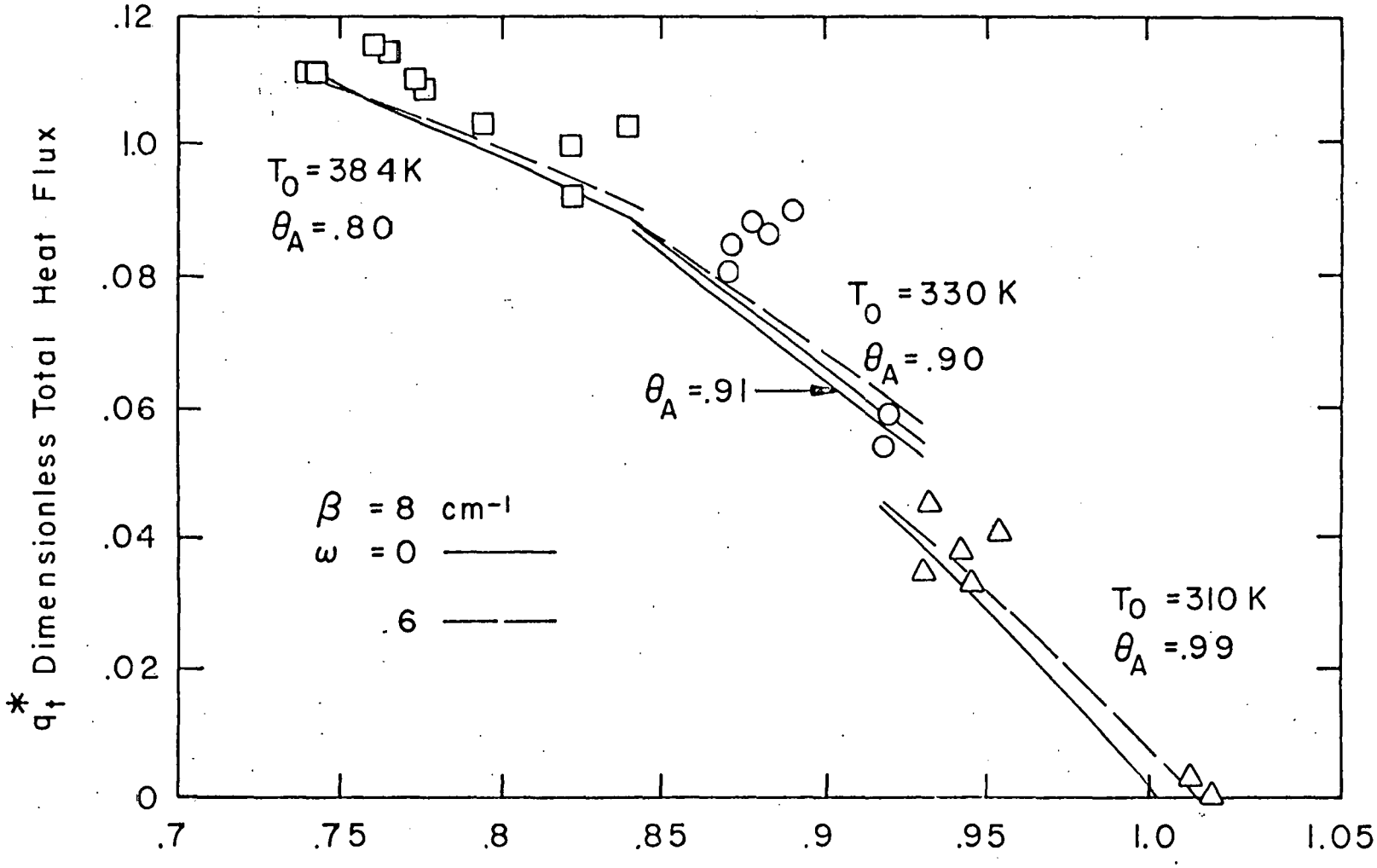

Fig. 4 Effect of θ_e and θ_a on q_t^*

a. absorbing media, and

b. convection and radiation suppressors.

This thesis reports the design, construction and preliminary testing of the test facility to meet the aforementioned objective. Two models of a Trombe wall were constructed and tested for various weather conditions to ensure that their performance was nearly identical. The walls were instrumented with thermocouples, heat-flow meters and radiation detectors. A data acquisition system was used to obtain the desired measurements. Environmental variables such as wind speed, ambient temperature and humidity were also measured. After the initial comparison, one of the models was used as reference and was compared to the other modified wall. The following two modifications were made:

a. Use of a double glass cover.

b. Single glass cover with fiber batt absorber.

The problems encountered at various phases of the project and techniques applied to overcome them are described. Some preliminary data for spring and summer months are presented.

The experimental study was conducted in three phases:

Phase I: Two Trombe wall test units were constructed and a single glass cover was used for both units. These two units were tested under the same weather conditions and pertinent data like temperatures, heat fluxes, solar flux and temperature profiles were collected. The data was reduced and analyzed to ensure that the two units had similar performances.

Phase II: One of the test units with a single glass cover was used as the control unit and a double-paned glass cover was used on the other unit. Data was collected to compare the performance of the two units.

Phase III: The control unit used had a double cover and the test unit had a fiber batt absorber surface with a single glass cover. Hourly data was collected continuously over a forty-eight hour period and the thermal performance of both units was compared.

CHAPTER 2

DESCRIPTION OF EXPERIMENTAL FACILITY

Small passive-solar test-boxes are an useful tool in the thermal-modelling of passively solar-heated building designs. Theoretical considerations for the test-box thermal modelling of passive-solar building designs have been discussed in a paper by Grimmer (1979). Solar gains are proportional to the area of glazing and thermal loads are proportional to the area of walls, floor and ceiling. In other words, it is possible to construct physical thermal models of a particular passive-solar design by normalizing appropriate thermal design parameters to the south-facing glazing area. Small test-boxes that incorporate the basic elements of passive solar design: glazings, thermal insulation and thermal storage capacity have been tested by Palmiter et al. (1978) and Grimmer et al. (1979). The test units have been found to provide a reasonably good estimate of the performance of passive solar designs that have a massive storage wall behind south-facing glazing, and heavily insulated and relatively massless roof, floor and walls. Details of the construction of the Trombe-wall test-units and the experimental equipment are described in this chapter.

The approaches used in this experiment includes two Trombe wall passive-solar units, a constant temperature bath, type T thermocouples, heat flow sensors, a pyranometer, an anemometer, a ten-channel scanner and multimeter. The data acquisition system consisted of a low-level amplifier - measurement and control processor connected to a minicomputer. Figure 5 shows the general schematic diagram of the apparatus.

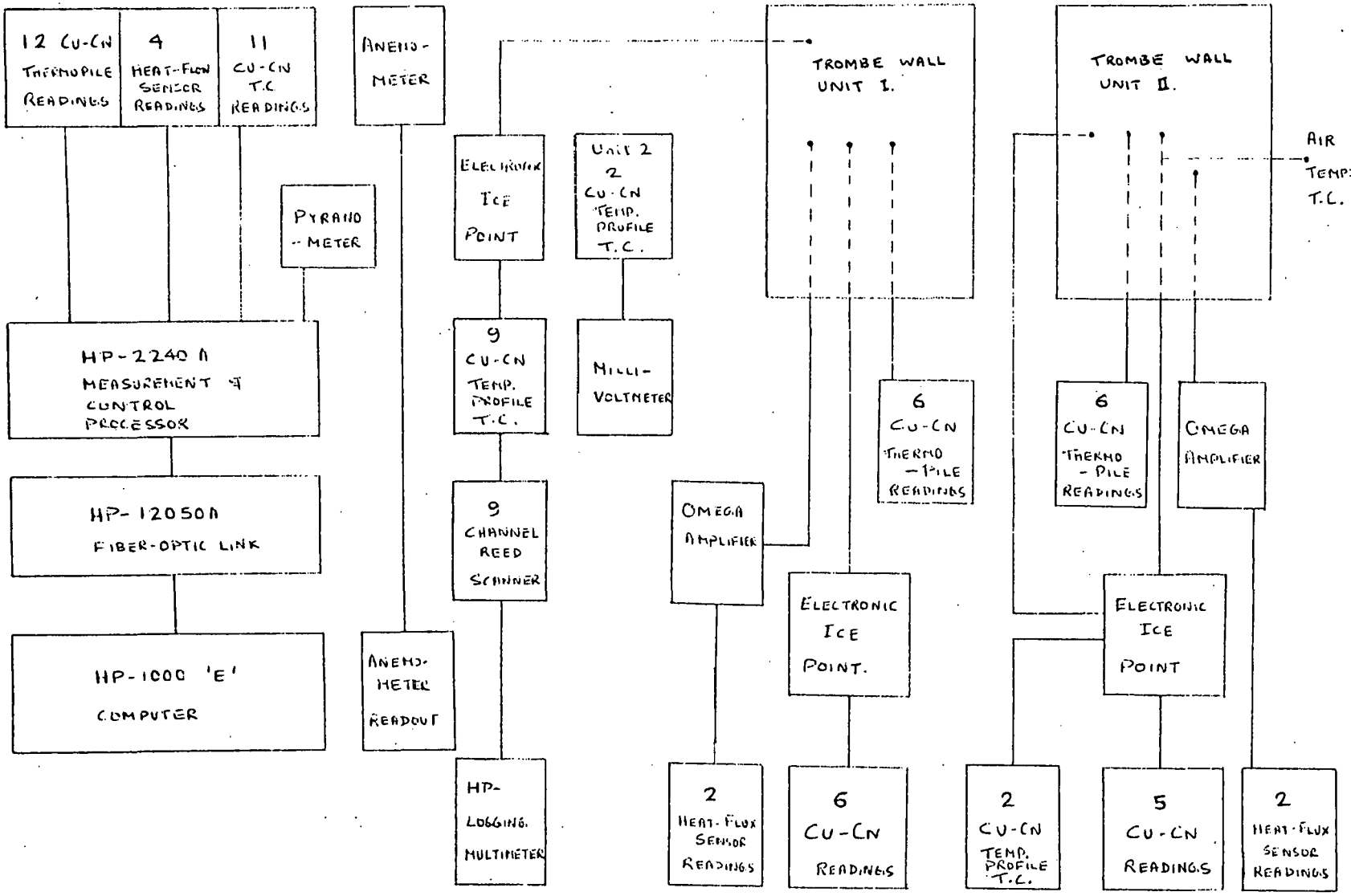

Fig. 5 Schematic Diagram of the Apparatus

2.1 Test Units

The Trombe wall test units described here are located in the quadrangle of the College of Engineering, University of Kentucky at Lexington, Kentucky. The masonry wall side of both test units are oriented due South. The presence of buildings on all four sides of the units result in a slightly shorter period of exposure to solar radiation than if they had been situated on the roof. However, the relatively large mass of the units prevented a roof location from being used. Figure 6, shows photographs of the test units during the testing stage.

In Figure 6(i) the test unit on the left is a conventional double glass cover Trombe wall unit and the one on the right has a single cover with a fiber-bed absorber (painted black). The thermocouple radiation shields and externally mounted pyranometer and anemometer can be seen. The photograph in Figure 6(ii) shows a side view of the set-up with the circulating bath and tubes. Figures 7(i) and (ii) show photographs of the rear view of units I and II respectively. The copper cooling plate, coolant tubes, linear amplifier, electronic ice-points, a ten channel scanner and a millivoltmeter can be seen.

2.1.1 Structure of the Test Units

The test units are basically a wood-frame structure supported on a metal frame on coasters to provide mobility. The outside dimensions of the passive-solar test units are 0.832 m long by 1.44 m deep by 1.873 m high. The interior box height is 1.667 m and width is 0.581 m. A plan view of the test unit is shown in Figure 8.

The side walls consist of plywood surfaces with 0.10 m thick fiber-glass building insulation material interposed between. The rear surface

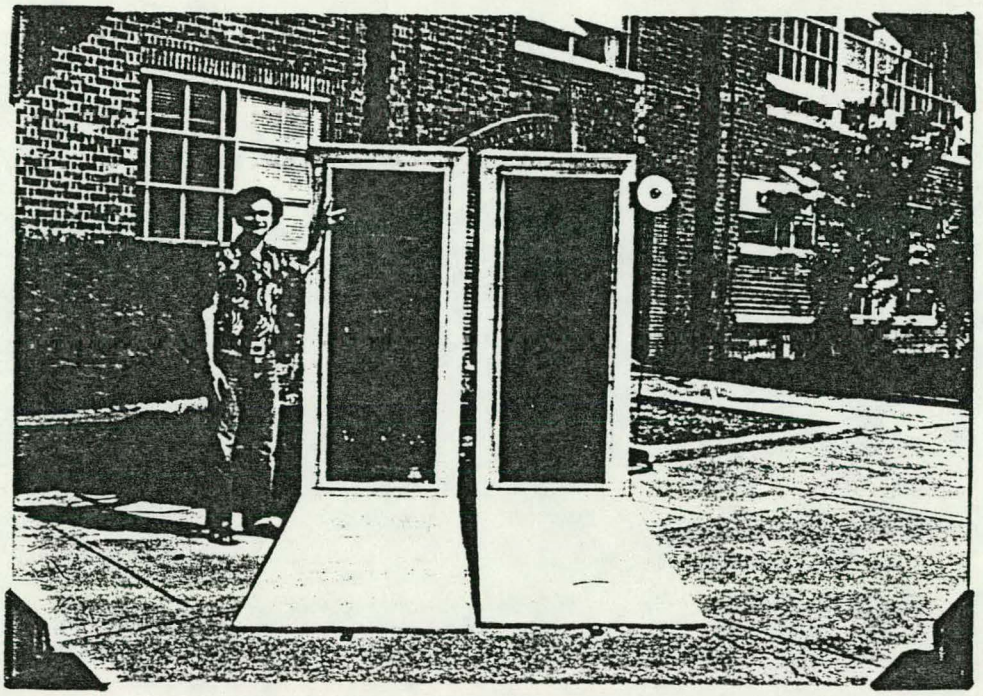

Fig. 6(i) Front View of Trombe Wall Test Units

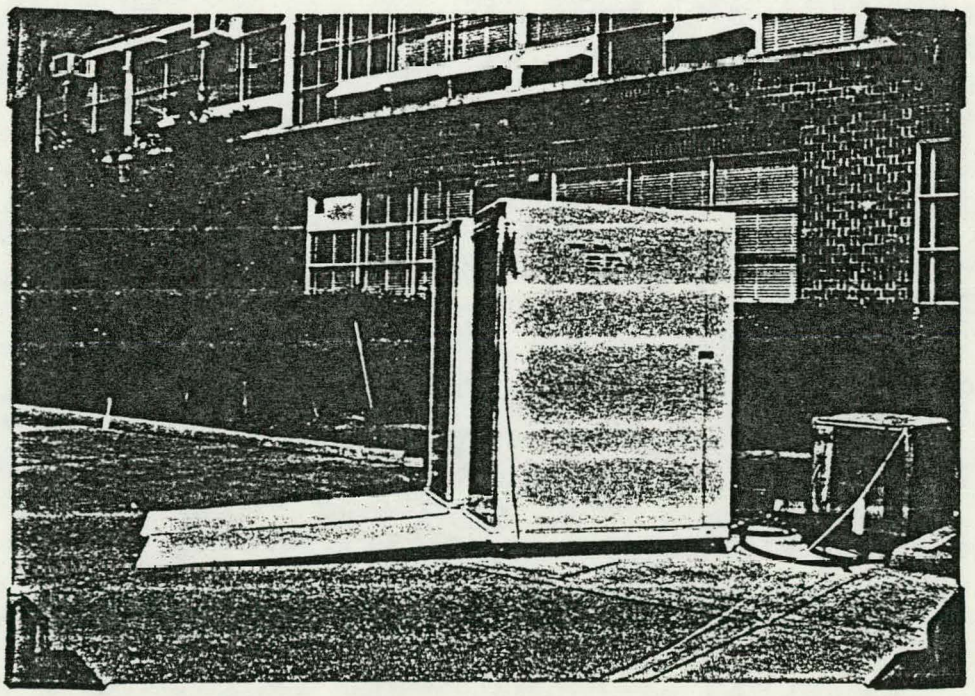

Fig. 6(ii) Side View of Trombe Wall Test Units

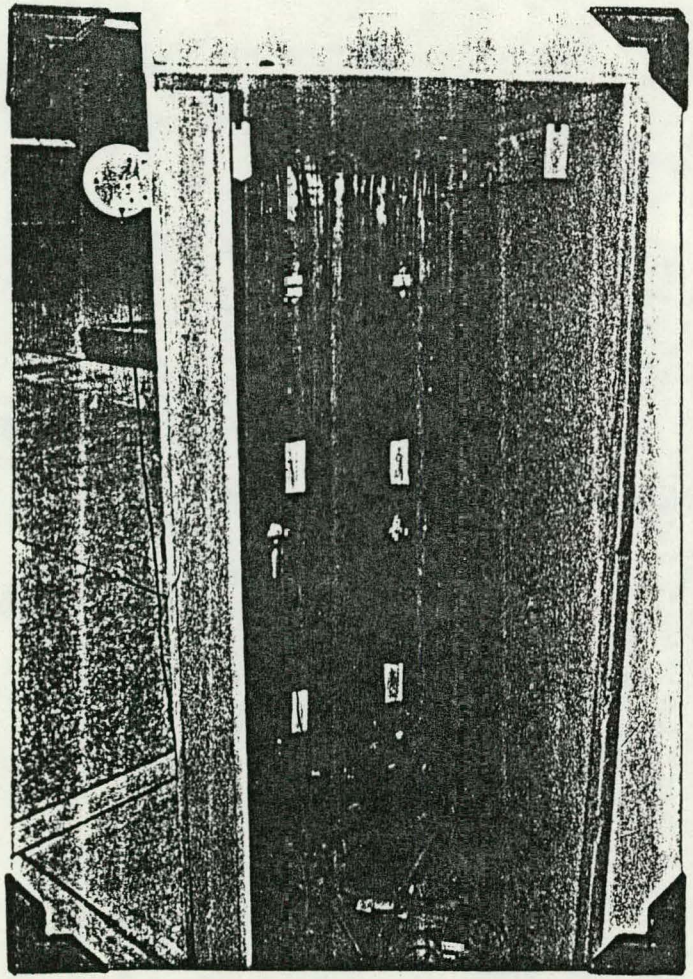

Fig. 7(i) Rear View of Trombe Wall Unit 1

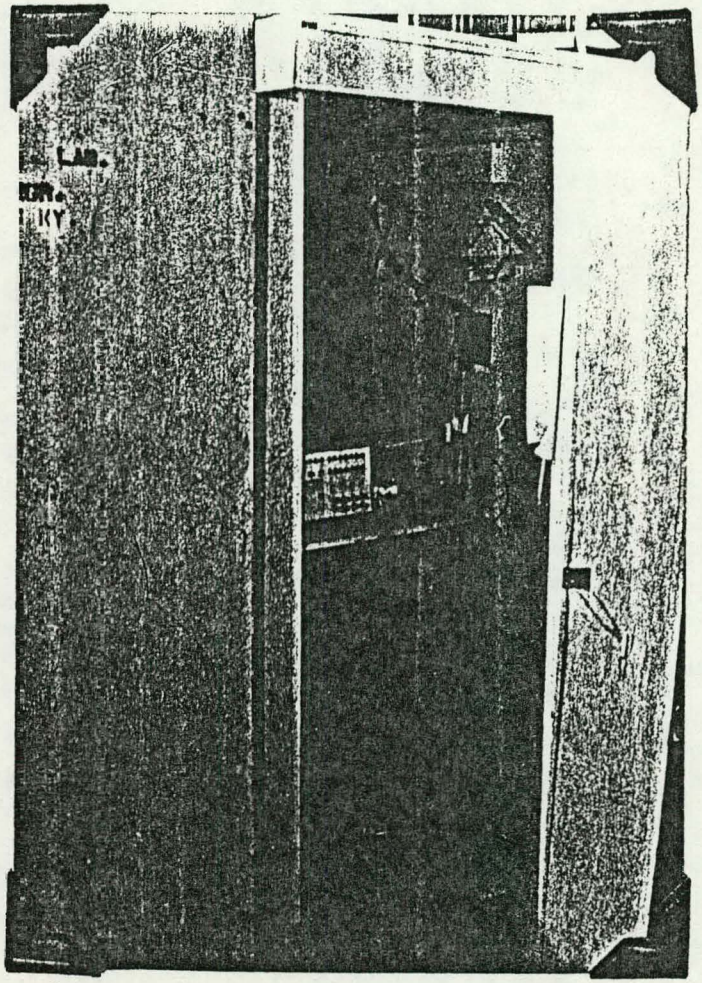

Fig. 7(ii) Rear View of Trombe Wall Unit 2

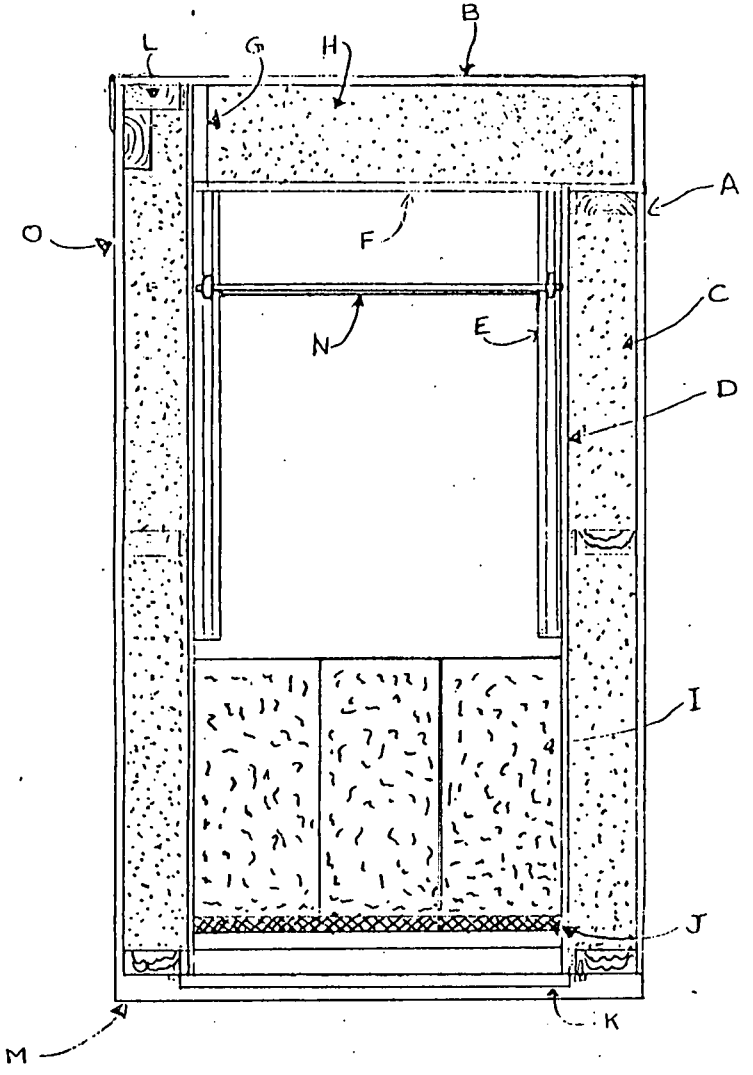

TOP VIEW WITH TOP OF BOX REMOVED.

LEGEND:

A - 1.27 cm thick plywood
B - 1.91 cm thick plywood
C - 10 cm thick building insulation
D - 0.95 cm thick plywood
E - Hanger for copper cooling plate
F - 1.27 cm thick plywood
G - 1.91 cm thick plywood
H - 15 cm thick building insulation
I - 19.4 x 19.4 x 39.7 cm thick concrete block
J - 3.81cm thick fiber batt
K - Glass cover
L - 2x4 supporting strut
M - 1.91 cm thick plywood base
N - 0.8 mm thick copper cooling plate
O - 1.27 cm thick plywood

Fig. 8 Plan View of a Trombe Wall Test Unit

of the box is hinged to provide access to the interior and is also made of plywood with 0.1524 m thick building insulation.

2.1.2 Masonry Wall

The Trombe wall in the test units consist of two types of blocks. The topmost and bottommost rows of blocks are 0.194 x 0.194 x 0.397 m thick concrete bond beam blocks to provide vents for thermo-circulation. The rest of the blocks are 0.194 x 0.194 x 0.397 m thick solid concrete blocks. The masonry wall is 0.581 m long, 1.667 m high and 0.397 m thick. The vents are 0.1524 m high and 0.0762 m wide and there are three in the top row and three in the bottom row.

The blocks are made of high density concrete obtained directly from the manufacturer. The density of the blocks is about 1432 Kg/m^3 and the specific heat is about 670 J/Kg-K. Some of the important data on the Trombe wall test units are summarized in Table 1. The outer surface of the Trombe wall was sprayed with two coatings of 3M Nextel$^{(R)}$ glarefree black paint. The paint pigment has a composition of 20.2% Carbon Black and 79.8% Silicon Dioxide and has an emissivity of 0.955.

2.1.3 Glass Cover

3.18 mm thick window glass was used in the cover units. An aluminum frame provided a seat for the glazings of which either one or two could be installed. Bead-type insulations strips were used on the aluminum frame and cover unit to prevent air infiltration. When double glazing was used the cover system consisted of two layers of 3.18 mm thick window glass separated by a 1.27 cm air space located 3.81 cm in front of the masonry wall. When one glass cover was used, the air gap was approximately 5.08 cm and when two glass covers were used the gap was reduced to 3.81 cm. In the test run with a fiber batt absorber,

Table 1. Test Unit Data

	Trombe Wall Unit I	Trombe Wall Unit II
Wall Thickness	0.397 m	0.397 m
Density of masonry block (ρ)	1432.0 Kg/m^3	1432.0 Kg/m^3
Volume of wall	0.36 m^3	0.36 m^3
Total mass	515.24 Kg	515.24 Kg
Specific heat (C_p)	670.0 J/Kg-K	670.0 J/Kg-K
Total Heat Capacity	345.21 KJ/K	345.21 KJ/K
Absorber surface (Phase I, II)	Masonry wall coated with carbon black paint	Masonry wall coated with carbon black paint
(Phase III)	3.81 cm thick Fiber Batt	Masonry wall coated with carbon paint
Glazing type	3.175 mm thick window glass	3.175 mm thick window glass
Number of glazings		
Phase I	single	single
Phase II	single	double
Phase III	single	double
Air gap		
Phase I	5.08 cm	5.08 cm
Phase II	5.08 cm	3.81 cm
Phase III	1.27 cm	3.81 cm
Type of heating/cooling	Constant temperature bath	Constant temperature bath
Thermostat setting	295 K	295 K

the air gap between the glass cover and the absorber was about 1.27 cm.

2.1.4 Cooling Plate

A 0.578 m long by 1.73 m high copper plate is situated directly behind the interior surface of the masonry wall. 0.953 cm O.D. copper tubing was soldered onto the 0.8 mm thick copper sheet as shown in Figure 9. Coolant fluid is circulated through the tubing from a constant temperature bath so that the air space between the plate and the masonry wall is maintained at nearly an uniform temperature.

2.1.5 Constant Temperature Bath

A Hotpack Refrigerated Bath circulator was used as the constant temperature bath in this experiment to maintain the interior of both test units at a specified temperature. The constant temperature bath was connected to the copper plates in the test units by heavily insulated plastic tubes as indicated in Figure 5. The operating temperature range for this bath is 253 K to 343 K. However, the coolant was generally kept at about 295 K to simulate room temperature in the test units.

2.2 Instrumentation:

Instrumentation in the test facility consisted of the following items:

(i) 27 thermocouples installed in the concrete wall of unit I at 27 locations.

(ii) 19 thermocouples installed in the concrete wall of unit II at 19 locations.

(iii) 6 thermocouples on the inside surface of the glass cover of each test unit at 6 locations.

(iv) 9 thermocouples in the air gap between cover and wall of each test unit at 9 locations.

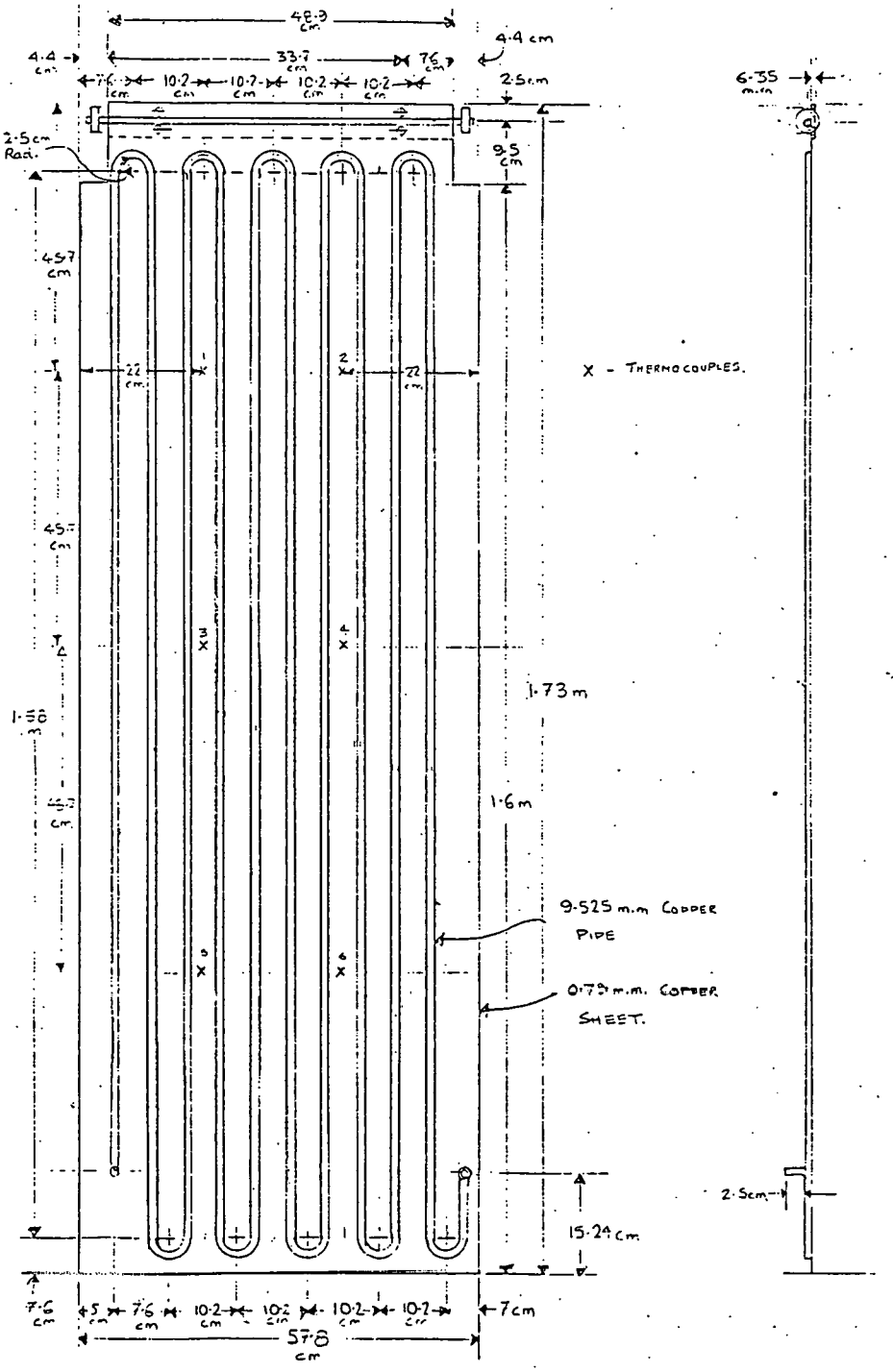

Fig. 9 Front and Side Views of a Copper Cooling Plate

(v) 6 thermocouples on the copper cooling plate at 6 locations in each test unit.

(vi) 4 thermocouples connected in series across the inlet and outlet of the copper cooling plate in each unit.

(vii) 3 thermocouples located on wiring connectors on the copper plate in each Trombe wall test box.

(viii) 2 foil heat flow meters installed in the concrete wall at 2 locations in each test unit.

(ix) 2 thermocouples located on the heat flow sensors in each test unit.

(x) 1 thermocouple measuring ambient air temperature.

(xi) 1 pyranometer mounted in the vertical plane on the south facing side of the test units.

(xii) 1 anemometer mounted on a test unit to measure wind speed.

2.2.1 Thermocouples

All thermocouples used in this experiment were constructed of Omega Engineering, Inc. copper-constantan wire. Most of the thermocouples were made of 20 gage wire (0.813 mm diameter) which was covered with a double-jacketed, Teflon insulator. The exceptions were the thermocouples located on the glass cover which were made of 36 gage wire (0.127 mm diameter). Thermocouples used to measure ambient temperature, connector temperatures, masonry wall temperature profiles and heat flow sensor temperatures were made of 30 gage nylon-jacketed wire (0.254 mm diameter).

Copper-constantan thermocouples (ANSI Symbol T) are suitable for applications where moisture is present and is recommended for low-temperature work since the homogeneity of the component wires can be maintained better than other base metal wires. Therefore, errors due to

inhomogeneity of wires in zones of temperature gradients is greatly reduced. The time constant of beaded type thermocouples made from 20 gage wire is about 3 seconds, as obtained from the Omega Temperature Measurement Handbook. The "Time Constant" or "Response Time" is defined as the time required to reach 63.2% of an instantaneous temperature change. Response times of 30 gage and 36 gage beaded thermocouples are 0.45 and 0.15 seconds respectively. The relatively long time constant of the 20 gage thermocouples was not a problem since temperature changes occurred slowly in all locations during the tests.

The limits of error for the thermocouple wire used are $\pm$ 1 C or $\pm$ 0.75% (whichever is greater) in the range 0 to 350 degrees Celsius. In the range -200 to 0 degrees Celsius the limits of error are $\pm$ 0.5 C or $\pm$ 0.8%, whichever is greater. The error in the measured temperatures can exceed the stated limits. This can occur if the thermocouple wires are exposed to large temperature gradients. A discussion of this conduction error phenomenon is presented in Appendix A. Omega-CJ electronic ice points were used with all the thermocouples to reference the thermocouple e.m.f.s to 0 degrees Celsius (273 K). The circuitry in the thermocouple reference junction was modified so it could be used simultaneously with a large number of thermocouples. The electronic ice points were calibrated regularly to compensate for battery aging.

Thermocouples-Masonry Wall Surfaces

The front and rear surfaces of the masonry wall had nine thermocouples installed on each surface. The location of the thermocouples are shown in Figure 10. Grooves were chipped in the block at each location and the thermocouple junctions were positioned flush with the surfaces. The thermocouple wires were placed in the grooves and the

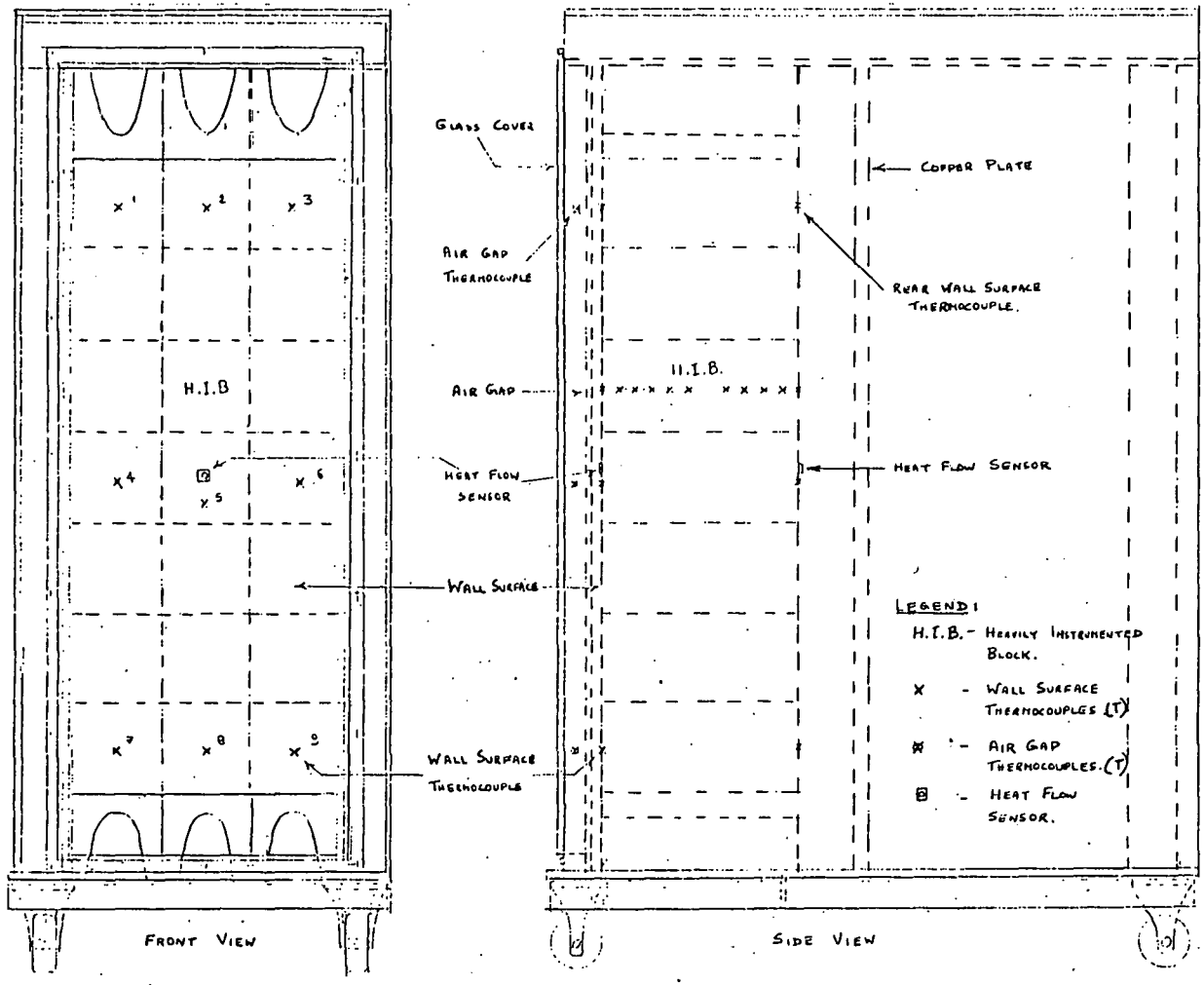

Fig. 10 Front and Side Views of a Trombe Wall Test Unit Showing the Locations of Thermocouples and Heat Flux Sensors

grooves were then filled with cement. The nine thermocouples on each surface were connected in series to form a thermopile reading the 'average' temperature of the surface. The cold junctions of the thermopile were placed in gold plated connectors which were in good thermal contact with the copper cooling plate near the rear surface of the wall. The thermopile, then, would read the temperature difference between the wall surface and the copper plate. Since the temperature of the connector would be known (from a thermocouple placed in the connector), the wall surface temperature would also be known.

Thermocouples-Masonry Wall Block

In one of the test units (to be called from now on test unit II) one block was "heavily" instrumented with thermocouples. The location of this block is shown on Figure 10.. Nine thermocouple junctions were installed in the interior of the block located along an axis running from the front surface of the block to the rear surface. The location of these thermocouples is shown in Figure 11 . At each location 10 cm deep holes were drilled perpendicularly to the top. The thermocouples were positioned with the junctions at the bottom of these holes, and the holes were filled with cement. The thermocouple junction locations in the blocks are known to within $\pm$ 2 mm's.

Trombe wall unit I had a "lightly" instrumented block in a similar location with two thermocouples located at the center of the block. Lack of extra channels in the data acquisition system prevented more thermocouples from being used.

Thermocouples-Glass Cover

Six thermocouples were attached to the inner glass cover surface, that is, the surface closest to the masonry wall. The thermocouple

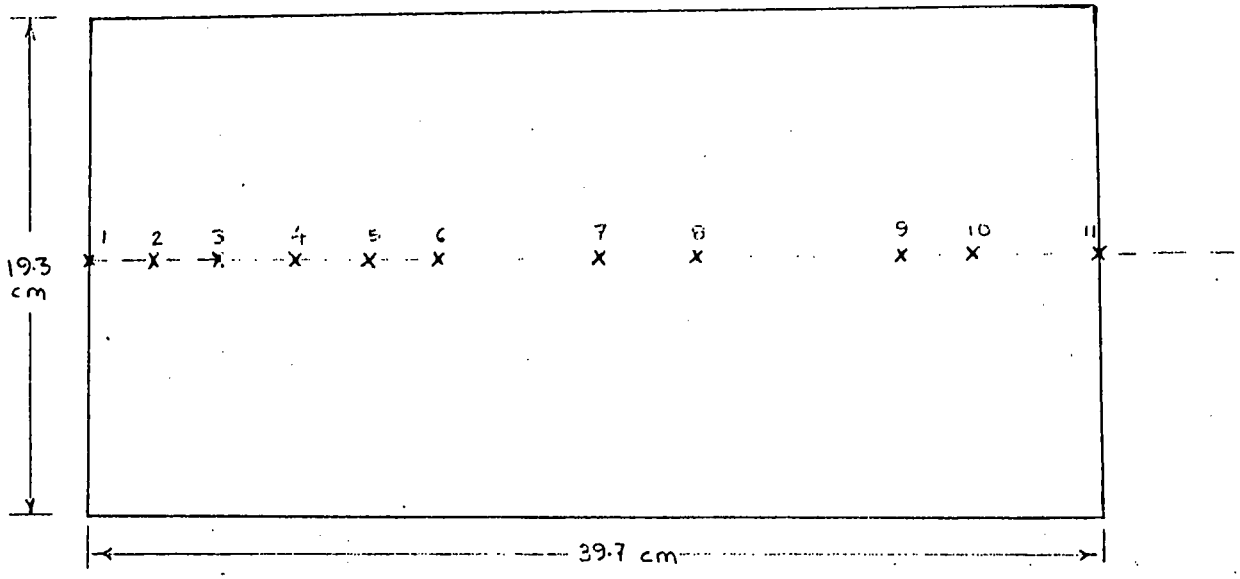

Thermocouple Number	1	2	3	4	5	6	7	8	9	10	11
Distance from front of block (cm)	0.0	2.54	5.1	8.1	10.95	13.7	18.8	27.2	32.2	34.9	39.7

Scale 1:3

Fig. 11 Top View of a Heavily Instrumented Block Showing the Location of Thermocouples

junctions were placed adjacent to the glass surface and then glued in place. Small aluminum foil radiation shields were placed on the glass directly in front of the thermocouples so that the thermocouples indicated the true glass temperature. The thermocouples were connected in series and the cold junctions were placed in a connector with good thermal contact with the copper cooling plate in each Trombe wall test unit. When divided by the multiplication factor (in this case, six) the thermocouple would indicate the 'average' temperature difference between the glass cover and the copper plate, whose temperature was known. The locations of the thermocouples are shown in Figure 12.

Thermocouples-Air Gap

Nine thermocouples were located in the air gap about 2.5 cm in front of the masonry wall at locations approximately opposite the nine surface thermocouples on the masonry wall. The thermocouples were suspended using fine nylon string and were shielded from direct radiation. A series connection was used for the thermocouples with the cold junctions situated in a connector bolted onto the copper cooling plate. The e.m.f. generated by the thermopile so formed, indicates the temperature difference between the air and the copper cooling plate, after taking into account the thermopile multiplication factor.

Thermocouples-Copper Plate

Six thermocouple junctions were glued onto the copper cooling plate in each Trombe wall test unit at locations shown in Fig. 9, using epoxy resin thermal glue and were connected in series. The cold junctions were located on a heat sink bolted to the copper plate itself. The temperature differences indicated by this thermopile were always negligible. A thermocouple was located on the heat sink so that at all times

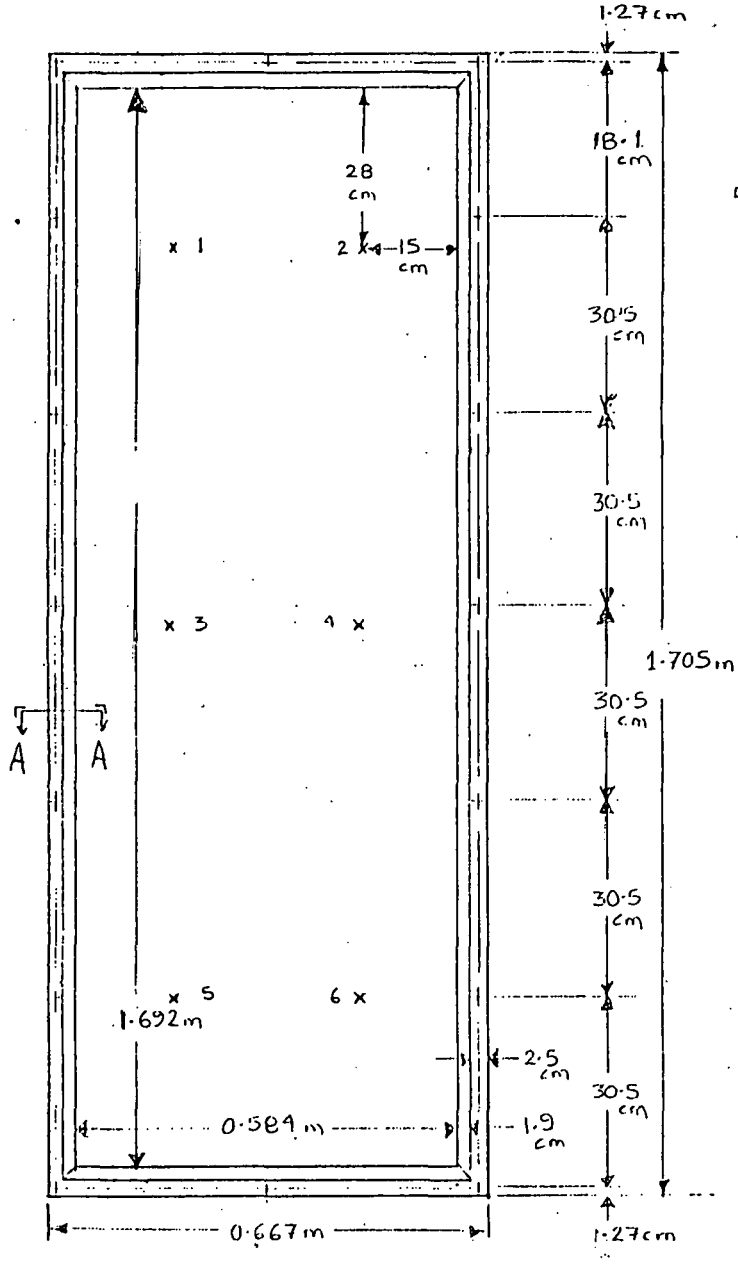

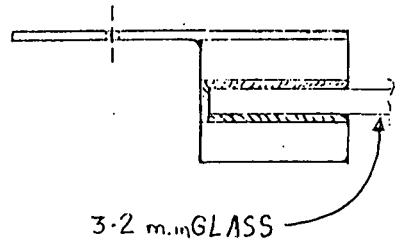

SECTION AA
Full Scale

x - Location of Thermocouples.

Fig. 12 Front View of a Glass Cover Showing the Location of Thermocouples

both the heat sink temperature and the copper cooling plate temperature (which were almost identical) were known.

Four thermocouples were located in the coolant inlet tube and four more were located in the coolant outlet tube of each copper plate across the flow stream. Two pieces of metal gauze were placed next to the thermocouples to ensure fluid mixing. The four inlet and outlet thermocouples were connected in series so that the temperature difference across the inlet and outlet could be read, after taking into account the thermopile multiplication factor. An individual thermocouple was located in the flow stream at the inlet to indicate the inlet coolant temperature.

Thermocouple-Ambient Temperature

One thermocouple was installed external to the test units. It extended about 5 cm from the East side of the test box and was shielded from direct beam radiation by an aluminum tubular shield painted black inside. This thermocouple provided an ambient air temperature measurement.

Thermocouples-Connectors

As mentioned before the cold junctions of the thermopiles on the glass covers, air gaps, masonry walls, coolant inlet-outlet tubes and copper cooling plates were located in gold-plated connectors in thermal contact with the copper cooling plate of each Trombe wall test unit. There are three such connectors in each unit and individual thermocouples are located in each connector. Thus, the temperature of the connector is known enabling the thermopile readings to be converted to absolute temperature values.

2.2.2 Heat Flow Sensors

Two RDF Corporation Micro-foil heat flow sensors were used to measure the total heat flux through a block in the masonry wall of each test unit. The location of this block is shown in Figure 10. The block is located approximately at the middle of the wall. The heat flow sensors contain a thermopile for high sensitivity, bi-directional heat flow measurements and an embedded ANSI Type T copper-constantan thermocouple for surface temperature measurement. They were attached with silicon heat transfer paste to the surfaces of the block. The calibration constants for these sensors are given in Chapter 3.

As will be mentioned later, the data acquisition system has a resolution of 10 microvolts with an input gain of 500. This is not sufficient to read the heat-flow sensors accurately and therefore linear amplifiers were used. Four Omega Engineering, Inc. Omni-Amp II amplifiers were connected to the heat-flow sensors (two for each wall). The amplifiers were used with a gain of 10 and noise was less than 50 microvolts RMS in the output. The output was coupled directly to the data acquisition system. The amplifiers were calibrated frequently by zeroing them and by using a known millivolt source.

2.2.3 Pyranometer

An Eppley Model PSP precision pyranometer was used to measure the insolation rate. The instrument was mounted on the vertical plane near the top of the glass cover on the west side of one of the Trombe wall test units. In this position, the pyranometer extended beyond the roofline and, consequently, was not shaded by the roof.

The pyranometer was temperature compensated in the range -20 to + 40°C. The e.m.f. developed by the instrument is linearly proportional

to the radiation intensity to within ± 0.5 percent up to an intensity of 700 W/m^2. Pyranometers mounted in the vertical plane are subject to error because of convection effects within the bulb of the instruments. However, as will be discussed later, the error can be taken into account.

2.2.4 Anemometer:

An Aeolian Kinetics Company model WPA-10 cup type anemometer was used to measure the average wind speed during the test runs of the experiment. The anemometer was mounted on a stub mast which was in turn mounted on top of one of the Trombe wall test units.

The anemometer contains a reed switch which is activated at a rate proportional to the wind speed. The reed switch is connected to an Aeolian Kinetics Company model WP-1000 microprocessor system which computes and displays both the instantaneous wind speed and an average wind speed over a specified period of time.

2.3 Data Acquisition System

A computer controlled data acquisition system was used for all three parts of this experiment. The heart of the system consisted of a Hewlett-Packard HP-1000 Series 'E' minicomputer with the following features:

(a) 192 K bytes main memory

(b) 16 Bit word length

(c) FORTRAN IV compiler

(d) 20 M byte disk for storage

(e) CRT displays

(f) Line printer.

The minicomputer was connected by a HP-12050A Fiber Optic link to a Hewlett-Packard HP-2240A Measurement and Control Processor (MACP).

The MACP was set up to read 32 analog channels but during the course of the experiment 4 channels were found to be defective. Therefore 28 channels of data were available.

The HP-2240A MACP has the following features:

(a) HP-22915A Low-Level Analog input cards (low-level amplifiers)

(b) HP-22900A Analog to Digital Converter.

(c) Automatic temperature calibration.

The MACP performs as an intelligent interface between the HP-1000 computer and the system of sensors. The HP-2240A MACP is microprogrammed to accept streams of commands from the controller (the HP-1000 computer) and then execute the commands in the real-time environment of the external system such as periodically gathering a group of measurements. The controller program specifies what the processor is to do; the processor performs the specified routines and returns any resulting data to the controller.

The input channel gain was set at 500 with a range of $\pm$ 20 millivolts. In this range the accuracy of the system was $\pm$ 0.5 percent full-scale. The HP-2240A has a 12 Bit A/D Converter plus a preamplifier gain of 500 to give a resolution of 10 microvolts. The input channels had offset potentiometers which were used frequently to calibrate the channels against a microvolt resolution digital voltmeter by both zeroing and using known millivolt sources.

Some of the data was not read automatically due to a limited number of channels being available. The nine thermocouples measuring the masonry wall temperature profile in the Trombe wall test unit II were read using a Dataplex 10 ten channel reed scanner connected to a HP-3467A Logging Multimeter. The multimeter has a sensitivity of 1

microvolt in the ± 20 millivolt range used. The two thermocouples located at the middle of one of the blocks in test unit I was read with Fluke 8600A Digital Multimeter.

All transducers were connected to the HP-2240A by shielded computer cable. The HP-2240 MACP was located close to the experiment location to minimize noise problems but even a close location necessitated use of fairly long cables (10 m long). Considerable noise problems were encountered with the cables picking up line frequency noise and acting as antennas. Many shielding configurations were tried before the standard deviation of the readings were brought down to acceptable values. Linear amplifiers were used to raise the signal level of the heat flux sensors. The connecting cable shield was connected to the negative side of all transducers near the transducers and at the HP-2240A MACP. While averaging the readings for each channel, a suitable sample size was used to minimize standard deviation values. Even though grounding problems were encountered with the constant temperature bath switched on, standard deviation values of 0.01 were finally obtained with a signal level of about 1 mv.

During Phase III of the experiment a 3.81 cm thick layer of fibrous material was attached to the masonry wall front surface. The air gap thermocouples would be measuring the temperature of the fiber bed 2.54 cm from the masonry wall surface. The true air gap temperature can be estimated by assuming a linear temperature profile in the fiber bed and then calculating the air-gap temperature.

CHAPTER 3

DATA ACQUISITION AND TEST PROCEDURE

3.1 General

The experimental program was begun after some preliminary tests had been completed to test the instrumentation and the data acquisition procedure. These tests were performed indoors with high intensity lamps to simulate solar insolation. Tests were made on all the thermocouples and thermopiles to ensure that their electrical resistance was of the same order for both Trombe wall test units. The coolant sub-system was tested for various ranges of operating temperatures. During the test runs proper the thermocouple electronic ice-points, heat flux sensor signal amplifiers and the low-level analog input cards were calibrated regularly to prevent drift.

3.2 Data Acquisition

Table 2 shows the input channel descriptions to the data acquisition system. Since only twenty-eight channels were available on the HP-2240A measurement and control processor only the more important measurements were made automatically.

As mentioned before, in Chapter 2, most of the temperature measurements (the cover, air gap, front wall surface, interior wall surface and copper plate surface) were made with thermocouples connected in series to form thermopiles, rather than individual thermocouples, that sense the temperature difference between the surface and the cold junctions situated on the copper plate. This arrangement has the advantage of magnifying the signal by the number of couples in series (permits detection of very small temperature differences) and one

Table 2. List of Instrumentation Used.

Device Description	Data Acquisition System Channel Numbers Wall # 1	Wall # 2
Interior Cover Surface Thermopile	1	17
Air Gap Thermopile	2	21
Exterior Wall Surface Thermopile	3	22
Interior Wall Surface Thermopile	4	23
Copper Cooling Plate Surface Thermopile	5	24
Coolant Flow Differential Thermopile	6	25
Coolant Inlet Temperature Thermocouple	7	26
37-Pin Connector Temperature Thermocouple	8	27
25-Pin Connector Temperature Thermocouple	9	—
13-Pin Connector Temperature Thermocouple	10	—
Exterior Wall Heat-Flux Sensor Thermocouple	11	28
Interior Wall Heat-Flux Sensor Thermocouple	12	29
Exterior Wall Heat-Flux Sensor	13	30
Interior Wall Heat-Flux Sensor	14	31
Pyranometer	16	—
Ambient Air Temperature Thermocouple	—	32

The following measurements were made without using the computer-controlled Data Acquisition System:

9 Masonry Wall Temperature Profile Thermocouples (Wall # 2)

2 Masonry Wall Temperature Profile Thermocouples (Wall # 1)

Anemometer

observation gives the arithmetic mean of the temperature differences sensed by the couples. Thus, for example, if nine thermocouples are situated on a surface, as on the masonry wall, with the cold junctions located in a connector on the copper cooling plate, the signal measured when divided by nine, would indicate the average temperature difference between the connector and the surface. This is necessary because a vertical surface on a Trombe wall is not at an uniform temperature. Experimenters have noted that measurable temperature stratification can occur due to shading effects. Therefore, either the wall has to be divided into several zones in the vertical direction and the individual zone temperatures measured, or the average temperature of the surface has to be measured. The first method, of course, requires a larger number of input channels on the data acquisition system and, therefore, was not used.

The HP-2240A Measurement and Control Processor was programmed to read each input channel 20 times sequentially and pass the results to the HP-1000 computer. There would be a time lag, of course, between reading the first channel and the last. However, the HP-2240A is extremely fast (for example, reading 32 channels 20 times each would take at most 690 mS to execute) and during the time lag the expected variation in the input signals would be negligible because of the large thermal mass of the system. The pyranometer signal was read 60 times over a period of 15 minutes (once every 15 seconds) and the average reading for the period was computed. This value was used as the "instantaneous" reading at the end of the 15 minute period. This procedure is necessary because pyranometer readings are proportional to the insolation (the solar radiation flux) which may fluctuate

considerably over short periods of time due to changing atmospheric conditions. Instantaneous values of the insolation may be quite misleading, so pseudo-instantaneous values are used instead. At the end of each 15 minute period all the other channels are read 20 times and then the process repeats itself. The logic of the data acquisition procedure is shown in Figure 13 which shows a flow chart of the data acquisition program "DATAQ". The program itself is written in FORTRAN IV language and is listed in Appendix B.

3.3 Test Procedure

As mentioned before in Chapter 1, the experiment was divided in three phases. During Phase I both Trombe wall units were tested with a single glass cover system. Phase II of the experiment consisted of testing unit 1 with a single glass cover and unit 2 with a double cover. A single glass cover with a fiber batt absorber was used on unit 1 during Phase III of the experiment. The performance of unit 1 was compared to that of unit 2 which had a double glass cover and a conventional masonry wall absorber. Further tests were made after painting the fiber-batt absorber surface with a carbon-black paint.

At this stage it must be noted that the weather conditions were not ideal during the course of the experiment. Trombe walls should be tested during cold, clear winter days when the sun is low and the angle of incidence of beam radiation is low. However, by the time the preliminary tests were completed and the apparatus was ready to take data, summer had arrived. The effects of the high summer sun and high ambient temperatures are discussed in Chapter 5. Also, air passages from the glazing side to the room side of the storage walls were sealed to eliminate thermosyphoning and thus avoid problems in maintaining uniform

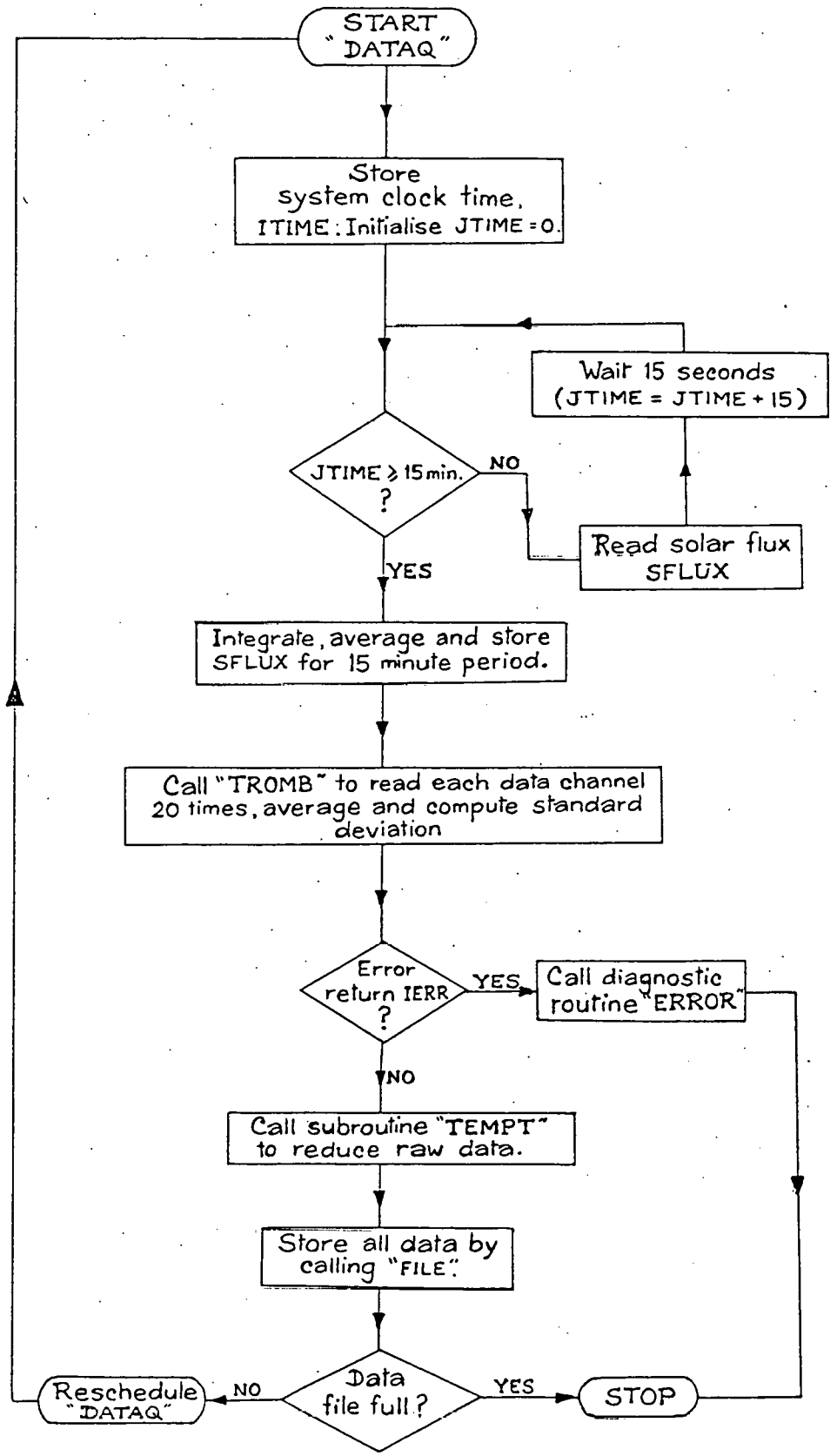

Fig. 13 Flow Chart of Data Acquisition Computer Program "DATAQ"

"room" temperature.

Each test run was made for two days at a time so that the units could be monitored continuously for 48 hours. The available disk storage capacity limited the data acquisition period to about 48 hours of data. The Trombe wall test units were left exposed to the environment for about 24 hours and the constant temperature bath cooling loop was switched on so that the temperature of the copper cooling plate in each unit could reach steady-state. The data acquisition program was loaded into the memory of the computer and a data file was created on the disk prior to running the program. The program was initialised at 12:00 A.M. at the beginning of each 48-hour period after switching on all electronic thermocouple ice-points and linear amplifiers.

The anemometer readout was also initialised to zero as the data acquisition procedure was started. The program switched itself off at the end of each 48-hour period but the anemometer readout had to be switched off manually. As mentioned before in this chapter the insolation (solar flux) data was read every 15 seconds and averaged for a 15 minute period. At the end of each 15 minute interval all other channels were read 20 times each. The averaged "instantaneous" data and standard deviations were stored by the control program in the data file on disk. The temperature profile data was read manually every hour using a nine-channel scanner and a millivoltmeter. The millivoltmeter was left switched on and was zeroed prior to reading each set of data. The average relative humidity for the test period was found by calling the Lexington Weather Forecast line.

CHAPTER 4

DATA REDUCTION AND ANALYSIS

The data reduction and analysis procedures described in this chapter have been incorporated in the data acquisition computer program "DATAQ" listed in Appendix B. Data in raw form (all in the order of millivolts) is fed to "DATAQ" every 15 minutes during the test period and the program converts and stores the data in reduced form. The standard deviation of each data set is calculated as

$$\left(\frac{\sum_{i=1}^{20} (x(i) - x_{avg})/G_D)^2}{Nmax - 1} \right)^{\frac{1}{2}} \tag{4}$$

where x(i) are the data (millivolts), x_{avg} is the average of the data set, G_D is the gain of the data acquisition system (500) and Nmax is the number of data points (20). The standard deviation is stored by "DATAQ" for all channels.

4.1 Thermocouple Data

As mentioned before, all thermocouples used in this experiment are A.N.S.I. type T copper-constantan thermocouples. Many data points were taken from the National Bureau of Standards Copper-Constantan Thermocouple Reference Tables and a least-squares polynomial fit was obtained through these data points. The program used was available on the IBM-370 Computer Statistical Software Package Library. The following sixth degree polynomial was obtained:

$$T = 9.172478 * 10^{-9} + 2.599973 * 10^{1} x_{TR} - 8.142306 * 10^{-1} x_{TR}^2 + 6.423569 * 10^{-2} x_{TR}^3 - 5.212138 * 10^{-3} x_{TR}^4 + 3.199713 * 10^{-4} x_{TR}^5 - 9.425144 * 10^{-6} x_{TR}^6 + 273 \tag{5}$$

where T is the temperature in degrees Kelvin and $x_{TR} = x_T/G_D$; where x_{TR} is the reduced thermocouple millivoltage, x_T is the raw thermocouple millivoltage and $G_D = 500$ is the gain factor of the data acquisition system.

4.2 Thermopile Data

4.2.1 Cover Surface Thermopiles

The raw millivolts read from the cover surface thermopiles were reduced to the corresponding temperatures as follows:

$$x_{CR} = x_C/(G_C * G_D) + x_p/(G_D) \tag{6}$$

where x_{CR} is the reduced cover thermopile millivoltage, x_C is the raw millivoltage, $G_C = 6$ is the gain factor of the thermopile, $G_D = 500$ is the gain factor of the data acquisition system and x_p is the raw millivolt reading of the thermocouple located on the cold-junction connector on the copper cooling plate. x_{CR} is converted to T_C, the cover temperature in degrees Kelvin by using equation (5) with x_{TR} replaced by x_{CR}.

4.2.2 Air Gap, Exterior and Interior Wall Surface Thermopiles

As in equation (6)

$$x_{AR} = x_A/(G_A * G_D) + x_p/G_D \tag{7}$$

$$x_{ER} = x_E/(G_E * G_D) + x_p/G_D \tag{8}$$

$$x_{IR} = x_I/(G_I * G_D) + x_p/G_D \tag{9}$$

where x_{AR}, x_{ER} and x_{IR} are the reduced air gap, exterior wall surface and interior wall surface thermopile millivoltages respectively. x_A, x_E and x_R are the corresponding raw quantities. $G_A = G_E = G_I = 9$ are the thermopile gains and G_D and x_p are as defined before in equation (6).

The reduced millivolts are converted to temperatures T_A, T_E and T_I by using equation (5).

4.2.3 Copper Cooling Plate and Coolant Flow Thermopiles

The copper plate average temperature T_{CP} is obtained from equation (5) by using x_{CPR} instead of x_{TR}, where

$$x_{CPR} = x_{CP}/(G_{CP} * G_D) + x_p/G_D \quad (10)$$

x_{CPR} is the reduced millivoltage from the copper plate thermopile, x_{CP} is the corresponding raw millivoltage and $G_{CP} = 6$. The coolant outlet temperature, T_o, is obtained by adding the coolant differential thermopile millivoltage to the millivoltage reading from the copper-constantan thermocouple at the inlet and then using equation (5).

$$x_{OR} = x_{CD}/(G_{CD} * G_D) + x_{IN}/G_D \quad (11)$$

x_{OR} - reduced millivoltage corresponding to outlet temperature.

x_{CD} - millivoltage of differential thermopile.

G_{CD} - gain of thermopile = 4.

x_{IN} - raw inlet thermopile reading (mV).

4.3 Heat Flux Sensor Data

Four RDF Corporation Micro-foil™ Heat Flux Sensors were used for heat flux measurements. The heat flux measurements were obtained as follows:

$$q = k * Z * x_{HF}/(G_{HF} * G_D) \quad (12)$$

where k is the sensor multiplication factor ($W/m^2/mV$) as supplied by the manufacturer, Z is the temperature correction factor to be obtained below, G_{HF} is the gain of the heat-flow sensor linear amplifier (10) and G_D is, as before, 500. q is the heat flux in W/m^2 and x_{HF} is the heat flux sensor reading in millivolts.

The temperature factor Z, is obtained from a second-degree polynomial that results from a curve-fit of data supplied by the manufacturer.

$$Z = 1.542994 - 2.524 \times 10^{-3} * T_{HF} + 2.0 * 10^{-6} * T_{HF}^2 \qquad (13)$$

where, T_{HF} is the temperature of the heat-flux sensor in degrees Kelvin. T_{HF} is obtained from the reading of a thermocouple located in the heat-flux sensor. The following table lists the heat-flux sensor multiplication factors as supplied by RDF Corporation:

Table 3. Heat Flux Sensor Multiplication Factors

Description of Sensor	Multiplication Factor k($W/m^2/mV$)
External Heat-Flow Sensor (Wall 1)	2.9557×10^2
Internal Heat-Flow Sensor (Wall 1)	3.0589×10^2
External Heat-Flow Sensor (Wall 2)	3.0738×10^2
Internal Heat-Flow Sensor (Wall 2)	3.03534×10^2

4.4 Pyranometer Data

The reduction of the pyranometer readings was very straight forward. The calibration constant of the instrument, as supplied by the Eppley Laboratory, Inc. is 96.8054211 $W/m^2/mV$. No temperature compensation is necessary because the pyranometer is self-compensating in the range - 25 to 40°C. This calibration constant has been obtained with the pyranometer in a horizontal position. Norris (1974) has noted that the response characteristics of pyranometers in inclined positions are slightly different due to convection effects. The effect is quite pronounced when the pyranometer is mounted in the vertical plane, as in Trombe wall tests and must be accounted for. As shown in Figure 14, a precision Eppley pyranometer may read as much as 10% more than the

actual value of insolation when mounted vertically. It is surprising that many researchers seem to ignore this important fact. A correction factor, $C_{PY} = 0.9$, as recommended by Norris, is taken into account when evaluating the incident solar flux by using the following calibration equation,

$$I_C = M_{PY} * C_{PY} * x_{PY}/G_D \qquad (14)$$

where I_C is the insolation (W/m^2), $M_{PY} = 96.8054211\ W/m^2/mV$ is the multiplication factor and x_{PY} is the pyranometer output in millivolts. $G_D = 500$, as before.

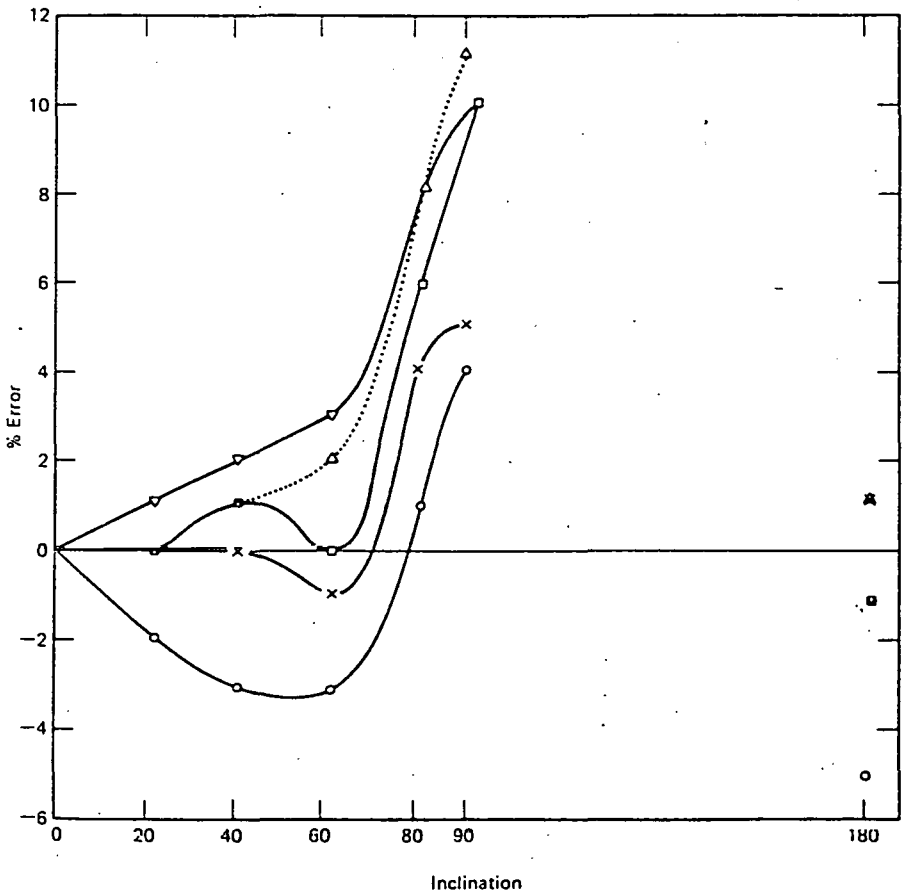

Figure 14. Effects of inclination of pyranometers on calibration. Instruments are: O, Eppley 180°; △, Precision Eppley; X, Trickett-Norris (CSIRO); □ Kipp, thermopile axis inclined; ▽, Kipp, thermopile axis horizontal. Adapted from Norris, Solar Energy, 16, 53 (1974).

4.5 Anemometer Data

The anemometer readout displays the total elapsed wind run and updates the reading continuously. The average wind speed, for each twenty-four hour period, is found by dividing the total wind run in kilometers by the number of hours the wind run has been accumulating.

CHAPTER 5

EXPERIMENTAL RESULTS AND DISCUSSION

The major objective of the experiment was to establish that a Trombe wall passive solar collector with a fiber batt absorber had an improved performance when compared with a conventional Trombe wall. Toward meeting this goal, a set of experiments was conducted to determine the thermal performance of two identically constructed Trombe wall test boxes. In the first part of the experiment, both test units had a similar configuration of single glass covers. Data is presented to show that the thermal characteristics of the test units are virtually identical.

In the second part of the experiment a single cover Trombe wall was compared with a double cover Trombe wall. In the final part a single cover fiber-batt absorber Trombe wall unit was compared with a double cover unit. Hourly data like cover temperatures, air gap temperatures, wall surface temperatures and heat flux measurements are presented for all three parts of the experiment over a 48 hour period. These results are plotted together with the hourly insolation and ambient temperature values over 48 hour periods. In the actual experiment, data was collected over a large number of days but only six days of data are presented as representative of the large amount of data collected. The temperature profile within a double cover Trombe wall test unit is presented for a 24 hour period. The energy gain of the fiber absorber single cover Trombe wall is compared with that of a double cover unit. Top loss coefficients are calculated for all three configurations of the Trombe wall units. The significance of the results are discussed in this chapter. All the data presented

in graphical form are also tabulated in Appendix D.

As mentioned before, the experiment was conducted over spring and summer months. The data presented in this chapter, therefore, is preliminary in nature and the conclusions drawn from them should be confirmed by supporting data obtained through a heating season. However, certain trends are quite clear from the data and many interesting conclusions can be drawn. Some information about the data collection periods like day numbers, relative humidity, wind speeds and weather conditions are presented in Table 4 below.

Table 4. Some Information about Data Collection Periods

Experiment	Day of Year (1982)	Relative Humidity(%)	Average Wind Velocity (m/s)	Weather Conditions
Phase I	113 (April 23)	62%	1.8	Intermittent Clouds
	114 (April 24)	59%	1.43	Light Clouds
Phase II	174 (June 24)	78%	2.86	Light Clouds
	175 (June 25)	63%	3.08	Clear
Phase III	196 (July 15)	68%	3.34	Light Clouds
	197 (July 16)	76%	3.66	Hazy

5.1 Comparison of Two Identical Test Units

In the first part of the experiment the two Trombe wall units were compared with single glass covers on both units. The 3.18 mm thick glass covers were installed 5.08 cm in front of the masonry wall surface. Rayleigh numbers obtained for this configuration were typically about 7×10^4 for the test period. The test period of this phase of the experiment was day 113 and 114 (April 23 and April 24, 1982). Day

113 was a cloudy day and day 114 had light clouds in the morning with clear sunshine in the afternoon. Both days were chilly with minimum temperatures dropping to 275.2 K on day 114. Figures 15 through 19 present thermal performance data like temperatures and masonry wall surface heat fluxes. The data is also tabulated in Table D.1 in Appendix D.

5.1.1 Cover Temperature Variation

The temperatures for the glass covers of test unit 1 and 2 are presented in Fig. 15. It can be seen that the cover temperatures are quite close for both test units (within 0.5 K of each other). The cover temperature of unit 1 seems to be slightly higher than that of unit 2 and this trend is observed in the air gap and front wall surface temperatures as well. The effects of clouds can be seen in day 113 when the insolation values vary considerably towards midday. Interestingly enough, the glass cover temperatures vary at the same time as the insolation showing the relatively low thermal time constant of the glass cover. The ambient temperature also shows a similar trend.

5.1.2 Air Gap Temperature Variation

The air gap temperatures measured are almost identical for both single-cover Trombe wall units, as is evident from the curves in Figure 16. Like the cover temperatures, the air gap temperatures of test unit 1 are slightly higher than that of unit 2 (by a maximum of 0.6 K). In day 113 the oscillation in the insolation curve has a marked effect on the air gap temperature curves. Nevertheless, both Trombe wall test units respond identically.

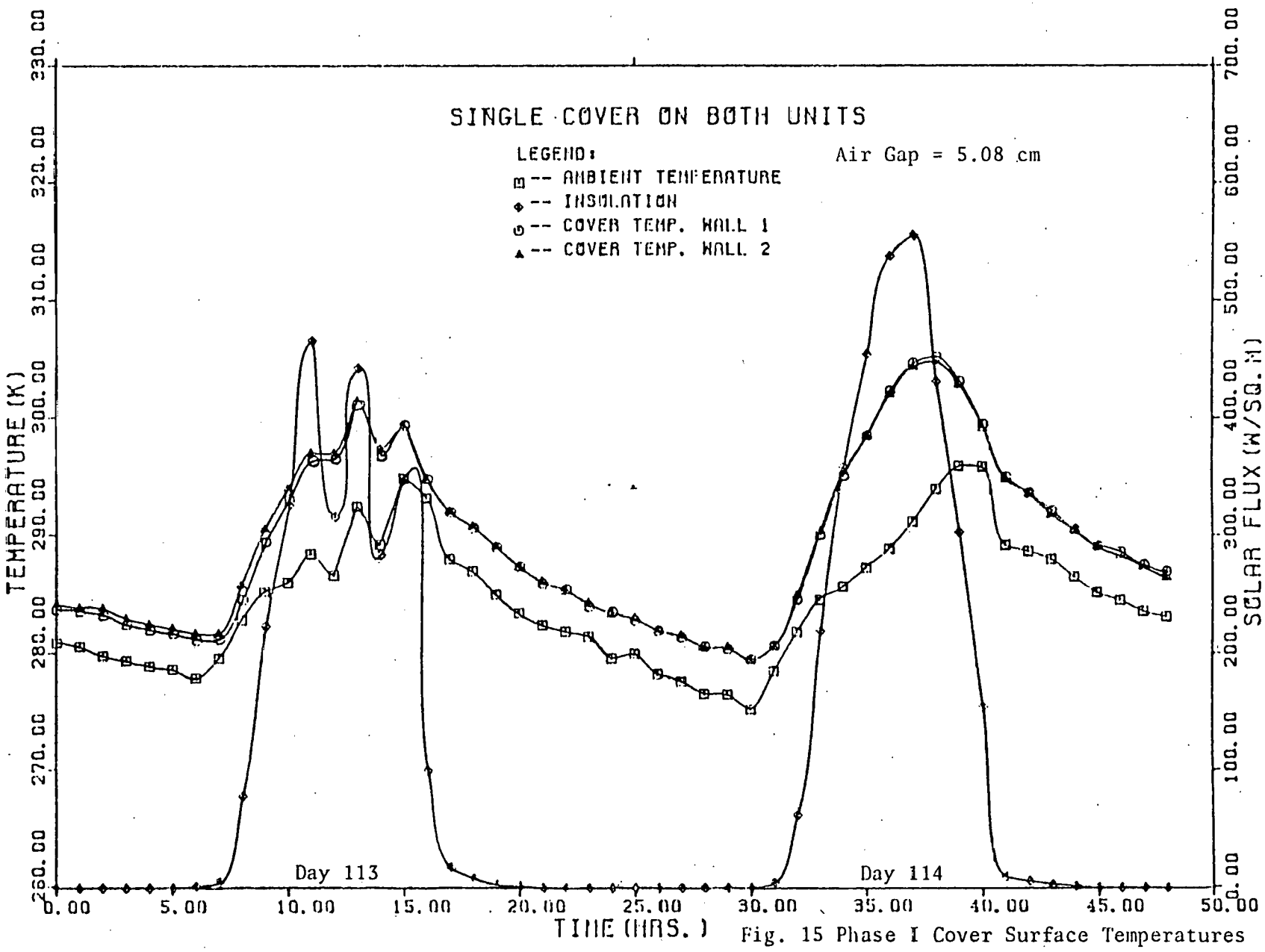

Fig. 15 Phase I Cover Surface Temperatures

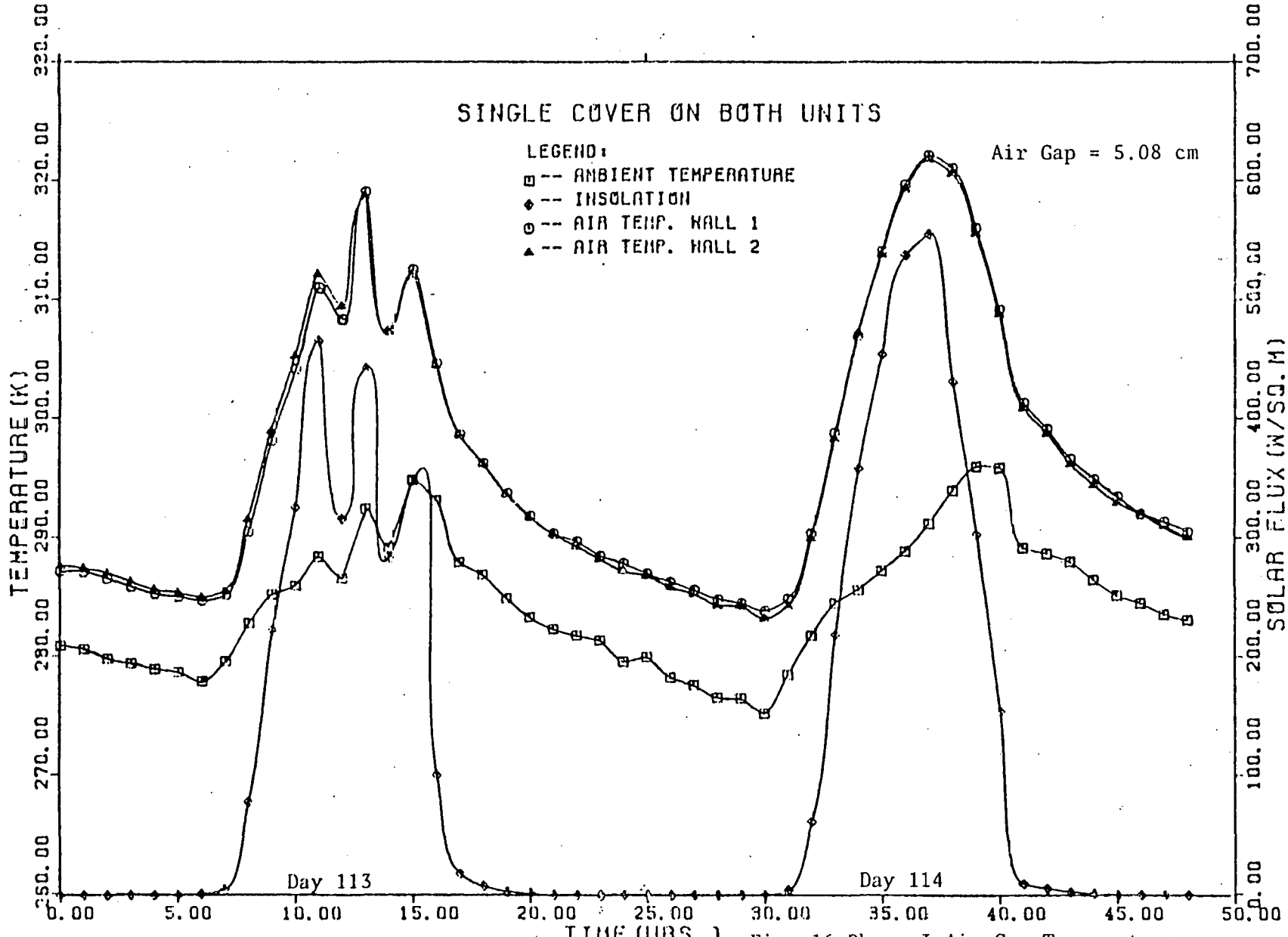

Fig. 16 Phase I Air Gap Temperatures

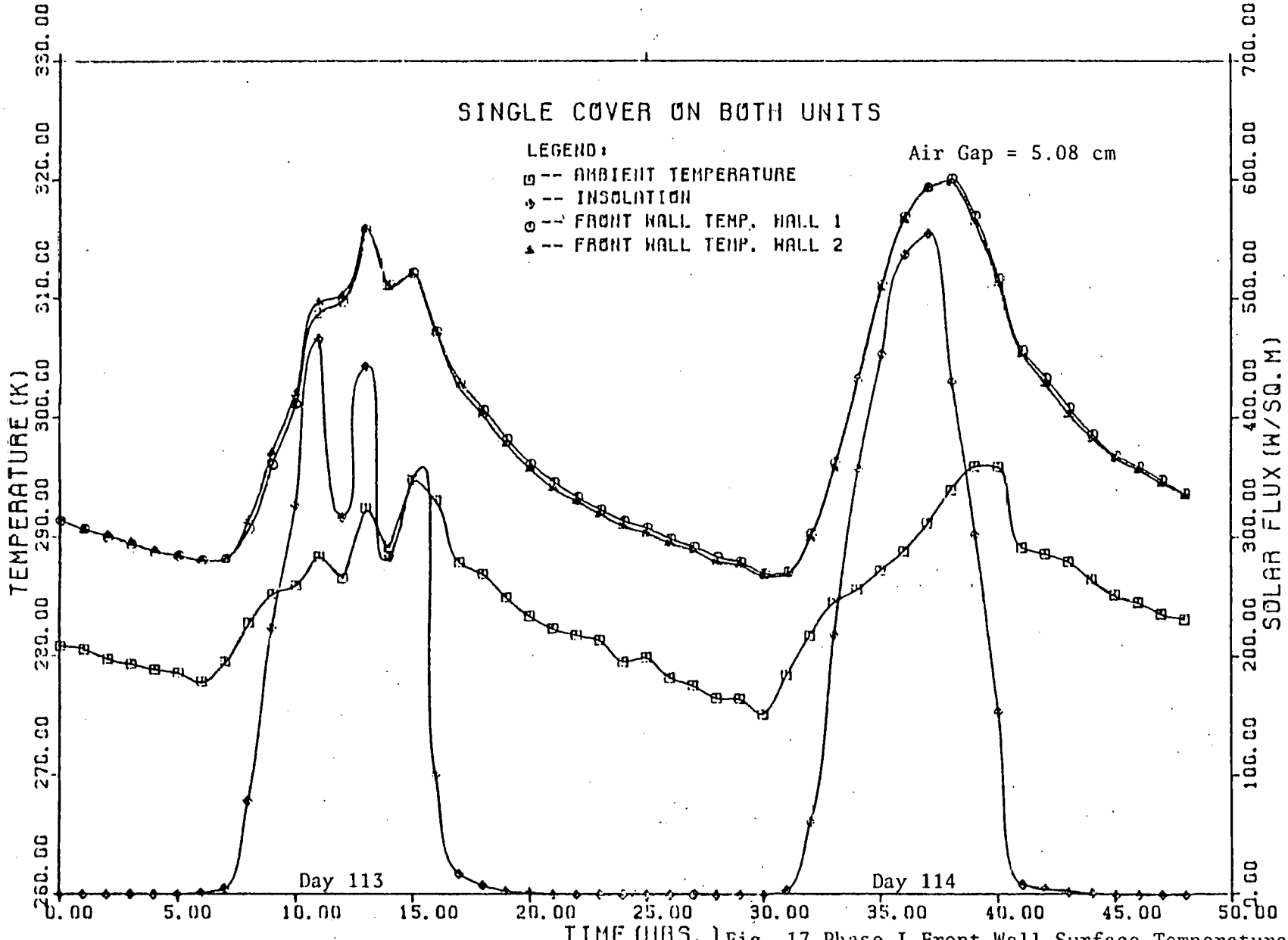

Fig. 17 Phase I Front Wall Surface Temperatures

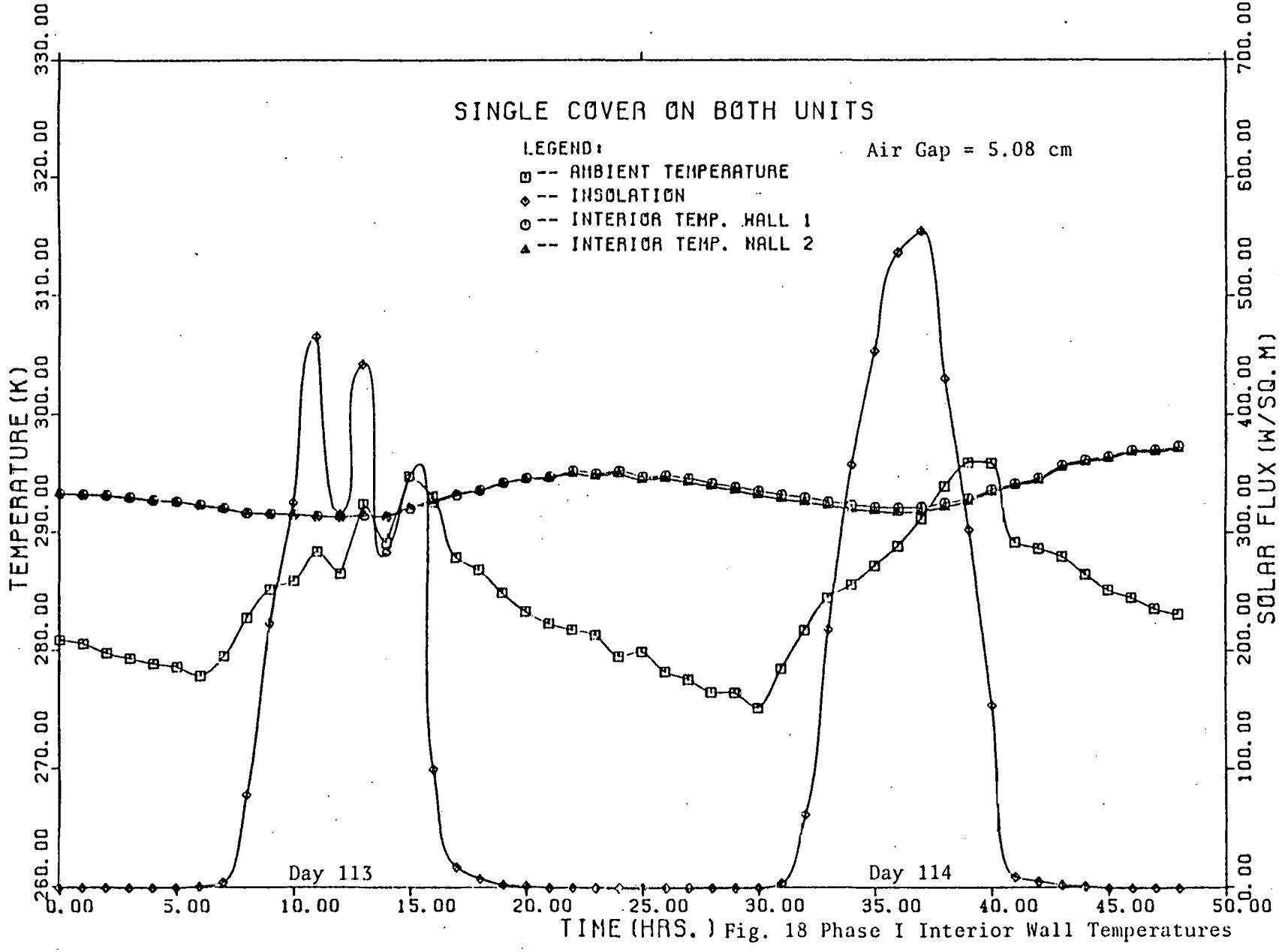

Fig. 18 Phase I Interior Wall Temperatures

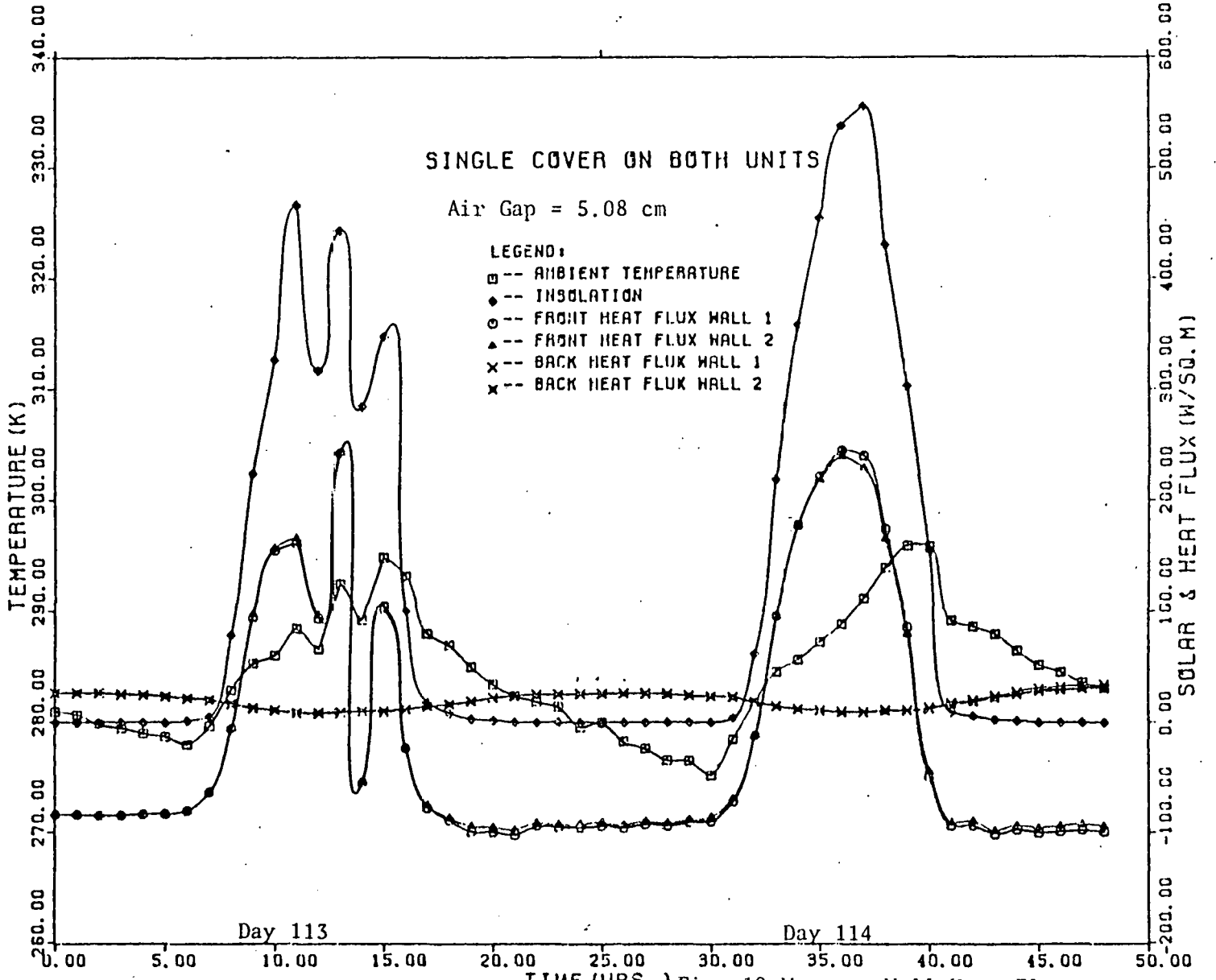

Fig. 19 Masonry Wall Heat Fluxes

5.1.3 Masonry Wall Front Surface Temperature Variation

Figure 17 shows the variation of the front masonry wall surface temperature with time. The trend is similar to the one observed in the air gap temperature. The temperature of the masonry wall surface increases with increase in the incident solar flux and decreases as the solar flux decreases. A minimum is reached when the ambient temperature reaches a minimum, because losses to the environment are maximum at this time. This minimum is at 6:00 AM on day 113 and 114. A maximum absorber surface temperature of about 320 K is reached at about 2:00 PM on day 114. However, rapid variations in the insolation, as on day 113, do not have such a marked effect on the wall surface temperatures as on the air gap temperatures, mainly because of the large thermal time constant of the masonry walls. Both test unit 1 and 2 have very similar masonry wall surface temperature curves with the unit 1 curve being occasionally slightly higher than the unit 2 curve, by a maximum of 0.5 K.

5.1.4 Masonry Wall Interior Surface Temperature Variation

Figure 18 shows a remarkably consistent behavior of the masonry wall interior surface temperatures of Trombe wall units 1 and 2. The temperatures in both units are very close together at all times of the test period with the interior surface temperature in unit 1 being sometimes slightly higher by about a maximum of 0.3 K. The curves exhibit a periodic behavior, reaching a maximum at about 11:00 PM and a minimum at about 12:00 in the afternoon. It can be observed that the interior surface temperature lags the front wall surface temperature by about 10 hours. Similar figures for the phase lag have been observed in studies for wall thicknesses close to the one used in

this experiment (Bilgen et al. (1978)).

5.1.5 Masonry Wall Surface Heat Flux Variation

The front wall surface and interior wall surface heat fluxes are plotted together with the insolation and ambient temperature variations in Figure 19. The results are consistent with the trends observed for the front wall and interior wall surface temperatures. Heat flux is taken as positive into the wall at the front surface and positive out of the wall at the interior surface. The front wall heat flux follows the trend of the insolation very closely, as is evident in day 113. At night the heat flux is outward from the front surface towards the environment and during hours of significant isolation, heat flux is into the wall. The heat flux curve of test unit 1 is somewhat higher than the curve of unit 2 during hours of peak insolation. However, generally speaking,it may be concluded that test units 1 and 2 behave similarly under identical environmental conditions.

The interior wall heat flux curves look very similar to the interior surface temperature curves in Figure 18, in fact, they have the same period and the maxima and minima occur at the same time. This is consistent with the fact that heat flux from the interior surface should be maximum and minimum when the interior surface temperature is maximum and minimum, assuming that the "room" temperature is held constant. The heat flux curves for units 1 and 2 are almost identical - the maximum difference being about 2.9 W/m^2. This difference was due to the calibration of the heat flux sensor and was later corrected for.

5.2 Comparison of a Single Cover Test Unit with a Double Cover Unit

The two Trombe wall test units were tested on days 174 and 175 (June 24 and 25, 1982) starting from 12:00 AM on day 174. Both days

were fairly sunny with some cloud towards midday on day 174. The effects of this cloudiness can be seen in the plot of insolation in figures 20 through 24 where the curve dips at 1400 hours. The peak value of the insolation is 384.8 W/m^2 at 1300 hours on day 174 which is quite a bit lower than the peak value of 555.8 W/m^2 measured during Phase I of the experiment. The reason, of course, is that the zenith angle is smaller in June than in April. In other words, the sun is higher in the sky in June so that the insolation measured in the vertical plane is lower.

Another observation that can be made is that the ambient curve lags the insolation curve by about 3 hours. Rayleigh numbers were in the order of 7×10^4 in the 5.08 cm air gap in the single cover test unit and about 1×10^3 in the 3.81 cm air gap for the double cover unit showing that the flow was well in the laminar region in both units. Some of the data obtained in the test period is plotted in Figures 20 through 24. The actual data is given in Table D.2 in Appendix D.

5.2.1 Cover Temperature Variation

Trombe wall test unit 1 had a single glass cover placed 5.08 cm in front of the masonry wall surface and unit 2 had a double cover (with the glass panes 1.27 cm apart) located 3.81 cm in front of the wall surface. In unit 2 the inner surface temperature of the inner cover was measured and in unit 1 the inner surface temperature of the only cover surface was measured. Figure 20 shows the variation of these temperatures with time. As can be seen from the plot, the cover temperature of unit 2 is consistently higher than that of unit 1 - by about 3 K. This is probably because of two reasons. The air gap temperature in the double cover unit is higher than in the single cover

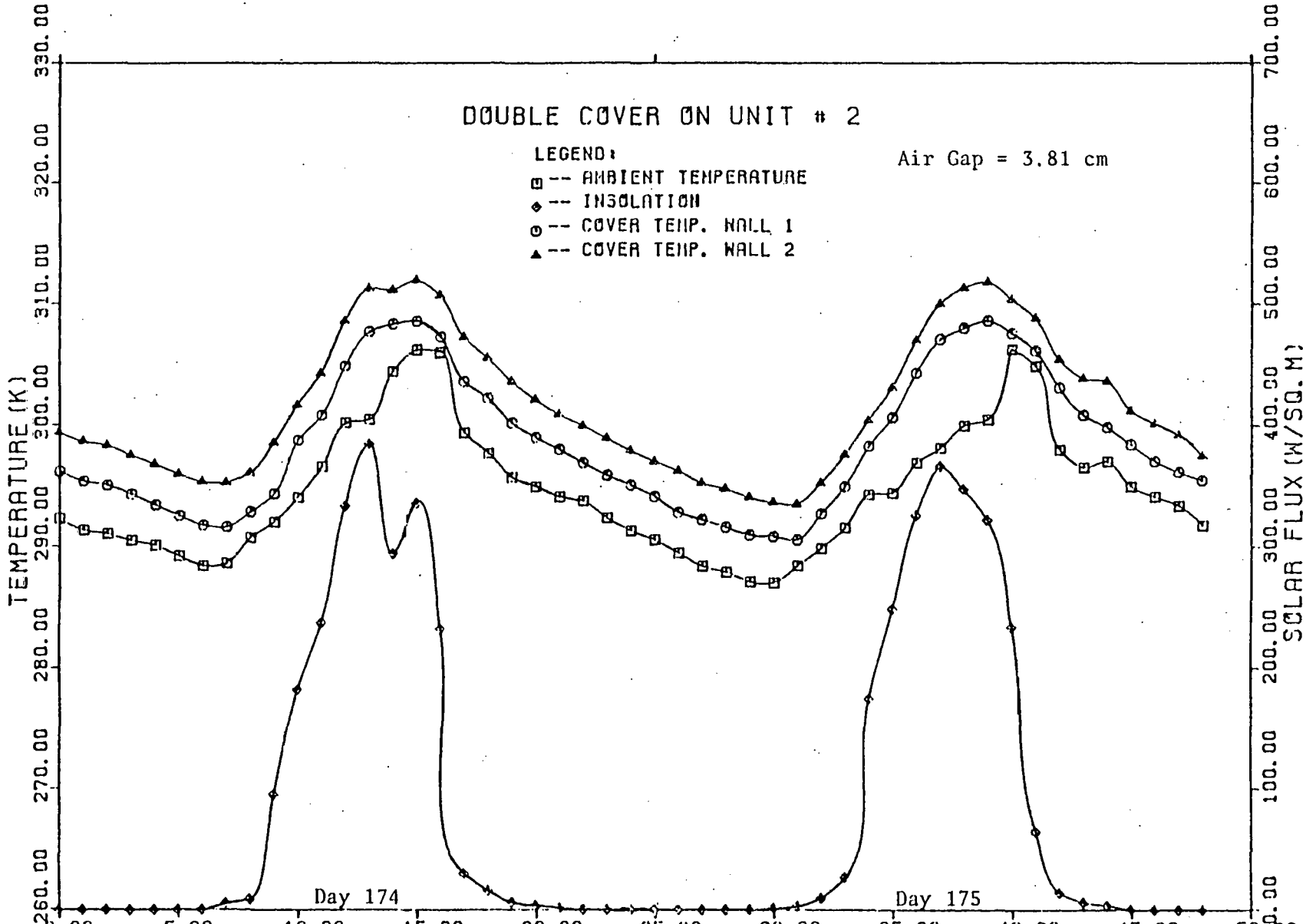

Fig. 20 Phase II Cover Surface Temperatures

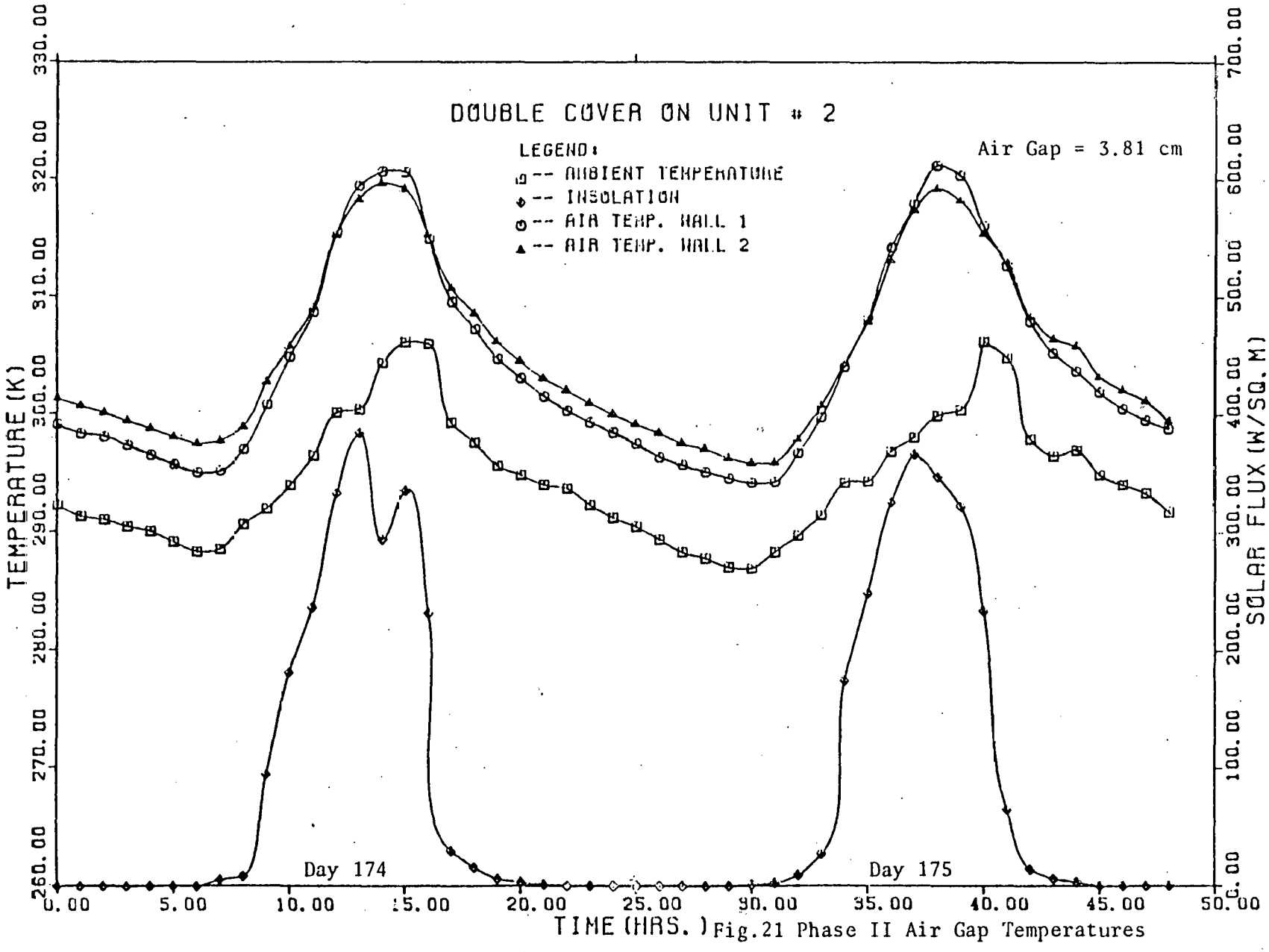

Fig.21 Phase II Air Gap Temperatures

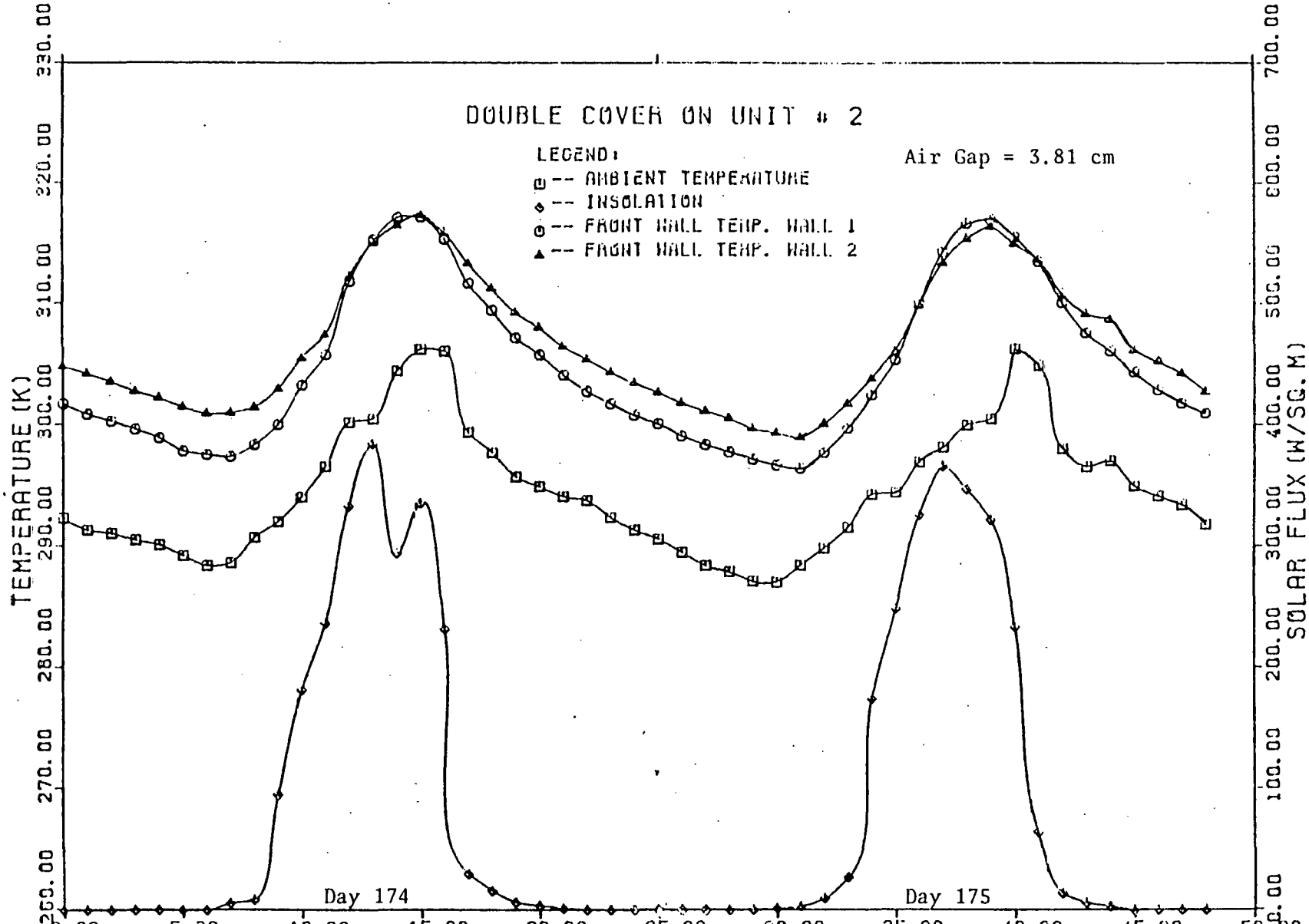

Fig. 22 Phase II Front Wall Temperatures

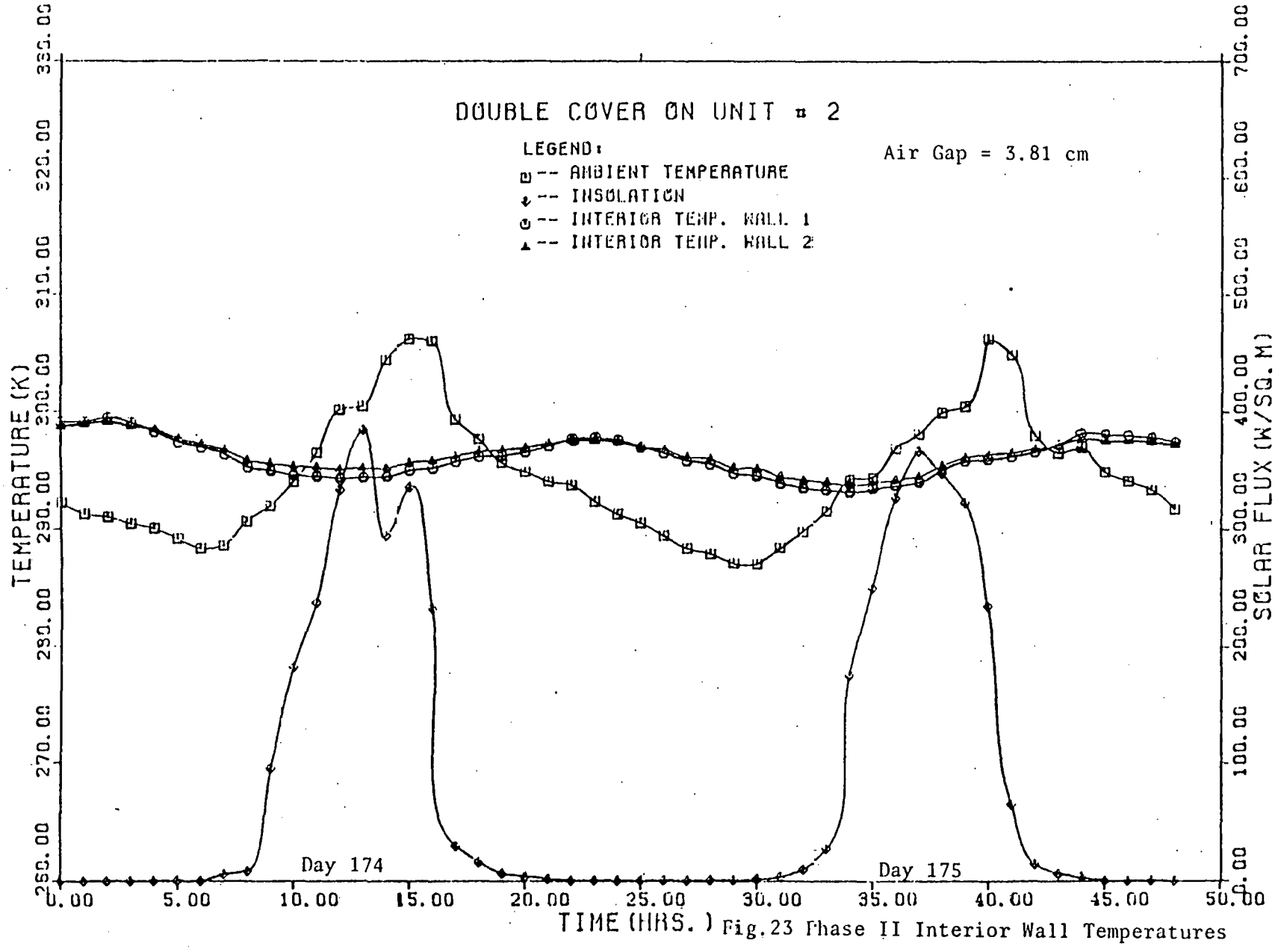

Fig.23 Phase II Interior Wall Temperatures

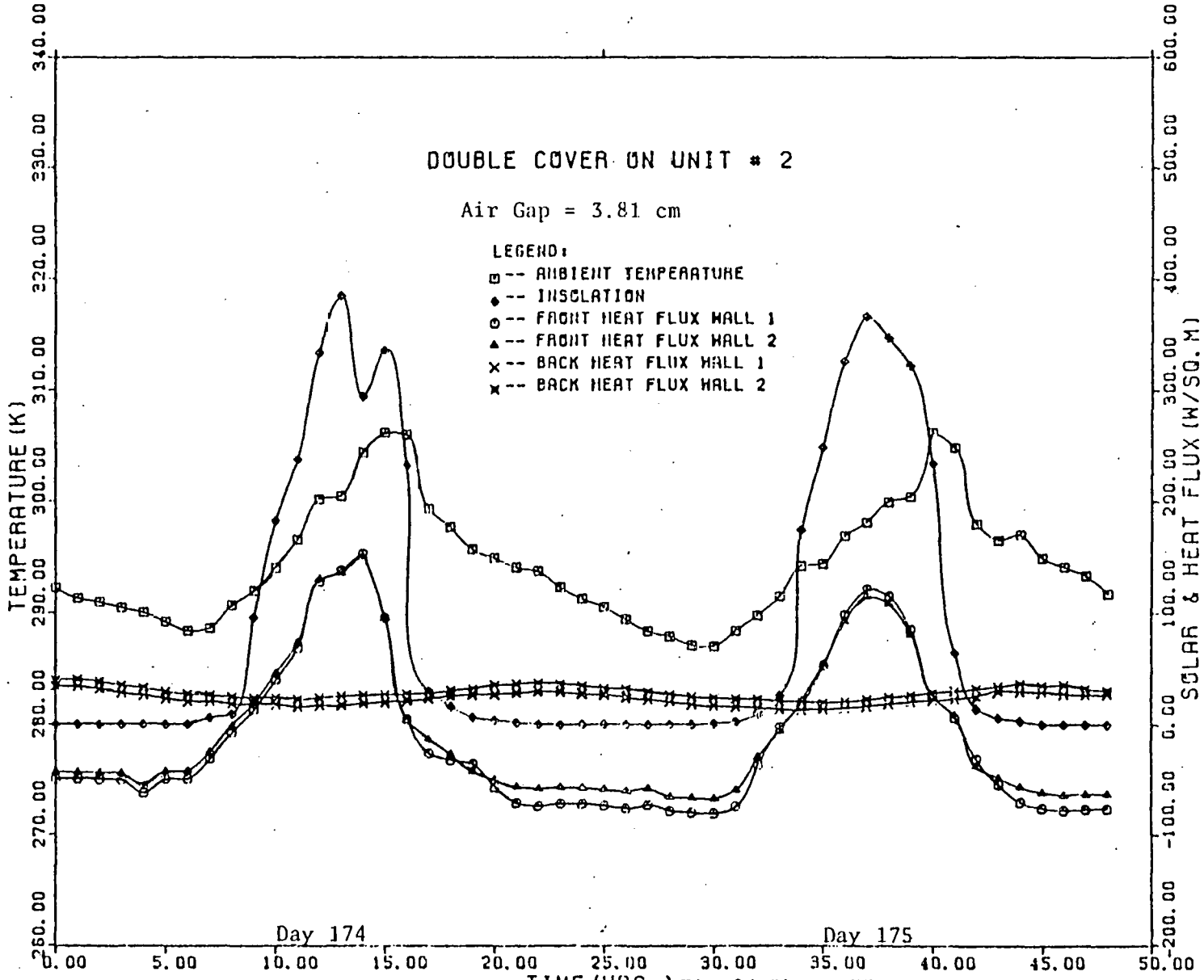

Fig.24 Phase II Masonry Wall Heat Fluxes

unit and also the cover in unit 1 is in direct interaction with the ambient unlike the inner cover in unit 2.

5.2.2 Air Gap Temperature Variation

Some interesting conclusions can be drawn from Figure 21 which shows the variation of the average air gap temperatures in the double cover and single cover units. As expected, over the 48 hour period, the air gap temperatures for the double cover unit are higher by as much as 2.6 K at night than that of the single cover unit. The improvement is more apparent when the temperatures are dropping and at night-time and early morning when the temperatures are low. The double cover unit has a lower top loss coefficient, U_t, compared to the single cover unit, as will be shown later. The single cover unit loses more energy to the environment thus decreasing air gap and wall surface temperatures. This conclusion can also be drawn from the wall heat flux measurements.

During midday, when the isolation is maximum, however, the air gap temperature is higher,by a maximum of 1.5 K, in the single cover unit for about three hours. The explanation for this phenomenon lies in the fact that the transmittance of a double cover decreases more rapidly with increase in the angle of incidence of solar radiation than the transmittance of a single cover. In summer months the angle of incidence of beam radiation on vertical surfaces near solar noon is quite high. Thus, lower transmittance values are to be expected for double covers. In winter, when the angle of incidence of solar radiation is low and ambient temperatures are low, double cover Trombe wall units are expected to have appreciably higher air gap and wall surface temperatures than single cover units.

5.2.3 Masonry Wall Front Surface Temperature Variation

The trend in the variation of the masonry wall absorber surface temperatures is similar to the variation in air gap temperatures, as can be seen in Figure 22. The double cover Trombe wall surface temperature is consistently higher than the single cover Trombe wall surface temperature, except during hours of peak insolation. The difference in surface temperatures becomes more apparent as the ambient temperature decreases to a minimum, proving that the use of a double cover improves thermal performance of a Trombe wall by cutting down on nighttime radiation losses to the environment. The double cover masonry wall surface temperature is higher by as much as 3.6 K compared to the single cover wall temperature when the temperature curves reach a minimum value early in the morning at 7:00 AM. The explanation for higher wall surface temperature during midday for unit 1 (single cover) is the same as that for higher air gap temperature given in section 5.2.2. During winter, the double cover test unit wall surface temperatures should be considerably higher than the temperatures for the single cover unit.

5.2.4 Masonry Wall Interior Surface Temperature Variation

The interior masonry wall surface temperature variations can be seen in Figure 23. The periodic nature of the curves is similar to the interior surface temperature curves obtained in Phase I of the experiment with the maxima occurring at about 11:00 PM and minima occurring at about 12:00 in the afternoon. The phase lag of these curves compared with the front wall surface temperature curves is about 9 to 10 hours. In other words, a temperature "wave" progresses from the front surface of the wall to the rear surface in that time. The

superior performance of the double cover Trombe wall is more apparent in the valleys of the curves where the double cover unit interior surface temperature is appreciably more than that of the single cover unit. When the curves reach a minima, the double cover unit temperature exceeds the single cover unit temperature by about 0.8 K. In keeping with the trend in the front wall temperature, the single cover Trombe wall interior surface temperature is slightly higher than the corresponding double cover quantity near the maxima (by about 0.4 K). The performance of the double cover unit should be quite appreciably better in winter when losses to the environment play an important role in determining the interior wall surface.

5.2.5 Masonry Wall Surface Heat Flux Variation

The results obtained for the masonry wall surface heat flux variations during the test period are consistent with the variations of the surface temperature, as is evident from Figure 24 which shows plots of both the front wall surface and interior surface heat fluxes. At the front surface, heat flux is positive for flow into the surface and at the interior wall surface heat flux is positive out of the surface. The front wall surface heat flux curves are in phase with the insolation curve - the heat flux curves peak when the insolation is maximum. The front wall surface heat fluxes are negative between 6:00 PM and 7:00 AM in the morning showing that during this period the walls lose heat to the environment. Except at midday, the front wall heat flux of Trombe wall test unit 2 (double cover) is greater than the figures for unit 1 (single cover). This is consistent with the higher front wall surface temperatures for unit 2 observed in Figure 22 and shows that the thermal performance of a double cover unit is superior to

that of a single cover unit for most of the day.

The interior wall surface heat flux curve, like the interior wall surface temperature, lags the insolation curve by about 10-12 hours. A phase lag of 10-12 hours is desirable because heating requirements for buildings are maximum during night and early morning and one would want to obtain maximum interior wall surface temperature and heat flux during this time. The interior wall heat flux for unit 2 is consistently higher than that of unit 1, by about 10 W/m^2, showing that a double cover Trombe wall unit has a more desirable thermal performance compared to a single cover unit.

5.3 Comparison of a Fiber Batt Absorber Test Unit with a Double Cover Unit

The last part of the experiment was performed during days 196 and 197 (July 15 and 16, 1982) with a double cover on test unit 2 and a single cover with a 3.81 cm thick fiber bed absorber attached to the masonry wall surface in unit 1. Day 196 had intermittent cloud cover towards midday leading to oscillations in the insolation curve observed in Figures 25 through 29. There were very few clouds in day 197 but some haziness existed in the atmosphere. After collecting 48 hours of data the fiber batt absorber surface was painted with glarefree black paint, as mentioned before, and the experiment was run over a 24 hour period. However, the Trombe wall unit with a black fiber absorber did not compare as favorably with the double cover unit as the unit with the clear fiber material. This is probably because painting the fiber batt black decreases the transmittance in the visible range.

During the test period the maximum value of insolation obtained was 411.9 W/m^2 at 1:00 PM on day 196. Ambient temperatures were quite

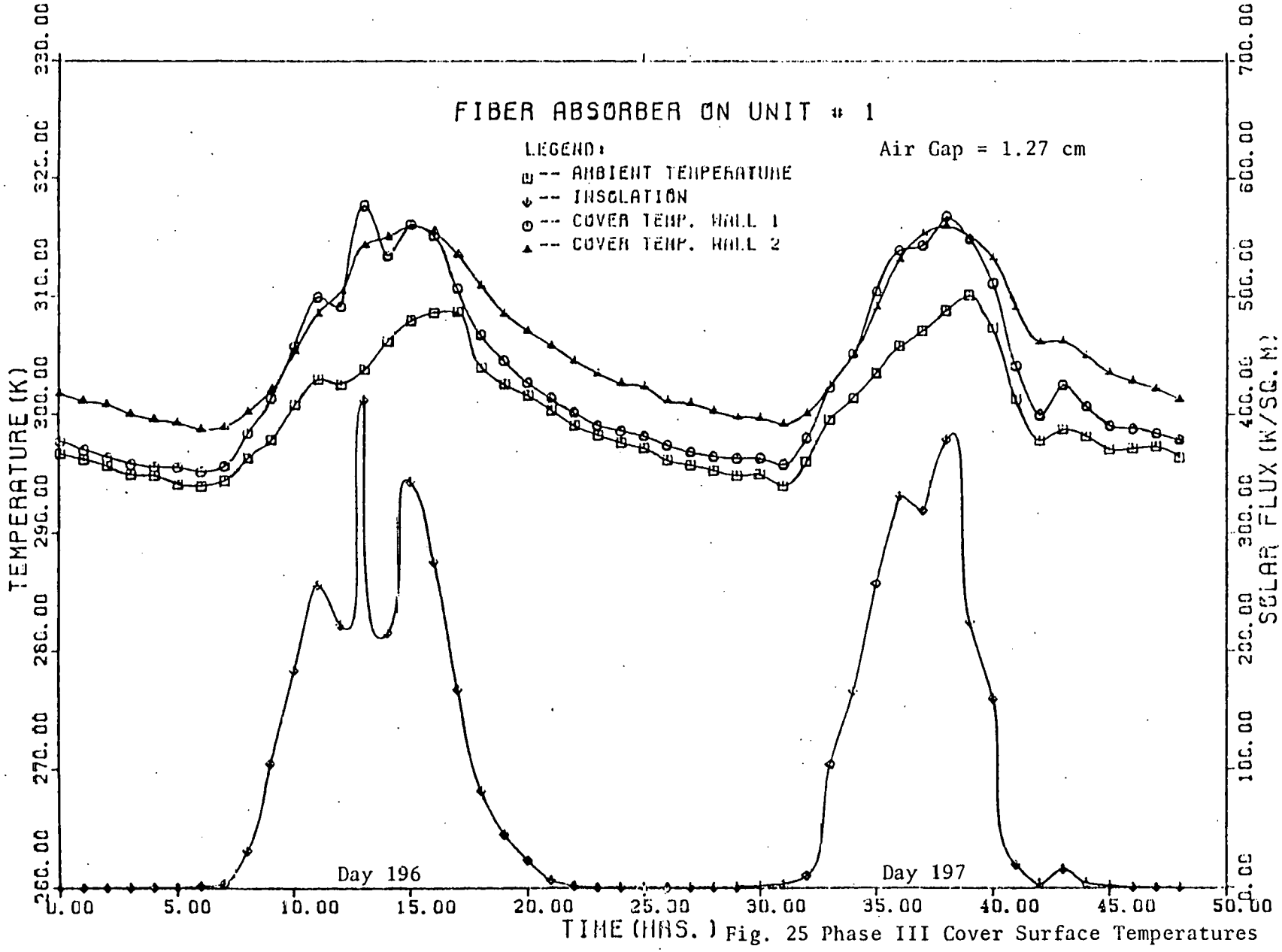

Fig. 25 Phase III Cover Surface Temperatures

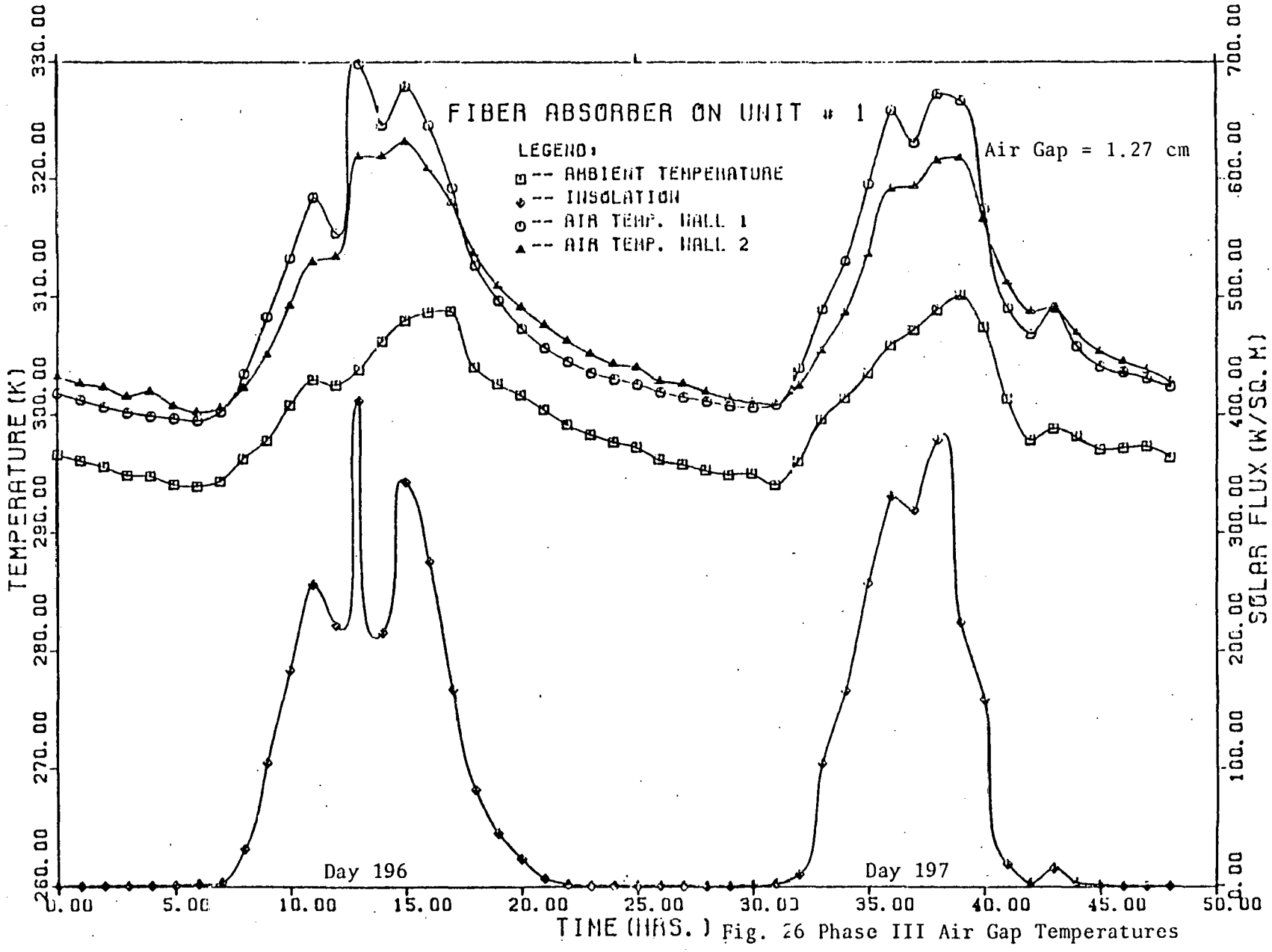

Fig. 26 Phase III Air Gap Temperatures

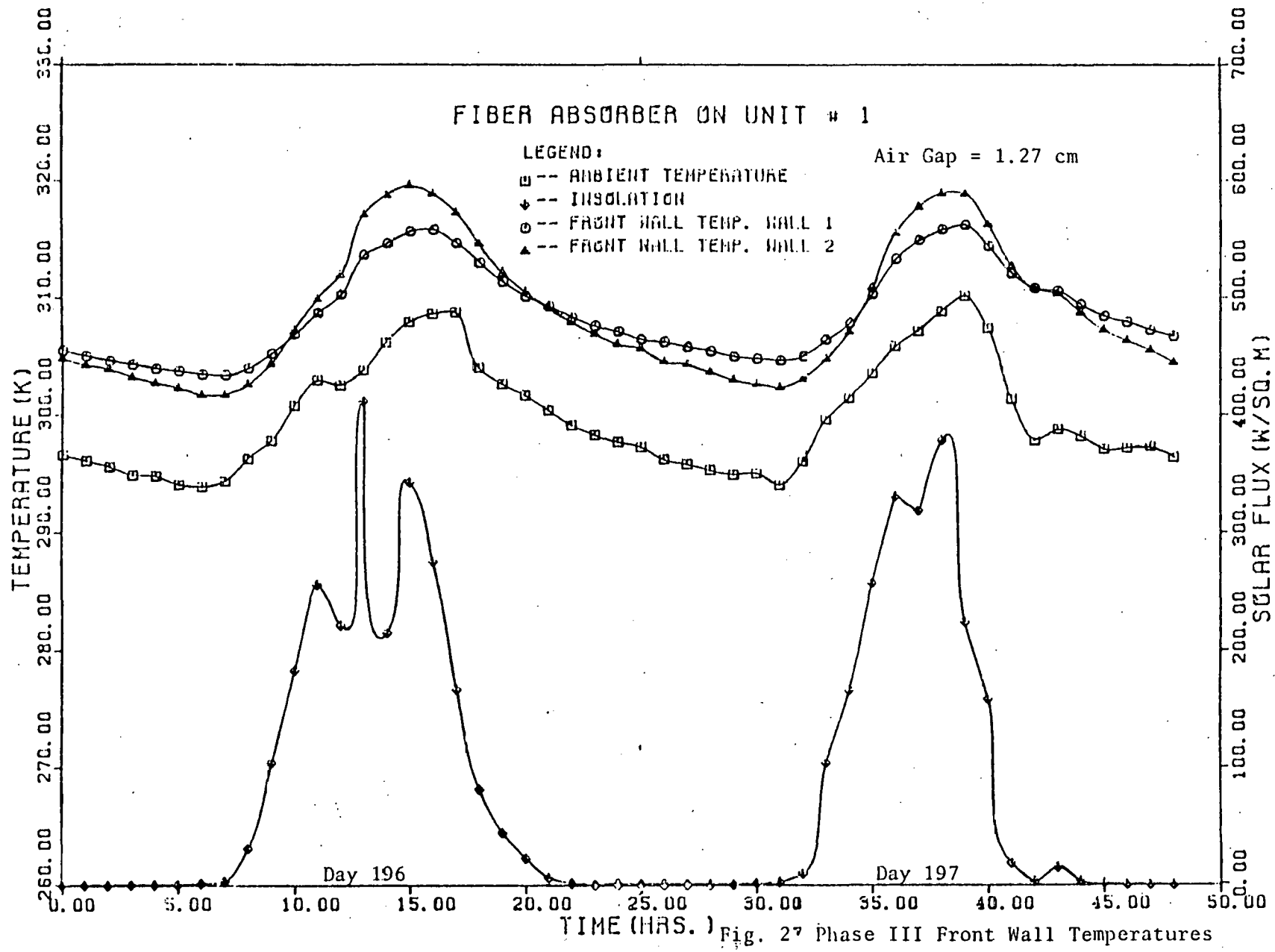

Fig. 27 Phase III Front Wall Temperatures

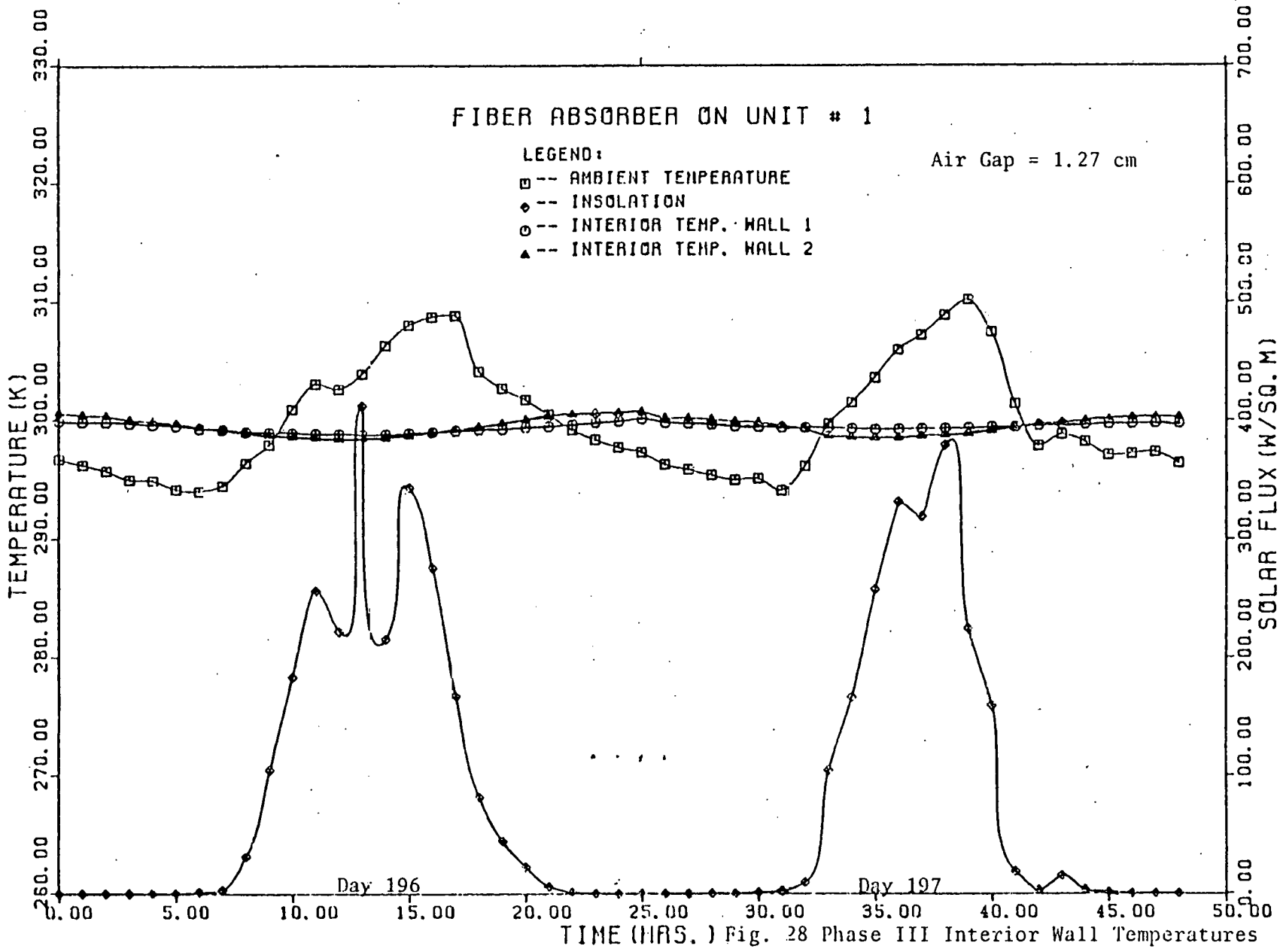

Fig. 28 Phase III Interior Wall Temperatures

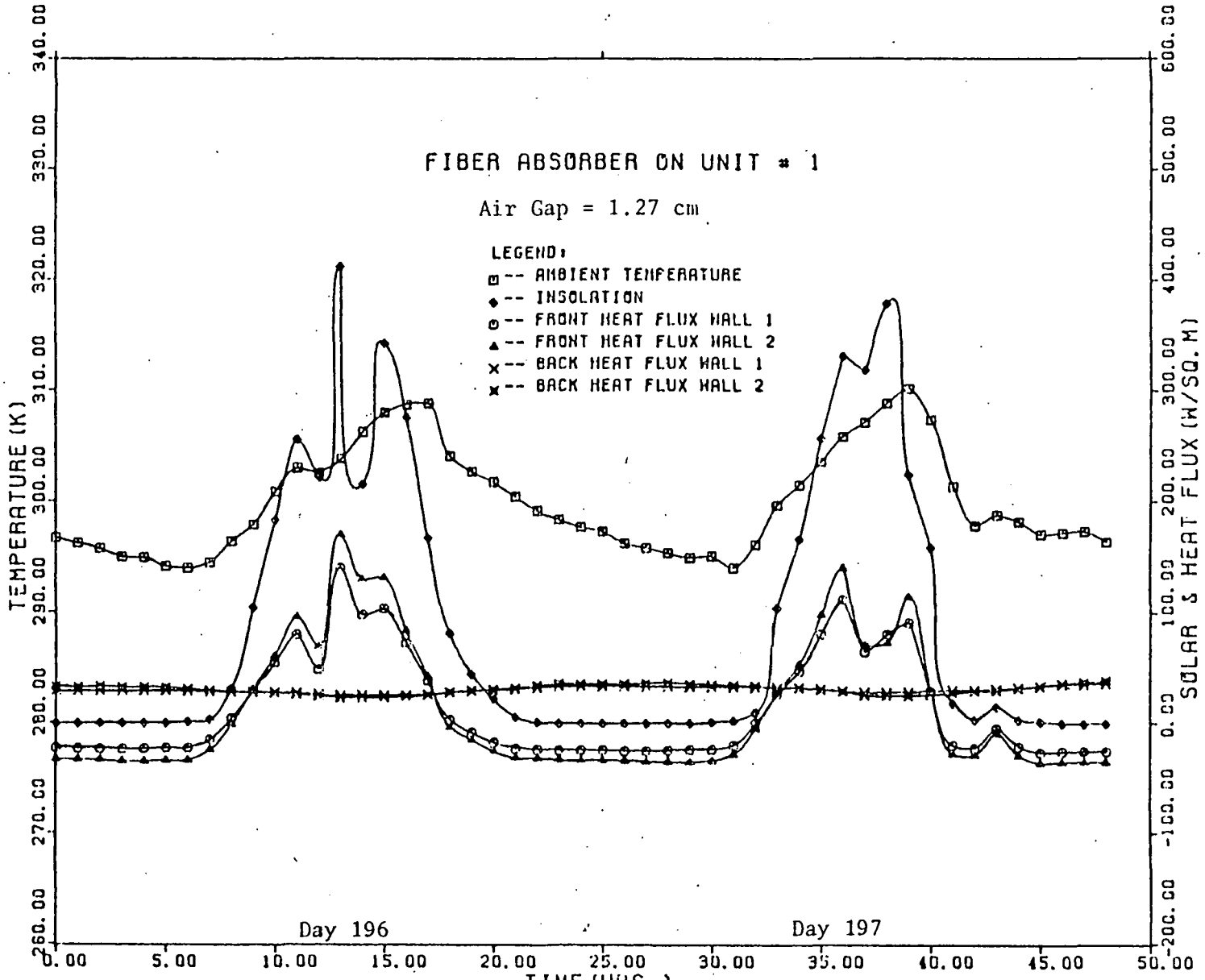

Fig. 29 Phase III Masonry Wall Heat Fluxes

high - the maximum being 310.2 K at 5:00 PM on day 197 and the minimum was 294 K at 6:00 AM on day 196. Rayleigh numbers obtained in the air gap of 1.27 cm were typically in the order of 9.5×10^2, which implies that the flow was laminar in the air gap. All the data used in obtaining plots 25 through 29 have been tabulated in Table D.3 in Appendix D.

5.3.1 Cover Temperature Variation

Figure 25 presents the cover temperatures of unit 1 and 2 as a function of time during the test period. As in Phase II of the experiment, in unit 1 the inner cover surface temperature was measured for the only cover and in unit 2 inner surface temperature of the inner cover was measured. It can be observed from the plot that the double surface temperature is higher than the single cover temperature for most of the test period except at midday when the solar insolation is maximum. At this time the single cover temperature exceeds the double cover temperature by as much as 3.3 K. This result is quite different from the one observed when an ordinary single cover unit was compared with a double cover unit where the cover temperature of the single cover unit was always less than that of the double cover Trombe wall. At night the temperature of the single cover is as much as 4 K less than the double cover temperature because the single cover is in direct interaction with the environment. During midday, the air gap temperature of the fiber batt absorber unit is briefly quite appreciably higher than the air gap temperature of the double cover unit. Since the cover is in direct contact with the air in the air gap, at midday the single cover has a higher temperature than the double cover. It is interesting to observe how the oscillations in the insolation curve in

day 196 affect the single cover surface temperature whereas the double cover surface seems to be affected not at all. This is because the air gap temperature in the fiber batt absorber Trombe wall unit is very sensitive to fluctuations in the insolation - as will be observed in the following section.

5.3.2 Air Gap Temperature Variation

As mentioned earlier the air gap temperature in unit 1 (the fiber batt absorber Trombe wall unit) is not really the air gap temperature but is the temperature 1.27 cm deep in the fiber bed. During hours of appreciable insolation values we observe that this fiber batt temperature is considerably higher than the air gap temperature in unit 2, probably because of convection suppression within the bed. The incident solar radiation heats the fiber batt and since the batt serves as a convection and radiation suppressor (and since it's thermal conductivity is low) most of the thermal energy is used in heating the fiber batt locally. Thus, local batt temperatures rise considerably. This local temperature rise is understandably quite sensitive to variations in the insolation curve as can be seen towards midday on day 196 in Figure 26. During nighttime the fiber batt acts as an infra-red radiation reflector and the batt temperature is lower compared to the air gap temperature in unit 2. It is expected that during sunshine hours in winter, when the insolation will attain higher values, the fiber batt interior will attain even higher temperatures. It may be possible to augment thermal energy delivery from the Trombe wall by filling the air gap with the fibrous material and arranging forced convection through the vents to take advantage of the high temperatures in the batt.

5.3.3 Masonry Wall Front Surface Temperature Variation

The front wall temperatures for units 1 and 2 are plotted in Figure 27. It is seen that the double cover unit performs better than the fiber batt absorber unit during daytime hours whereas at night the performance of the fiber batt absorber unit is superior in terms of higher wall surface temperatures. For example, at 2:00 PM on day 197, the front wall temperature for the double cover unit is 319 K whereas for the fiber batt absorber unit the corresponding temperature is 316 K. However, at 6:00 AM on day 197, the double cover unit front wall temperature is 302.7 K whereas the fiber bed absorber Trombe wall front wall temperature is 304.8 K. This result is, of course, quite reasonable since during the day solar radiation is incident directly onto the masonry wall surface in the double cover unit whereas in the single cover unit the radiation has to pass through the fiber batt. Even though the fiber batt functions almost like a glass cover in being more transparent in the visible range than in the infrared, less radiation penetrates through to the masonry wall surface. Some of the radiation is absorbed, emitted and scattered within the fiber batt. However, at night, the fiber batt suppresses infra-red radiation emission from the masonry wall surface to the ambient. Heat loss from the Trombe wall front surface to the ambient is reduced considerably - this conclusion will also be drawn in the discussion on the heat flux plots in section 5.3.5.

The introduction of the fiber batt has the effect of increasing the thermal resistance for energy loss to the ambient. This is confirmed by the fact that the top loss coefficient, U_t, evaluated later in section 5.4 is lower for the fiber batt absorber Trombe wall test

unit than for the double cover unit under identical environmental conditions. During winter months, when ambient temperatures are much lower, a fiber batt absorber Trombe wall unit should be clearly superior to a double glass cover Trombe wall unit in terms of reduced energy losses.

5.3.4 Masonry Wall Interior Surface Temperature Variation

Figure 28 shows plots of the masonry wall interior surface temperature as a function of time. As observed in the comparison of single and double cover walls, the interior surface temperature for both the double cover wall and the single cover fiber-batt absorber wall lags the front surface temperature by about 9 to 10 hours. The interior wall surface temperature for unit 1 (the fiber-batt absorber unit) is flatter than the corresponding curve for unit 2 leading to the conclusion that the addition of a fiber batt reduces the amplitude of the oscillation in the temperature due to an added thermal resistance. The interior wall surface temperature curves for unit 1 and unit 2 exhibit a similar behavior as the front wall surface temperature curves, except about 10 hours later. In other words, at noon, when the interior wall surface temperature curves are at a minimum, the unit 1 temperature curve exceeds the unit 2 curve by about 0.6 K. Near 11:00 PM, when the curves are at their maxima, the unit 2 (double cover unit) inner wall surface temperature curve is about 0.6 K higher than the unit 1 curve. In winter the improved energy loss characteristics of the fiber-batt absorber Trombe wall should have a more pronounced effect on the interior wall surface temperature.

5.3.5 Masonry Wall Surface Heat Flux Variation

The front wall surface and interior wall surface heat fluxes for

both the conventional double cover Trombe wall and the fiber-batt absorber single cover Trombe wall are plotted in Figure 29 together with the ambient temperature and the insolation. Both the double cover and the fiber-batt absorber Trombe wall front surface heat fluxes reach a maximum energy loss of -36.5 and -27.1 W/m^2 at 10:00 PM on day 197. The maximum energy gain for the front wall surface is 140.1 W/m^2 for the fiber-absorber unit and 169.9 W/m^2 for the double cover unit at 1:00 PM on day 196. The results show that the front wall heat flux of the double cover Trombe wall is larger than that of the fiber absorber unit between 9:00 AM and 4:00 PM in the daytime. This is consistent with the higher front wall surface temperatures attained by the double cover Trombe wall test unit in this time period. In the hours when significant solar radiation is incident on the Trombe walls, the added thermal resistance introduced by the fiber-batt layer lowers the heat flux into the wall compared with the double cover unit.

An opposite effect is noticed between 5:00 PM and 8:00 AM when both walls are losing energy to the environment. During this period the fiber-batt absorber Trombe wall loses less thermal energy with the maximum difference in loss rates being about 10 W/m^2 less than the double cover Trombe wall. The interior wall surface heat flux plots lead to the same conclusion but the difference in the magnitude of the heat fluxes is not so dramatic as in the front wall heat fluxes. The interior wall surface heat flux curves lag the front wall heat flux curves by about 11 hours. The maximum heat flux from the rear surface of the walls are 39.8 W/m^2 and 36.9 W/m^2 at 12:00 PM on day 197 for the double cover and fiber absorber Trombe wall units respectively. The minimum heat fluxes of 25.3 W/m^2 and 22.7 W/m^2 for the fiber-absorber

and double cover Trombe wall unit interior wall surfaces are attained at 1:00 PM on day 196. The energy yield rate from the double cover Trombe wall unit walls surface interior is greater between 7:00 PM and 8:00 AM whereas the energy yield rate for the fiber absorber Trombe wall is greater between 9:00 AM and 6:00 PM.

5.3.6 Comparison of Energy Gain for the Test Units

One method to compare the performance of the fiber-batt absorber and double cover Trombe wall units is to compute the energy gains for the two walls over a period of time by integrating the front wall heat flux values plotted in Figure 29, as follows:

$$Q = \int_{o}^{\bar{t}} q dt \qquad (15)$$

where Q is the net energy gain over the time period $\bar{t}$ in J/m^2; q is the hourly average front wall surface heat flux W/m^2 and $\bar{t}$ is taken as 48 hours. A Simpson quadrature rule was used to numerically integrate the heat flux values at hourly intervals over a 48 hour period. The results for test units 1 and 2 are plotted in Figure 30 and also tabulated in Table D.4 in Appendix D.

It may be concluded from the plot that at the end of the 48 hour test period the fiber-batt absorber surface Trombe wall has a larger energy gain than the double cover unit (577.2 J/m^2 versus 532.7 J/m^2). It is also clear from Figure 30 that the double cover unit performs better during the time insolation values are near maximum and the fiber-batt unit performs better when the insolation is near zero. On the whole, the fiber-batt unit appears to be more efficient than the double cover unit.

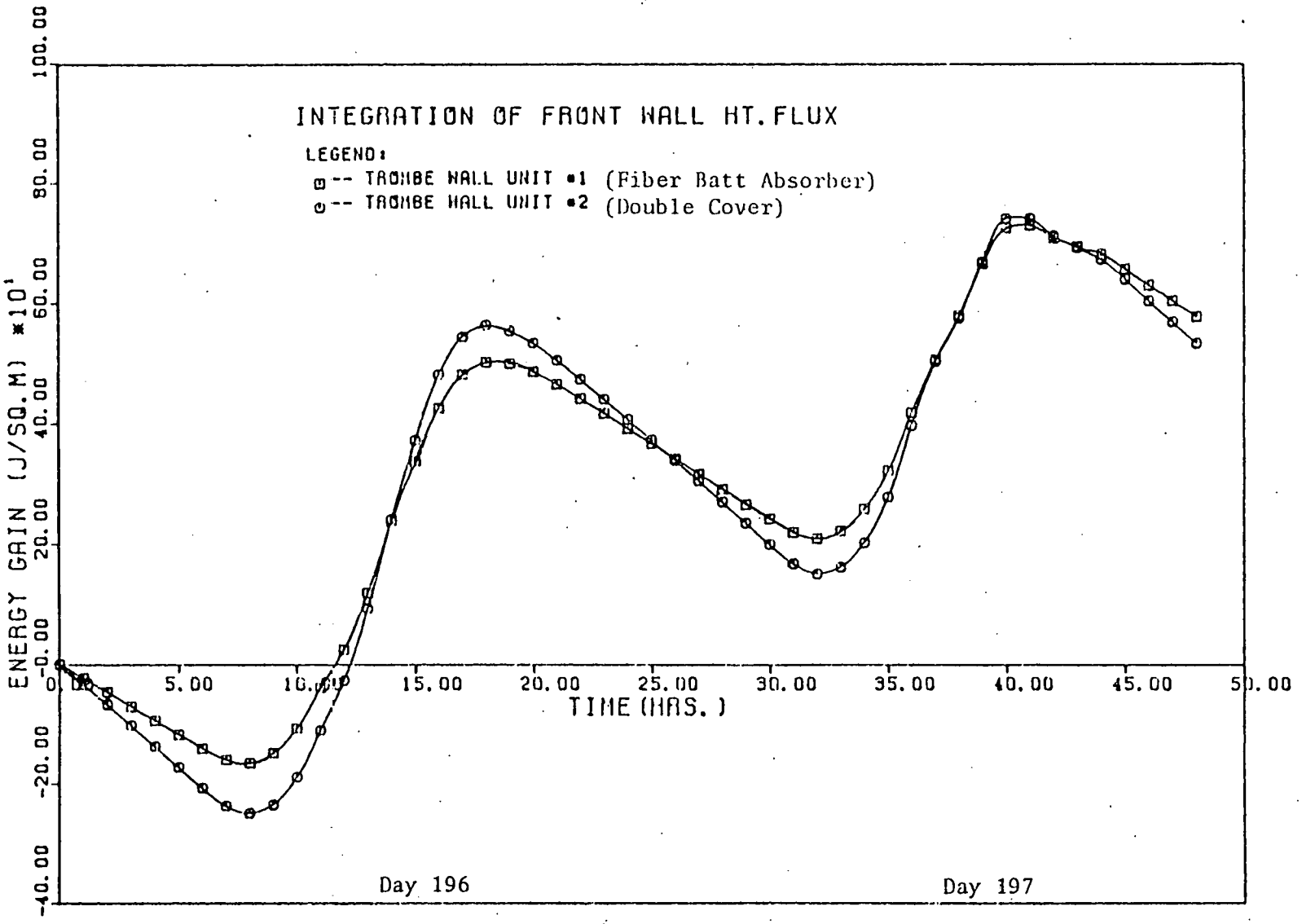

Fig. 30 Energy Gains of Trombe Wall During Phase III of the Experiment

5.4 Comparison of Top Loss Coefficients

The top loss coefficient, U_t in W/m^2, is calculated for the single cover, the double cover and the fiber-batt absorber Trombe wall test units during Phase II and III of the experiment. The procedure followed in making these computations is given in detail in Appendix C. The top-loss coefficient, U_t, is an indication of the energy loss through the front cover of a solar collector. Solar collector design is often an exercise in optimization the objective of which is to minimise U_t without seriously decreasing the transmittance-absorptance of the cover-absorber surface system. The top-loss coefficients obtained from the computations and the corresponding Rayleigh numbers are tabulated in Table 5. The Rayleigh number indicates laminar flow for natural convection in this geometry for $Ra < 10^6$. As can be seen, the flow patterns in the Trombe wall channels were well in the laminar regime.

5.4.1 Comparison of Single Cover Unit with Double Cover Unit

From Table 5 it is clear that the double cover unit top loss coefficient is less than the single cover unit top loss coefficient by almost 40%. We would expect this in the light of the results obtained for the temperature and heat flux variations for Phase II of the experiment discussed in section 5.2. The introduction of a second glass cover cuts down on the longwave radiation losses from the front absorbing surface of the Trombe wall.

5.4.2 Comparison of Single Cover Fiber-Batt Absorber Unit with Double Cover Unit

The values of U_t listed for the fiber-batt absorber Trombe wall unit are about 18% less than the values obtained for the double cover

Table 5. Rayleigh Numbers and Top-Loss Coefficients for Phase II and III of Experiment

	Comparision of Single Coure unit vs. Double Cover				Comparision of Fiber-Batt unit vs. Double Cover unit.			
	Single Cover		Double Cover		Fiber-Batt Absorber		Double Cover	
HOUR	RAYLEIGH	UTOP	RAYLEIGH	UTOP	RAYLEIGH	UTOP	RAYLEIGH	UTOP
1	0.7040E 05	0.4785E 01	0.1074E 04	0.2805E 01	0.8086E 03	0.2351E 01	0.1074E 04	0.2854E 01
2	0.7123E 05	0.4758E 01	0.1138E 04	0.2872E 01	0.8482E 03	0.2343E 01	0.1138E 04	0.2842E 01
3	0.6858E 05	0.4737E 01	0.1134E 04	0.2858E 01	0.8761E 03	0.2335E 01	0.1134E 04	0.2828E 01
4	0.7041E 05	0.4719E 01	0.1095E 04	0.2844E 01	0.8947E 03	0.2328E 01	0.1095E 04	0.2814E 01
5	0.7366E 05	0.4701E 01	0.1031E 04	0.2836E 01	0.8913E 03	0.2323E 01	0.1031E 04	0.2806E 01
6	0.7207E 05	0.4666E 01	0.1061E 04	0.2822E 01	0.8607E 03	0.2321E 01	0.1061E 04	0.2793E 01
7	0.8033E 05	0.4667E 01	0.1119E 04	0.2811E 01	0.8982E 03	0.2317E 01	0.1119E 04	0.2781E 01
8	0.7965E 05	0.4662E 01	0.1048E 04	0.2814E 01	0.9609E 03	0.2324E 01	0.1048E 04	0.2784E 01
9	0.7325E 05	0.4686E 01	0.7406E 03	0.2828E 01	0.9889E 03	0.2359E 01	0.7406E 03	0.2799E 01
10	0.7068E 05	0.4736E 01	0.9665E 03	0.2842E 01	0.1263E 04	0.2407E 01	0.9665E 03	0.2812E 01
11	0.5175E 05	0.4801E 01	0.1136E 04	0.2885E 01	0.1253E 04	0.2464E 01	0.1136E 04	0.2855E 01
12	0.5361E 05	0.4889E 01	0.1092E 04	0.2917E 01	0.1314E 04	0.2523E 01	0.1092E 04	0.2887E 01
13	0.6749E 05	0.5108E 01	0.1150E 04	0.3018E 01	0.1002E 04	0.2505E 01	0.1150E 04	0.2987E 01
14	0.6803E 05	0.5215E 01	0.1537E 04	0.3060E 01	0.1605E 04	0.2651E 01	0.1537E 04	0.3028E 01
15	0.7750E 05	0.5289E 01	0.8120E 03	0.3120E 01	0.1595E 04	0.2602E 01	0.8120E 03	0.3087E 01
16	0.7640E 05	0.5295E 01	0.6300E 03	0.3145E 01	0.1604E 04	0.2641E 01	0.6300E 03	0.3112E 01
17	0.7873E 05	0.5240E 01	0.4511E 03	0.3124E 01	0.1334E 04	0.2615E 01	0.4511E 03	0.3091E 01
18	0.8642E 05	0.5118E 01	0.1081E 04	0.3052E 01	0.1308E 04	0.2556E 01	0.1081E 04	0.3020E 01
19	0.7987E 05	0.5041E 01	0.1100E 04	0.3009E 01	0.9852E 03	0.2487E 01	0.1100E 04	0.2978E 01
20	0.8074E 05	0.4969E 01	0.1151E 04	0.2969E 01	0.8913E 03	0.2452E 01	0.1151E 04	0.2938E 01
21	0.8046E 05	0.4924E 01	0.1041E 04	0.2950E 01	0.8348E 03	0.2424E 01	0.1041E 04	0.2919E 01
22	0.7412E 05	0.4865E 01	0.9836E 03	0.2920E 01	0.7922E 03	0.2404E 01	0.9836E 03	0.2889E 01
23	0.7290E 05	0.4822E 01	0.8688E 03	0.2902E 01	0.8186E 03	0.2388E 01	0.8688E 03	0.2872E 01
24	0.7501E 05	0.4792E 01	0.9616E 03	0.2879E 01	0.8679E 03	0.2375E 01	0.9616E 03	0.2848E 01
25	0.7356E 05	0.4759E 01	0.9888E 03	0.2861E 01	0.8562E 03	0.2367E 01	0.9888E 03	0.2831E 01
26	0.7842E 05	0.4743E 01	0.9781E 03	0.2847E 01	0.8671E 03	0.2360E 01	0.9781E 03	0.2817E 01
27	0.8405E 05	0.4718E 01	0.1057E 04	0.2829E 01	0.9063E 03	0.2352E 01	0.1057E 04	0.2799E 01
28	0.8386E 05	0.4696E 01	0.1097E 04	0.2817E 01	0.9349E 03	0.2345E 01	0.1097E 04	0.2787E 01
29	0.8497E 05	0.4678E 01	0.1107E 04	0.2805E 01	0.9508E 03	0.2340E 01	0.1107E 04	0.2776E 01
30	0.8651E 05	0.4661E 01	0.1139E 04	0.2788E 01	0.9093E 03	0.2335E 01	0.1139E 04	0.2759E 01
31	0.8193E 05	0.4642E 01	0.1071E 04	0.2783E 01	0.8821E 03	0.2333E 01	0.1071E 04	0.2754E 01
32	0.8204E 05	0.4637E 01	0.7048E 03	0.2784E 01	0.1040E 04	0.2332E 01	0.7048E 03	0.2756E 01
33	0.6697E 05	0.4657E 01	0.7590E 03	0.2799E 01	0.1149E 04	0.2363E 01	0.7590E 03	0.2770E 01
34	0.6068E 05	0.4709E 01	0.8689E 03	0.2821E 01	0.1186E 04	0.2419E 01	0.8689E 03	0.2792E 01
35	0.4876E 05	0.4771E 01	0.8453E 03	0.2857E 01	0.1324E 04	0.2464E 01	0.8453E 03	0.2827E 01
36	0.5067E 05	0.4866E 01	0.1324E 04	0.2883E 01	0.1391E 04	0.2539E 01	0.1324E 04	0.2853E 01
37	0.5647E 05	0.5030E 01	0.1509E 04	0.2946E 01	0.1677E 04	0.2608E 01	0.1509E 04	0.2915E 01
38	0.6778E 05	0.5185E 01	0.1778E 04	0.3015E 01	0.1252E 04	0.2597E 01	0.1778E 04	0.2983E 01
39	0.7620E 05	0.5267E 01	0.1634E 04	0.3066E 01	0.1414E 04	0.2640E 01	0.1634E 04	0.3033E 01
40	0.7498E 05	0.5278E 01	0.1622E 04	0.3090E 01	0.1639E 04	0.2631E 01	0.1622E 04	0.3057E 01
41	0.7632E 05	0.5247E 01	0.3566E 03	0.3107E 01	0.9808E 03	0.2543E 01	0.3566E 03	0.3075E 01
42	0.7474E 05	0.5179E 01	0.3484E 03	0.3081E 01	0.8667E 03	0.2447E 01	0.3484E 03	0.3049E 01
43	0.7691E 05	0.5061E 01	0.1016E 04	0.3005E 01	0.1273E 04	0.2411E 01	0.1016E 04	0.2973E 01
44	0.7735E 05	0.4982E 01	0.1027E 04	0.2969E 01	0.1160E 04	0.2435E 01	0.1027E 04	0.2938E 01
45	0.7372E 05	0.4932E 01	0.8830E 03	0.2953E 01	0.9388E 03	0.2402E 01	0.8830E 03	0.2932E 01
46	0.7153E 05	0.4871E 01	0.8556E 03	0.2913E 01	0.9482E 03	0.2380E 01	0.8556E 03	0.2888E 01
47	0.7187E 05	0.4826E 01	0.8256E 03	0.2897E 01	0.9043E 03	0.2374E 01	0.8256E 03	0.2867E 01
48	0.7126E 05	0.4792E 01	0.7954E 03	0.2878E 01	0.9006E 03	0.2367E 01	0.7954E 03	0.2849E 01
49	0.7083E 05	0.4764E 01	0.8056E 03	0.2851E 01	0.8731E 03	0.2358E 01	0.8056E 03	0.2821E 01

RAYLEIGH – RAYLEIGH NUMBER UTOP – TOP LOSS COEFFICIENT (W/M²)

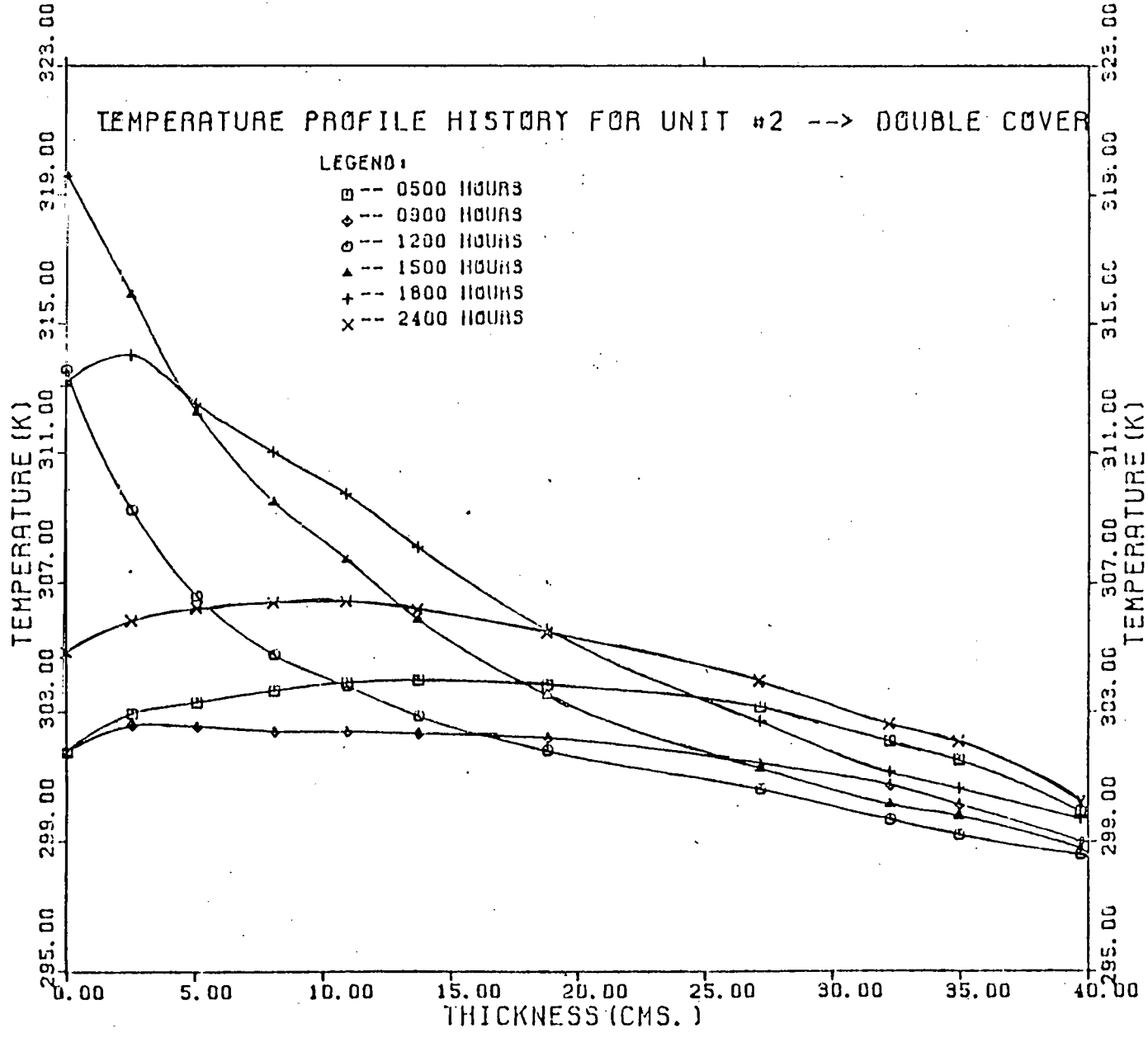

Fig. 31 Temperature Profiles of a Double Cover Trombe Wall at Different Times

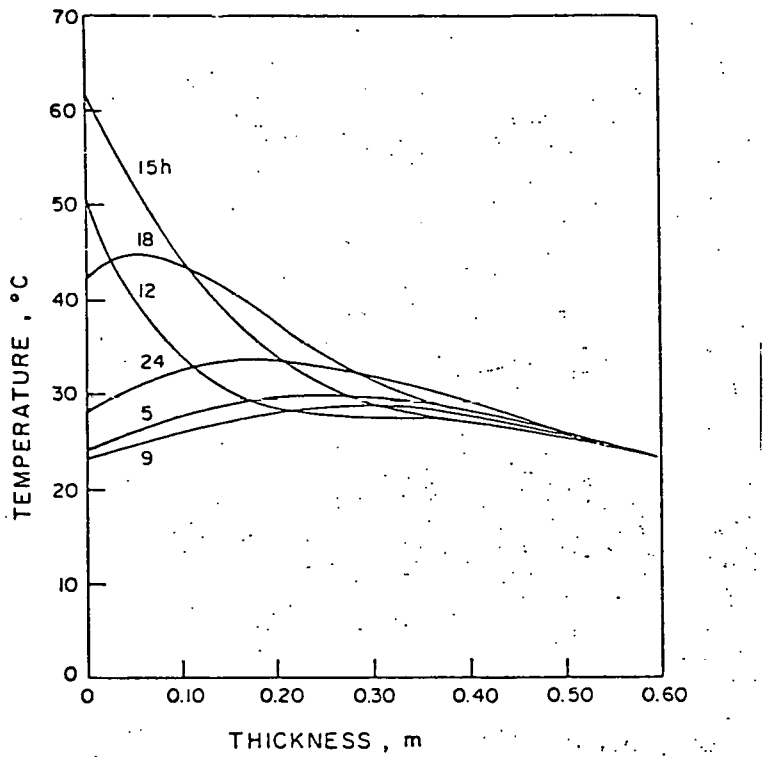

Fig. 32 Temperature Profiles of a Double Cover Trombe Wall at Different Times (Analytical). From Bilgen and Jeldres (1978)

unit during Phase III of the experiment. The conclusion from this result reinforces the statement made earlier in this chapter that the introduction of a layer of fibrous material serves to reduce thermal energy losses to the environment. The energy loss through the front of a Trombe wall is the result of convection and radiation losses to the environment. In winter, when the difference between the absorber surface and ambient temperature (which is the driving potential for energy loss) is large, we would expect the fiber-batt absorber Trombe wall unit to perform considerably better than a conventional double cover unit.

5.5 Temperature Profile Results

In Phase II of the experiment temperature profiles in the heavily instrumented block located in the double cover Trombe wall unit, were measured. The temperature profiles obtained are representative of profiles in the cross-section of the Trombe wall unit. Figure 31 shows the temperature profiles obtained at different times in a 24 hour period. The data points have been tabulated in Table D.5 in Appendix D. A temperature "wave" progresses from the front surface of the wall to the inside surface with time. Figure 32 shows a similar plot obtained in an analytical study by Bilgen and Jeldres (1978). In the case they studied, the wall thickness was 0.6 m as opposed to the 0.4 m thick wall used in this experiment. They also assumed that the inner wall surface could be held constant at one fixed temperature. In practice, of course, this would not be the case. However, qualitatively, it is clear that the general shape of the profiles in Figures 31 and 32 are remarkably similar.

CHAPTER 6

CONCLUSIONS

The most important conclusion drawn from this set of experiments is that a single cover Trombe wall passive solar collector, using a fiber-batt absorber surface is an attractive alternative to a more expensive, conventional double cover Trombe wall system. Data has been collected to compare the two systems over summer months. The results indicate that the fiber-absorber Trombe wall has a top-loss coefficient about 18% less than a conventional double-cover Trombe wall. Consequently, superior front wall surface and interior wall surface temperatures are attained during the night and day times respectively. The total energy gain for the fiber-batt absorber Trombe wall unit has been found to be about 7% more than the double cover unit for a 48 hour heating and cooling cycle. Plots of the front wall heat flux and interior wall surface heat flux show that even though the fiber absorber Trombe wall gains less energy during periods of exposure to solar radiation, it's superior energy loss characteristics at night, compared with that of a double cover Trombe wall, lead to a better performance.

In the first set of experiments the two Trombe wall units had single glass covers installed and their thermal performance has been compared. Their performance has been found to be very similar under the same environmental conditions with all temperatures measured being within 0.6 K and heat fluxes agreeing to within 5% of each other. During the second set of experiments a single cover Trombe wall unit was compared to a double cover unit and their performance has been evaluated. The double cover unit has been found to have a superior performance in terms of higher front wall and interior wall surface

temperatures, air gap temperatures and larger heat fluxes into the front wall surface and out of the rear wall surface. Energy losses to the environment have been found to be lower at night for the double cover unit. Temperature profile data has been obtained at different times of a 24 hour period and the profiles agree well with those obtained by an analytical study by Bilgen and Jeldres (1978).

Though this experiment indicates the effectiveness of using double glass covers and single covers with fiber batt absorbers, it must be recalled that the data has been obtained over spring and summer months. According to theory, a double cover Trombe wall unit should perform even better compared to a single-cover unit during a heating season. Correspondingly, the merits of a single-cover fiber-batt absorber Trombe wall unit compared with a conventional double cover Trombe wall unit should be more apparent in winter. This, however, needs to be verified by obtaining data through winter months.

APPENDIX A

ERROR ANALYSIS OF THE SYSTEM

A.1 Heat Flux Sensors

The heat flux sensors used in this experiment were RDF Corporation micro-foil heat flow sensors as described in Chapter 2. The calibration equation for these sensors is

$$q = k*Z*V \tag{A1}$$

where q is the heat flux measured in W/m^2, k is the sensor multiplication factor ($W/m^2/mV$), Z is the temperature correction factor and V is the millivolt output of the sensor. Equation (A1) can also be written as

$$q = M*V \tag{A2}$$

where the multiplication factor M is obtained by combining k and Z. The temperature compensation factor, Z, is obtained from equation (13) in Chapter 4

$$Z = 1.542994 - 2.524x10^{-3}* T_{HF} + 2.0x10^{-6}* T_{HF}^{2} \tag{A3}$$

where T_{HF} is the mean temperature of the heat flux sensors. Taking the natural log of both sides of the equation (A1)

$$\ln q = \ln k + \ln Z + \ln V \tag{A4}$$

On differentiating Equation (A4) we obtain

$$\frac{dq}{q} = \frac{dV}{V} + \frac{dZ}{Z} \tag{A5}$$

where dq/q is the error percentage of the total heat flux measurement, and the terms dV/V and dZ/Z are the error percentage of the voltage measurement and temperature compensation factor estimation, respectively. As mentioned before, the accuracy of voltage measurement on the HP-2240A MACP is $\pm$ 10 microvolts. However, by using Omega Omni-Amp II

linear amplifiers with a gain of 10, the resolution is improved to $\pm$ 1 microvolt. The term dZ/Z can be calculated from Equation (A3) as follows

$$\ln Z = \ln (1.542994 - 2.524\times10^{-3} * T_{HF} + 2.0\times10^{-6} * T_{HF}^{2}) \qquad (A6)$$

After differentiating, we obtain

$$\frac{dZ}{Z} = (- 2.524\times10^{-3} + 4.0\times10^{-6} * T_{HF})\ dT_{HF}/1.542994$$
$$- 2.524\times10^{-3} * T_{HF} + 2.0\times10^{-6} * T_{HF}^{2}) \qquad (A7)$$

where the accuracy of the temperature measurement, dT_{HF} is $\pm$ 1.0 K. Once the mean temperature is calculated, the error in the heat flux measurement due to temperature can be calculated.

Usually, the error percentage caused by temperature measurement is small, while the error due to voltage measurement is larger. The following three examples show the percentage error of the heat flux measurement caused by each factor.

Ex. 1 T_{HF} = 325.56 K

V = 73.34 μV

% error caused by temperature measurement is 0.131%

% error caused by voltage measurement is 1.364%

Total % error caused in the heat flux measurement is 1.495%

Ex. 2 T_{HF} = 324.1 K

V = 28.6 μV

% error caused by temperature measurement is 0.132%

% error caused by voltage measurement is 3.5%

Total % error in the heat flux measurement is 3.63%

Ex. 3 T_{HF} = 321.104 K

V = 7.73 μV

% error caused by temperature measurement is 0.133%

% error caused by voltage measurement is 12.94%

Total % error in the heat flux measurement is 13.073%

It is clear that the dominant error in the total heat flux measurement is the voltage measurement. When the voltage was greater than 20 microvolts, the percentage error was less than 5%, which is acceptable. Most of the heat flux sensor readings were greater than 20 microvolts.

A.2 Thermocouples

In this experiment all thermocouples were made of copper-constantan wire with limits of error ± 1 K. The calibration equation for copper-constantan thermocouples as written in Chapter 4 (Equation 5) is as follows

$$T = 9.172478*10^{-9} + 2.599973x10^{1}*x - 8.142306x10^{-1}*x^2 + 6.423569x10^{-2}*x^3 - 5.212138x10^{-3}*x^4 + 3.199713x10^{-4}*x^5 - 9.425144x10^{-6}*x^6 + 273 \quad \text{(A8)}$$

where T is the temperature in degrees K and x is the thermocouple voltage in millivolts.

Taking the natural log of both sides,

ln T = ln (right hand side of Eqn. (A8))

differentiating,

$$\frac{dT}{T} = (2.599973*10^{1} - 1.62846x + 1.927*10^{-1}x^2 - 2.0848552*10^{-2}x^3 + 1.28*10^{-3}x^4 - 5.6551*10^{-5}x^5)\, dx/(\text{r.h.s. of (A8)}) \quad \text{(A9)}$$

where dT is the uncertainty in the temperature due to voltage measurement and dx is the error in voltage measurement = $\pm$ 10 microvolts.

The following two examples give an idea of the magnitude of the errors involved:

Ex. 1 x = 2.131mV

T = 325.695 K

% error caused by voltage measurement is 0.071% (0.232 K)

% error caused by thermocouple errors is 0.397% (1 K)

Total error = 0.468% (1.232 K)

Ex. 2 x = 0.7105mV

% error caused by voltage measurement is 0.086% (0.25 K)

% error caused by thermocouple errors is 0.344% (1 K)

Total error = 0.43% (1.25 K)

It is clear that thermocouple errors dominate. For thermopiles, however, the percent error will be lesser because of the fact that the voltage output of thermopiles is higher by a factor equal to the number of thermocouples connected in series.

In the above analysis, it has been assumed that the thermocouple error is less than $\pm$ 1 K. In some temperature measurements larger errors can occur when the thermocouple leads are exposed to large temperature gradients. However, in this experiment, the temperature gradients were not large. In any case, error due to conduction in the thermocouple wire was almost identical in both test units and did not affect the comparison of results between units.

A.3 Pyranometer

As mentioned in Chapter 2 a Precision-Eppley pyranometer was used to measure the incident solar flux (insolation). The calibration error

is given as $\pm$ 0.5% by the manufacturer. The calibration equation of the pyranometer as obtained from Chapter 4 is

$$I_c = M_{py} * C_{py} * x_{py} / G_D \qquad \text{(A10)}$$

where I_c is the solar insolation (W/m^2), M_{py} is the multiplication factor of the instrument, C_{py} is the correction factor, G_D is the data acquisition system gain and x_{py} is the output of the instrument in millivolts.

Taking the natural logarithm of both sides and differentiating, we obtain

$$\frac{dI_c}{I_c} = \frac{dx_{py}}{x_{py}}$$

dI_c is the uncertainty in the solar insolation due to the uncertainty $dx_{py} = \pm$ 10 microvolts, in voltage measurement.

Ex. 1 x_{py} = 5.0 millivolts

I_c = 435.625 W/m^2

% error in the insolation rate due to the uncertainty is 0.2% (0.87 W/m^2)

% error in the insolation rate due to calibration is 0.5% (2.18 W/m^2)

Total % error in the insolation rate 0.7% (3.05 W/m^2)

In other words, when the insolation is high, the calibration error dominates.

Ex. 2 x_{py} = 0.5 mV

I_c = 43.5625 W/m^2

% error in the insolation rate due to dx_{py} = 2% (0.87 W/m^2)

% error in the insolation rate due to calibration = 0.5 % (0.22 W/m^2)

Total error in the insolation rate due = 2.5% (1.09 W/m^2)

Or, at lower insolation rates the error due to uncertainty in the voltage reading dominates.

APPENDIX B

DATA ACQUISITION AND REDUCTION PROGRAM "DATAQ"

```
&DATAQ T=00004 IS ON CR29793 USING 00076 BLKS R=0000

0001   FTN4
0002           PROGRAM DATAQ(3,50)
0003   C
0004   C       THIS PROGRAM PERFORMS THE FOLLOWING TASKS ::
0005   C          (1) COLECTS SOLAR FLUX DATA EVERY 15 SECONDS.
0006   C          (2) AVERAGES THE SOLAR FLUX DATA OVER 15 MINUTES.
0007   C          (3) AFTER AVERAGING THE PYRANOMETER DATA FOR 15 MINUTES
0008   C              CALLS DATA ACQUISITION PROGRAM "TROMB" WHICH TAKES
0009   C              28 CHANNELS OF DATA FROM THE TROMBE WALLS #1 & #2.
0010   C          (4) WHEN "TROMB" TERMINATES "DATAQ" SCHEDULES ITSELF
0011   C              TO RUN AGAIN FOR THE NEXT 15 MINUTES.
0012   C
0013   C          THE SUBROUTINES CALLED BY "DATAQ" ARE::
0014   C              "TROMB": COLLECTS DATA FROM TROMBE WALLS.
0015   C
0016   C          PROGRAM "TROMB" IN TURN CALLS THE FOLLOWING SUBROUTINES:
0017   C          (1) "ERROR": LISTS ERRORS, IF ANY, IN THE DATA ACQUISITION
0018   C              PROCESS.
0019   C          (2) "TEMPT": CONVERTS THERMOCOUPLE MILLIVOLTAGES TO
0020   C              TEMPERATURES.
0021   C          (3) "FILE" : STORES THE DATA TAKEN BY "TROMB" IN A DATA
0022   C               FILE NAMED "DTROM1".
0023   C
0024   C          VARIABLE LIST FOR PROGRAM "DATAQ"::
0025   C          (1) "ITER"-) NUMBER OF TIMES SOLAR DATA IS TO BE COLLECTED
0026   C              (INPUT).
0027   C          (2) "IOFST"-) THE INTERVAL IN SECONDS BETWEEN SUCCESIVE DATA
0028   C              COLLECTION RUNS AND HAS TO BE NEGATIVE (INPUT).
0029   C          (3) "NMAX"-) SAMPLE SIZE FOR DATA COLLECTION (INPUT).
0030   C          (4) "ICOUN"-) LOOP COUNTER.
0031   C          (5) "ITIME"-) ARRAY CONTAINING THE TIME OF DAY.
0032   C          (6) "MACP" -) LOGICAL UNIT NUMBER OF THE MEASUREMENT AND
0033   C              CONTROL PROCESSOR.
0034   C          (7) "GAIN" -) GAIN SETTING ON THE LOW LEVEL ANALOG INPUT
0035   C              BOARD.
0036   C          (8) "SMULT"-) MULTIPLICATION FACTOR FOR PYRANOMETER READING.
0037   C          (9) "VOLT" -) ARRAY USED TO STORE DATA RETURNED FROM THE MACP.
0038   C          (10)"COND" -) CONDITION CODE FOR DATA ACQUISITION PROCESS.
0039   C          (11)"AVG"  -) INSTANTANEOUS VALUE PYRANOMETER MILLIVOLTAGE.
0040   C          (12)"FLUX" -) INSTANTANEOUS VALUE OF SOLAR FLUX (WATTS SQ.M)
0041   C          (13) "F"   -) AVERAGE VALUE OF PYRANOMETER MILLIVOLTAGE.
0042   C          (14) "H"   -) AVERAGE VALUE OF SOLAR FLUX (WATTS/SQ.METER)
0043   C          (15) "R"   -) STANDARD DEVIATION OF SOLAR FLUX READINGS.
0044   C          (16) "ITY" -) VARIABLE INDICATING IF "DATAQ" IS TO BE RUN
0045   C               ONCE (IF ITY# 1) OR IF IT IS TO BE RUN CONTINOUSLY( ITY=1)
0046   C           (17) CRRCT -) CORRECTION FACTOR FOR VERTICAL PYRANOMETER
0047   C                MOUNTING (CRRCT=0.9)
0048           INTEGER JTIME(5),IVOLT(20),COND,KTIME(5)
0049           REAL VOLT(20),A(60),B(60),C(60)
0050   C
0051   C       THE VALUES OF ITER, IOFST, NMAX AND ITY ARE READ IN.
0052   C
0053           WRITE(1,8910)
0054   8910    FORMAT(1X,'  ITER  _')
0055           READ(1,*) ITER
0056           WRITE(1,8911)
0057   8911    FORMAT(1X,'  IOFST _')
0058           READ(1,*) IOFST
0059           WRITE(1,8912)
0060   8912    FORMAT(1X,'  NMAX _')
0061           READ(1,*)'NMAX
0062           WRITE(1,8913)
0063   8913    FORMAT(1X,'  ITY _')
0064           READ(1,*) ITY
0065   C
0066   C        ALL ARRAYS AND CONSTANTS TO BE USED IN THE CALCULATIONS ARE INITIAL
0067   C                                                                    -SED
0068   1000    ICOUN=0
0069   C
0070   C       THE TIME AT WHICH CALCULATION STARTS IS STORED IN ARRAY JTIME.
0071   C
0072           CALL EXEC(11,JTIME)
0073   90      MACP=31
0074           GAIN=500.
0075           SMULT=96.8054211
0076           ICOUN=ICOUN +1
0077           IF(ICOUN.GT.ITER) GO TO 100
0078           DO 5 L=1,NMAX
```

```
0079          IVOLT(L)=0
0080    5     VOLT(L)=0.
0081    C
0082    C     THE PRESENT TIME IS WRITTEN TO THE TERMINAL TO SHOW THAT DATA IS
0083    C     BEING TAKEN.
0084    C
0085          CALL EXEC(11,KTIME)
0086          WRITE(1,10)(KTIME(6-I),I=1,5)
0087    C
0088    C     A COMMAND IS WRITTEN TO THE MACP TO READ SOLAR FLUX DATA NMAX TIMES
0089    C
0090          CALL CLEAR(MACP,1)
0091          WRITE(MACP,15)
0092    15    FORMAT("SN!")
0093          WRITE(MACP,17)
0094    17    FORMAT("AC,1!")
0095          WRITE(MACP,20)NMAX
0096    C
0097    C     THE VALUES ARE READ FROM THE MACP AND THE INSOLATION AND STANDARD
0098    C     DEVIATION ARE CALCULATED.
0099    C
0100          READ(MACP,*) COND,(IVOLT(I),I=1,NMAX)
0101          IF(COND.EQ.0) GO TO 31
0102          WRITE(1,30)
0103          CALL ERROR
0104          STOP 1
0105    31    TOTAL=0.0
0106          SW=0.0
0107          DO 40 J=1,NMAX
0108          VOLT(J)=FLOAT(IVOLT(J))/GAIN
0109    40    TOTAL=TOTAL +VOLT(J)
0110          AVG=TOTAL/(FLOAT(NMAX))
0111          DO 45 J=1,NMAX
0112    45    SW=SW+(VOLT(J) -AVG)**2
0113          SD=SQRT(SW/FLOAT(NMAX-1))
0114          FLUX=AVG*SMULT
0115          A(ICOUN)=AVG
0116          B(ICOUN)=FLUX
0117          C(ICOUN)=SD
0118    10    FORMAT(1X,"DAY:",I3,2X,"HOUR:",I3,2X,"MIN.:",I3,2X,"SEC.:",
0119         &I3,2X,"MILLISEC.:",I3)
0120    20     FORMAT("RP ",I2,";AI,1,16,1;WN,1;NX!")
0121    30    FORMAT(1X,"CONDITION CODE INDICATES ERROR")
0122    C
0123    C     "DATAQ" IS RESCHEDULED TO RUN AGAIN IN 15 SECONDS LATER.
0124    C
0125          CALL EXEC(12,0,2,0,IOFST)
0126          GO TO 90
0127    C
0128    C     AVERAGE VALUES FOR MILLIVOLTAGES, SOLAR FLUX AND STANDARD DEVIATION
0129    C     ARE CALCULATED.
0130    C
0131    100   E=0.0
0132          G=0.0
0133          Q=0.0
0134          DO 60 I=1,ITER
0135          E=E+A(I)
0136          G=G+B(I)
0137    60    Q=Q+C(I)
0138          F=E/FLOAT(ITER)
0139          H=G/FLOAT(ITER)
0140          R=Q/FLOAT(ITER)
0141    C
0142    C
0143    C     SUBROUTINE "TROMB" IS CALLED TO TAKE DATA FROM DEVICES IN TROMBE
0144    C     WALLS.
0145    C
0146          CALL TROMB(F,H,R,JTIME,NMAX)
0147          IF(ITY.EQ.1) GO TO 1000
0148          STOP
0149          END
0150    C
0151          SUBROUTINE TROMB(F,H,R,JTIME,NMAX)
0152    C
0153    C     SUBROUTINE TROMB PERFORMS THE FOLLOWING TASKS WHEN CALLED
0154    C     BY THE MAIN PROGRAM "DATAQ":
0155    C     (1) COLLECTS 28 CHANNELS OF DATA FROM THE MEASUREMENT AND
0156    C         CONTROL PROCESSOR NMAX TIMES AND AVERAGES THEM.
0157    C     (2) REDUCES THE DATA FROM THE RAW FORM TO VARIOUS QUANTITIES
0158    C         LIKE TEMPERATURES, HEAT FLUXES AND SOLAR FLUXES.
```

```
0159  C      (3) STORES THE REDUCED DATA AND THE TIME OF EXECUTION IN A
0160  C          DATA FILE NAMED "DTROM1" BY CALLING SUBROUTINE "FILE".
0161  C
0162  C      VARIABLE LIST FOR SUBROUTINE TROMB::
0163  C          (1)NMAX-) SAMPLE SIZE OF DATA.
0164  C          (2)MACP-) LOGICAL UNIT NUMBER OF MEASUREMENT AND CONTROL
0165  C          PROCESSOR.
0166  C          (3)AVG -) ARRAY CONTAINING THE RAW DATA (MILLIVOLTS) READ
0167  C          FROM THE MACP (AFTER EACH CHANNEL IS AVERAGED).
0168  C          (4)XAVG-) ARRAY CONTAINING THE REDUCED DATA (TEMPERATURES
0169  C          HEAT FLUXES AND SOLAR FLUX).
0170  C          (5)SD  -) ARRAY CONTAINING THE STANDARD DEVIATION CALCULATED
0171  C          DURING THE REPEATED READING OF EACH CHANNEL.
0172  C          (6)VOLT-) TWO DIMENSIONAL ARRAY INTO WHICH THE RAW DATA FROM
0173  C          THE MACP IS READ PRIOR TO DATA REDUCTION.
0174  C          (7)GAIN-) THE GAIN SETTING ON THE LOW LEVEL ANALOG INPUT
0175  C          BOARD.
0176  C          (8)ITIME-) ARRAY IN WHICH THE TIME OF DAY IS STORED.
0177  C          (9)COND -) CONDITION CODE FOR DATA ACQUISITION PROCESS.
0178  C          (10)SMULT-) MULTIPLICATION FACTOR FOR PYRANOMETER READING.
0179  C          (11)MULTF-) ARRAY CONTAINING THE MULTIPLICATION FACTORS
0180  C          USED IN CONVERTING THE THERMOPILE READINGS.
0181  C          (12)HMULT-) ARRAY CONTAINING THE MULTIPLICATION FACTORS
0182  C          USED IN CONVERTING THE HEATFLOW METER READINGS.
0183  C          (13) Z    -) TEMPERATURE CORRECTION FACTOR FOR HEATFLOW
0184  C          METERS.
0185  C
0186  C          IT SHOULD BE NOTED THAT ALTHOUGH 32 CHANNELS ARE READ BY
0187  C          "TROMB" THE READINGS FROM CHANNEL #15,18,19 & 20 ARE
0188  C          IGNORED BECAUSE THESE CHANNELS ARE DEFECTIVE AND NO DEVICES
0189  C          ARE CONNECTED TO THEM.
0190  C
0191  C          CHANNEL LISTING::
0192  C          WALL #1   WALL #2   DEVICE DESCRIPTION
0193  C          -------   -------   ------------------------------------------
0194  C              1         17     INTERIOR GLASS SURFACE THERMOPILE
0195  C              2         21     AIR GAP THERMOPILE
0196  C              3         22     EXTERIOR WALL SURFACE THERMOPILE
0197  C              4         23     INTERIOR WALL SURFACE THERMOPILE
0198  C              5         24     COPPER PLATE SURFACE THERMOPILE
0199  C              6         25     COOLANT FLOW DIFFERENTIAL THERMOPILE
0200  C              7         26     COOLANT INLET TEMPERATURE THERMOCOUPLE
0201  C              8         27     37-PIN CONNECTOR TEMPERATURE THERMOCOUPLE
0202  C              9         -      25-PIN CONNECTOR TEMPERATURE THERMOCOUPLE
0203  C             10         -      13-PIN CONNECTOR TEMPERATURE THERMOCOUPLE
0204  C             11         28     EXTERNAL WALL HEATFLOW METER THERMOCOUPLE
0205  C             12         29     INTERNAL WALL HEATFLOW METER THERMOCOUPLE
0206  C             13         30     EXTERNAL WALL SURFACE HEATFLOW METER
0207  C             14         31     INTERNAL WALL SURFACE HEATFLOW METER
0208  C             16         -      PYRANOMETER
0209  C              -         32     AMBIENT AIR TEMPERATURE THERMOCOUPLE
0210  C          ------------------------------------------------------------
0211  C
0212  C
0213        INTEGER COND,ITIME(5),INAME(3),IVOLT(32,20)
0214        REAL AVG(32),MULTF(12),HMULT(4),XAVG(32),SD(32)
0215        DATA MULTF/6.,9.,9.,9.,6.,4.,6.,9.,9.,9.,6.,4./,HMULT/
0216       &295.57,305.89,307.38,303.534/
0217  C
0218  C     ARRAYS AND CONSTANTS TO BE USED IN THE COMPUTATIONS ARE INITIALISED
0219  C
0220        MACP=31
0221        GAIN=500.
0222        DO 2 I=1,32
0223        AVG(I)=0.0
0224        XAVG(I)=0.0
0225        SD(I)=0.0
0226        DO 1 J=1,NMAX
0227        IVOLT(I,J)=0
0228  1     CONTINUE
0229  2     CONTINUE
0230  C
0231  C     ANALOG INPUT BOARD #1 (CHANNELS 1 THROUGH 16) IS READ NMAX TIMES,
0232  C     THE CONDITION CODE IS EXAMINED AND THE AVERAGE & THE STANDARD
0233  C     DEVIATION OF EACH CHANNEL IS COMPUTED.
0234  C
0235        CALL CLEAR(MACP,1)
0236        WRITE(MACP,15)
0237  15    FORMAT("3N!")
0238  17    FORMAT("AC,1!")
```

```
0239          WRITE(MACP,20) NMAX
0240    20    FORMAT("BK,16;RP,",I2,";AI,1,1,16;WN,1;NX!")
0241          READ(MACP,*) COND
0242          IF(COND.EQ.0) GO TO 21
0243          CALL ERROR
0244          STOP 1
0245    21    DO 23 J=1,NMAX
0246    23    READ(MACP,*)(IVOLT(I,J),I=1,16)
0247          DO 27 I=1,16
0248          TOTAL=0.0
0249          SW1=0.0
0250          DO 29 J=1,NMAX
0251          TOTAL=TOTAL+FLOAT(IVOLT(I,J))/GAIN
0252    29    CONTINUE
0253          AVG(I)=TOTAL/(FLOAT(NMAX))
0254          DO 26 J=1,NMAX
0255    26    SW1=SW1+(FLOAT(IVOLT(I,J))/GAIN-AVG(I))**2
0256          SD(I)=SQRT(SW1/FLOAT(NMAX-1))
0257    27    CONTINUE
0258    C
0259    C     ANALOG INPUT BOARD #2 (CHANNELS 17 THROUGH 32) IS READ AND IF THE
0260    C     CONDITION CODE IS GOOD, THE AVERAGE VALUE & STANDARD DEVIATION
0261    C     OF EACH CHANNEL IS COMPUTED.
0262    C
0263          CALL CLEAR(MACP,1)
0264          WRITE(MACP,15)
0265          WRITE(MACP,1111)
0266    1111    FORMAT("AC,2!")
0267          WRITE(MACP,30) NMAX
0268    30    FORMAT("BK,16;RP,",I2,";AI,2,1,16;WN,1;NX!")
0269          READ(MACP,*)COND
0270          IF(COND.EQ.0) GO TO 31
0271          CALL ERROR
0272          STOP 2
0273    31    DO 33 J=1,NMAX
0274    33    READ(MACP,*)(IVOLT(I,J),I=17,32)
0275          DO 37 I=17,32
0276          TOTAL=0.0
0277          SW1=0.0
0278          DO 39 J=1,NMAX
0279          TOTAL=TOTAL+FLOAT(IVOLT(I,J))/GAIN
0280    39    CONTINUE
0281          AVG(I)=TOTAL/(FLOAT(NMAX))
0282          DO 38 J=1,NMAX
0283    38    SW1=SW1+(FLOAT(IVOLT(1,J))/GAIN-AVG(I))**2
0284          SD(I)=SQRT(SW1/FLOAT(NMAX-1))
0285    37    CONTINUE
0286    C
0287    C     THE NEXT PART OF THE PROGRAM CONVERTS THE THERMOPILE MILLIVOLTS
0288    C     TO THE TRUE MILLIVOLTS BY DIVIDING BY THE MULTIPLICATION FACTORS
0289    C     AND THEN ADDING THE REFERENCE MILLIVOLTS.
0290    C
0291          AVG(1)=AVG(1)/MULTF(1) +AVG(9)
0292          AVG(2)=AVG(2)/MULTF(2) +AVG(8)
0293          AVG(3)=AVG(3)/MULTF(3) +AVG(8)
0294          AVG(4)=AVG(4)/MULTF(4) +AVG(8)
0295          AVG(5)=AVG(5)/MULTF(5) +AVG(10)
0296          AVG(6)=AVG(6)/MULTF(6) +AVG(7)
0297          AVG(17)=AVG(17)/MULTF(7) +AVG(27)
0298          AVG(21)=AVG(21)/MULTF(8) +AVG(27)
0299          AVG(22)=AVG(22)/MULTF(9) +AVG(27)
0300          AVG(23)=AVG(23)/MULTF(10) +AVG(27)
0301          AVG(24)=AVG(24)/MULTF(11) +AVG(27)
0302          AVG(25)=AVG(25)/MULTF(12) +AVG(26)
0303    C
0304    C     NEXT ALL THE THERMOCOUPLE VOLTAGES ARE CONVERTED TO TEMPERATURES
0305    C     (DEGREES KELVIN) BY CALLING THE SUBROUTINE "TEMPT".
0306    C
0307          DO 60 I=1,32
0308          IF(I.EQ.13.OR.I.EQ.14.OR.I.EQ.15.OR.I.EQ.16.OR.I.EQ.18.
0309         &OR.I.EQ.19.OR.I.EQ.20.OR.I.EQ.30.OR.I.EQ.31) GO TO 60
0310          CALL TEMPT(AVG(I),TK,IF)
0311          XAVG(I)=TK
0312    60    CONTINUE
0313    C
0314    C     THE HEATFLOW METER VOLTAGES ARE CONVERTED TO HEAT FLUXES BY
0315    C     MULTIPLYING BY THE MULTIPLICATION FACTORS AND BY THE TEMPERATURE
0316    C     CORRECTION FACTORS. THE SOLAR FLUX (INSOLATION) IS ALSO CALCULATED
0317    C     AFTER CORRECTING FOR VERTICAL PYRANOMETER POSITION.
0318    C
```

```
0319          SMULT=96.8054211
0320          CRRCT=0.9
0321          DO 65 I=13,14
0322          AVG(I)=AVG(I)/10.
0323          Z=1.542994-2.524E-3*AVG(I-2)+2.E-6*AVG(I-2)**2
0324          XAVG(I)=HMULT(I-12)*Z*AVG(I)
0325    65    CONTINUE
0326          XAVG(16)=SMULT*CRRCT*AVG(16)
0327          DO 67 I=30,31
0328          AVG(I)=AVG(I)/10.
0329          Z=1.542994-2.524E-3*AVG(I-2)+2.E-6*AVG(I-2)**2
0330          XAVG(I)=HMULT(I-27)*Z*AVG(I)
0331    67    CONTINUE
0332    C
0333    C     THE TIME AT THE END OF THE CALCULATION RUN IS STORED IN THE
0334    C     ARRAY ITIME.
0335    C
0336          CALL EXEC(11,ITIME)
0337    C
0338    C     THE RAW AND REDUCED DATA IS STORED IN A DATA FILE NAMED "DTROM1"
0339    C     BY CALLING THE SUBROUTINE "FILE".
0340    C
0341          CALL FILE(AVG,XAVG,ITIME,SD,F,H,R,JTIME)
0342          RETURN
0343          END
0344    C
0345    C
0346          SUBROUTINE ERROR
0347    C
0348    C     THIS SUBROUTINE LISTS THE TYPE OF ERROR ENCOUNTERED WHILE
0349    C     READING DATA FROM THE MACP IF IT IS CALLED BY THE MAIN PROGRAMS.
0350    C
0351          WRITE(31,57)
0352    57    FORMAT("$T2")
0353          READ(31,*)E1,E2,E3,E4
0354          IF(E2.EQ.1) GO TO 58
0355          IF(E2.EQ.2) GO TO 59
0356          IF(E2.EQ.3) GO TO 60
0357          IF(E2.EQ.4) GO TO 61
0358          IF(E2.EQ.5) GO TO 62
0359          IF (E2.EQ.6) GO TO 63
0360          IF(E2.EQ.7) GO TO 64
0361          IF(E2.EQ.8) GO TO 65
0362          IF(E2.EQ.9) GO TO 66
0363          IF(E2.EQ.10) GO TO 67
0364    58    WRITE(1,70) E3
0365    70    FORMAT("CMD#",I4,3X,"NOT RECOGNISED")
0366          GO TO 80
0367    59    WRITE(1,71)E4,E3
0368    71    FORMAT("PARAMETER",1X,I4,"IN CMD #",I4," INVALID")
0369          GO TO 80
0370    60    WRITE(1,72)E3
0371    72    FORMAT("BUFFER OVERFLOW ON CMD #",I4)
0372          GO TO 80
0373    61    WRITE(1,73)E4,E3
0374    73    FORMAT("NO RESPONSE FROM SLOT#",I4," ON CMD #",I4)
0375          GO TO 80
0376    62    WRITE(1,74)E4,E3
0377    74    FORMAT(" READBACK ERROR FROM SLOT #",I4," ON CMD #",I4)
0378          GO TO 80
0379    63    WRITE(1,75)E4,E3
0380    75    FORMAT(" CALIB IN SLOT #",I4,"OUT OF RANGE, CMD #",I4)
0381          GO TO 80
0382    64    WRITE(1,76)E3,E4
0383    76    FORMAT(" CMD #",I4," IO UNCALIBRATED CARD IN SLOT #",I4)
0384          GO TO 80
0385    65    WRITE(1,77)E4
0386    77    FORMAT("NOISY READINGS DURING ANLG CALIB IN SLOT#",I4)
0387          GO TO 80
0388    66    WRITE(1,78)E4,E3
0389    78    FORMAT(" SLOT #",I4," EMPTY OR CMD #",I4," IMPROPER")
0390          GO TO 80
0391    67    WRITE(1,79)E4
0392    79    FORMAT(" SELF TEST ERROR #", E4)
0393    80    CONTINUE
0394          RETURN
0395          END
0396    C
0397          SUBROUTINE TEMPT(X,TK,TF)
0398    C
```

```
0399  C      THIS SUBROUTINE ACCEPTS MILLIVOLTS(X) FROM CU-CN THERMOCOUPLES
0400  C      AND RETURNS TEMPERATURE TK IN DEGREES KELVIN AND TF IN DEGREES
0401  C      FAHRENHEIT.  THE FIT IS GOOD FROM -40 TO 200 DEGREES C. WITH
0402  C      UNCERTAINTY OF LESS THAN 0.01 DEGREES C.THE FIT IS THROUGH A
0403  C      SIXTH DEGREE POLYNOMIAL.
0404  C
0405         TK=9.172478E-3+25.99973*X-0.8142306*X**2+0.06423569*X**3
0406        &-5.212138E-3*X**4 +3.199713E-4*X**5 -9.425144E-6*X**6
0407         TK=TK+273.
0408         TF=(TK-273.)*9/5 +32.
0409         RETURN
0410         END
0411  C
0412         SUBROUTINE FILE(AVG,XAVG,ITIME,SD,F,H,R,JTIME)
0413  C
0414  C      THIS SUBROUTINE STORES THE DATA TAKEN IN THE MAIN PROGRAM
0415  C      IN A DATA FILE NAMED DTROM1.BESIDES THE DATA ITSELF, THE
0416  C      TIME AT WHICH THE MAIN PROGRAM WAS CALLED IS ALSO STORED.
0417  C
0418         INTEGER IBUF(60),NAME(3),IDCB(256),ITIME(5),IBUFF(256)
0419         INTEGER JTIME(5)
0420         REAL AVG(32),XAVG(32),SD(32)
0421         DATA NAME/2HDT,2HRO,2HM1/
0422         CALL OPEN(IDCB,IERR,NAME,2B)
0423  5      CALL READF(IDCB,IERR,IBUFF,256,LEN)
0424         IF(LEN.NE.-1) GO TO 5
0425         IF(IERR.GE.0) GO TO 15
0426         WRITE(1,7) IERR
0427  7      FORMAT(" FMP ERROR ",I3)
0428         STOP 4
0429  15     DO 8 I=1,60
0430  8      IBUF(I)=2H
0431         CALL CODE
0432         WRITE(IBUF,10)
0433  10     FORMAT(1X,115("*"))
0434         CALL WRITF(IDCB,IERR,IBUF,60)
0435         DO 20 I=1,60
0436  20     IBUF(I)=2H
0437         CALL CODE
0438         WRITE(IBUF,25)
0439  25     FORMAT(5X,"WALL#1 & #2 WITH SINGLE COVER.")
0440         CALL WRITF(IDCB,IERR,IBUF,60)
0441         DO 26 I=1,60
0442  26     IBUF(I)=2H
0443         CALL CODE
0444         WRITE(IBUF,27)(JTIME(6-I),I=1,5)
0445  27     FORMAT(5X,"START:::",2X,"DAY:",I3,2X,"HOUR:",I3,2X,"MIN.:",
0446        &I3,2X,"SEC.:",I3,2X,"M.SEC.:",I3)
0447         CALL WRITF(IDCB,IERR,IBUF,60)
0448         DO 30 I=1,60
0449  30     IBUF(I)=2H
0450         CALL CODE
0451         WRITE(IBUF,35)(ITIME(6-I),I=1,5)
0452  35     FORMAT(5X,"FINISH:::",2X,"DAY:",I3,2X,"HOUR:",I3,2X,"MIN.:",
0453        &I3,2X,"SEC.:",I3,2X,"M.SEC.:",I3)
0454         CALL WRITF(IDCB,IERR,IBUF,60)
0455         DO 36 I=1,60
0456  36     IBUF(I)=2H
0457         CALL CODE
0458         WRITE(IBUF,37)F,H,R
0459  37     FORMAT(5X,"SFLUX M.VOLT=",F10.6,2X,"SFLUX=",F10.6,2X,
0460        &"STD.DEV.=",F10.6)
0461         CALL WRITF(IDCB,IERR,IBUF,60)
0462         DO 40 I=1,60
0463  40     IBUF(I)=2H
0464         CALL CODE
0465         WRITE(IBUF,43)
0466  43     FORMAT(3X,"CHANNEL#",3X,"MILLIVOLTS",3X,"QUANTITIES",
0467        &8X,"STD.DEVIATION",3X,"CHANNEL#",5X,"MILLIVOLTS",3X,
0468        &"QUANTITIES",5X,"STD.DEVIATION")
0469         CALL WRITF(IDCB,IERR,IBUF,60)
0470         DO 50 I=1,60
0471  50     IBUF(I)=2H
0472         CALL CODE
0473         WRITE(IBUF,55)
0474  55     FORMAT(3X,"---------",3X,"-----------",3X,"-----------"
0475        &8X,"-------------",3X,"---------",5X,"-----------",3X,"-----------"
0476        &5X,"-------------")
0477         CALL WRITF(IDCB,IERR,IBUF,60)
0478         DO 60 I=1,60
```

```
0479   60     IBUF(I)=2H
0480          DO 65 I=1,16
0481          J=I+16
0482          IF(I.GT.1.AND.I.LT.9) GO TO 90
0483          IF(I.EQ.9.OR.I.EQ.10) GO TO 99
0484          IF(I.GT.10.AND.I.LT.15) GO TO 100
0485          IF(I.EQ.15) GO TO 65
0486          IF(I.EQ.16) GO TO 101
0487          CALL CODE
0488          WRITE(IBUF,62)I,AVG(I),XAVG(I),SD(I),J,AVG(J),XAVG(J),SD(J)
0489   62     FORMAT(1X,I5,8X,3(F10.6,5X),I5,8X,3(F10.6,5X))
0490          CALL WRITF(IDCB,IERR,IBUF,60)
0491          IF(IERR.GE.0) GO TO 65
0492          WRITE(1,75)
0493          GO TO 65
0494   90     K=I+19
0495          CALL CODE
0496          WRITE(IBUF,62)I,AVG(I),XAVG(I),SD(I),K,AVG(K),XAVG(K),SD(K)
0497          CALL WRITF(IDCB,IERR,IBUF,60)
0498          IF(IERR.GE.0) GO TO 65
0499          WRITE(1,75)
0500          GO TO 65
0501   75     FORMAT(1X," FMP ERROR ",I3)
0502   99     L=27
0503          CALL CODE
0504          WRITE(IBUF,62)I,AVG(I),XAVG(I),SD(I),L,AVG(L),XAVG(L),SD(L)
0505          CALL WRITF(IDCB,IERR,IBUF,60)
0506          IF(IERR.GE.0) GO TO 65
0507          WRITE(1,75)
0508          GO TO 65
0509   100    MI=I+17
0510          CALL CODE
0511          WRITE(IBUF,62)I,AVG(I),XAVG(I),SD(I),MI,AVG(MI),XAVG(MI),SD(MI)
0512          CALL WRITF(IDCB,IERR,IBUF,60)
0513          IF(IERR.GE.0) GO TO 65
0514          WRITE(1,75)
0515          GO TO 65
0516   101    N=I+16
0517          CALL CODE
0518          WRITE(IBUF,62)I,AVG(I),XAVG(I),SD(I),N,AVG(N),XAVG(N),SD(N)
0519          CALL WRITF(IDCB,IERR,IBUF,60)
0520          IF(IERR.GE.0) GO TO 65
0521          WRITE(1,75)
0522   65     CONTINUE
0523          CALL CLOSE(IDCB)
0524          RETURN
0525          END
0526          END$
```

APPENDIX C

CALCULATION OF TOP LOSS COEFFICIENTS

A.1 Double Cover Trombe Wall Unit

In the analysis of solar collectors it is useful to develop the concept of an overall loss coefficient U. In computing U we first have to find the top loss coefficient U_t. The magnitude of U_t gives an idea of the energy loss through the top cover (in the case of Trombe walls, the front)of a solar collector.

Figure 33 shows the thermal network used for calculating U_t for a two-cover system. At some typical location on the absorber, where the temperature is T_b, the solar energy absorbed is S. The energy loss through the top is the result of convection and radiation between parallel plates. The energy transfer between the absorber at T_b and the first cover at T_{c1} is

$$q_{loss,top} = (h_{b-c1} + h_{r,b-c1})\ (T_b - T_{c1}) \qquad (C1)$$

where

$$h_{r,b-c_1} = \frac{(T_b + T_{c1})(T_b^2 + T_{c1}^2)}{\frac{1}{\varepsilon_b} + \frac{1}{\varepsilon_c} - 1} \qquad (C2)$$

T_b = temperature of Absorber Surface (K)
T_{c1}= temperature of Cover 1 (K)
ε_b = emissivity of Absorber Surface (taken as 0.95)
ε_c = emissivity of Cover (taken as 0.88)

The convective heat transfer coefficient h_{b-c1} is calculated as follows:

$$h = \frac{Nu \cdot k}{L} \qquad (C3)$$

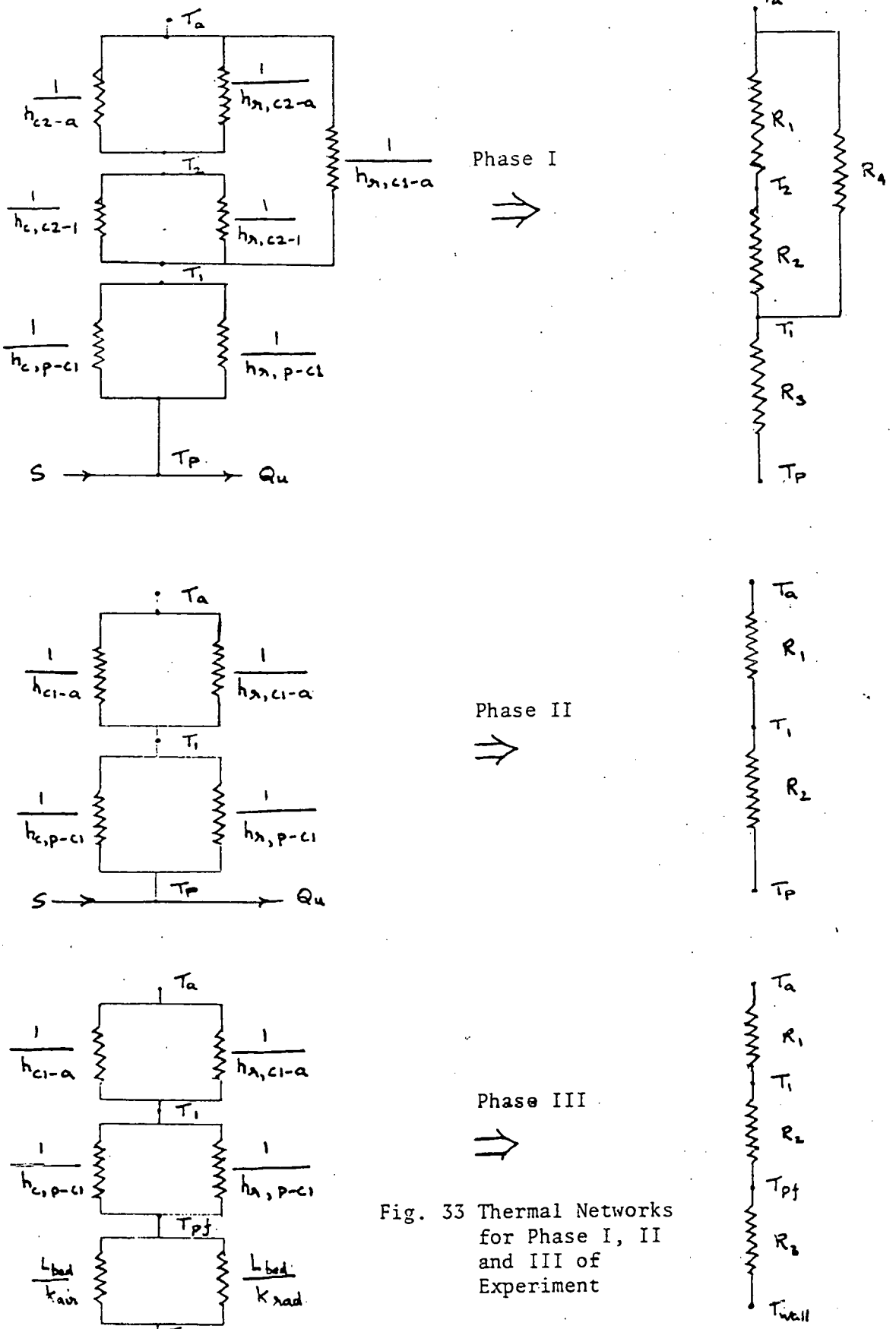

Fig. 33 Thermal Networks for Phase I, II and III of Experiment

$$Nu = 1 + 1.44 \left[1 - \frac{1708}{Ra \cos\beta}\right]^{+} \left(\frac{1 - (\sin 1.8\beta)^{1.6}\ 1708}{Ra \cos\beta}\right) + \left[\left(\frac{Ra \cos\beta}{5830}\right) - 1\right]^{+} \quad (C4)$$

$$Ra = \frac{g\beta' \Delta T L^3}{\nu\alpha} \quad (C5)$$

$$Pr = \nu/\alpha \quad (C6)$$

where

h = heat transfer coefficient (W/m^2K)
L = plate spacing (m)
k = thermal conductivity (W/mK)
g = gravitational constant (9.81 m/s^2)
β' = volumetric coefficient of expansion ($\beta'=1/T$)
ΔT = temperature difference between plates
ν = kinematic viscosity (m^2/s)
α = thermal diffusivity (m^2/s)
Nu = Nusselt number
Ra = Rayleigh number
Pr = Prandtl number
β = tilt angle

Equation (C4) has been obtained by Hollands et al. (1976) for free convection heat transfer between two plates inclined at an angle β between 0 to 75°. The meaning of the + exponent is that only positive values of the terms in the square brackets are to be used (i.e. zero is to be used if the term is negative). Duffie and Beckman (1980) recommend that for vertical surfaces the tilt angle be set to 75°. The predictions for the Nusselt number so obtained will be reasonable or conservative.

The resistance, R_3, can then be expressed as

$$R_3 = \frac{1}{h_{b\text{-}c1} + h_{r,b\text{-}c2}}$$

A similar expression can be written for R_2, the resistance between the cover plates. The absorber surface and the first cover also interact with the surroundings but the interaction of the absorber surface with the surroundings is not significant. The linearized radiative heat transfer coefficient for energy transfer between the ambient and the first cover is given by

$$h_{r,c1-e} = \frac{\varepsilon_{c1}\tau_{c2}\sigma\ (T_{c1} + T_e)(T_e^{\ 2} + T_{c1}^{\ 2})}{1 - \rho_{c1}\,\rho_{c2}} \qquad \text{(C7)}$$

where

ε_{c1} = emissivity of cover 1 (taken as 0.88)
τ_{c2} = transmissivity of cover 2 (taken as 0.04)
σ = Stefan-Boltzmann constant = 5.6997×10^{-8} W/m^{2}K^4
T_{c1} = temperature of cover 1 (K)
T_e = ambient temperature (K)
ρ_{c1} = reflectivity of cover 1 = 0.08 ($\rho = 1-\varepsilon-\tau$)
ρ_{c2} = reflectivity of cover 2 = 0.08

The resistance, R_4, is now

$$R_4 = \frac{1}{h_{r,c1-e}}$$

The thermal resistance to the surroundings R_1 is defined as

$$R_1 = \frac{1}{h_{wind} + h_{r,c2-e}}$$

The heat transfer coefficient due to the wind, h_{wind}, can be calculated as recommended by Duffie and Beckman (1980)

$$h_{wind} = \max\left[5,\ \frac{8.6V^{0.6}}{L^{0.4}}\right] \qquad \text{(C8)}$$

where

V = wind velocity (m/s)

L = cube root of enclosure volume (m)

The radiant heat transfer from top cover to ambient is

$$h_{r,c2-e} = \frac{\varepsilon_{c2}\sigma\,(T_{c2} + T_e)(T_{c2}^2 + T_e^2)}{(T_{cs} - T_e)} \qquad (C9)$$

The net resistance, R_{net}, is then

$$R_{net} = \frac{(R_1 + R_2)R_4}{R_1 + R_2 + R_4} + R_3$$

The top loss coefficient is

$$U_t = \frac{1}{R_{net}} \quad W/m^2 \cdot K \qquad (C10)$$

A.2 Single Cover Trombe Unit

From the thermal network in Figure 33 the net thermal resistance, R_{net}, is computed as

$$R_{net} = R_1 + R_2$$

where

$$R_2 = \frac{1}{h_{b-c} + h_{r,b-c}}$$

$$R_1 = \frac{1}{h_{wind} + h_{r,c-a}}$$

The heat transfer coefficients are calculated as in the preceding section.

$$U_t = \frac{1}{R_{net}}$$

A.3 Single Cover with Fiber Absorber Trombe Unit

The thermal network for the fiber absorber Trombe wall unit is shown in Figure 33. Thermal resistances R_1 and R_2 are calculated as in section A.2 using the fiber absorber surface temperature T_{bf}

instead of T_b. An additional resistance R_3 appears because of the fiber batt.

$$R_3 = \frac{R_r R_{cond}}{R_r + R_{cond}}$$

where R_r = thermal resistance due to radiation interchange.

R_{cond} = thermal resistance due to conduction.

Studies of heat transfer characteristics of fiber batts with one free surface show that gas conduction and radiation interchange are the dominant modes of heat transfer so natural convection effects may be neglected.

The porosity of the fiber batt is very high, in the order 0.98, so solid conduction may be neglected and the thermal conductivity of the fiber batt may be taken as that of air.

$$R_{cond} = \frac{H}{k_a}$$

H = thickness of bed (0.0381 m)

k_a = conductivity of air (W/mK)

In calculating the radiation resistance, R_r, an equation suggested by Davis (1972) is used

$$R_r = \frac{H}{k_r}$$

and

$$k_r = \frac{4\sigma T_m^3}{\overline{\sigma}\ \beta} \qquad \text{(C11)}$$

where

σ = Stefan-Boltzmann constant
T_m = mean bed temperature = $(T_{wall} + T_{bf})/2$
T_{bf} = fiber bed surface temperature (K)

$\bar{\sigma}$ = extinction coefficient = 0.06 m^{-1}
β = scattering parameter = 1.0

The top loss coefficient is

$$U_t = \frac{1}{R_1 + R_2 + R_3}$$

A.4 Computation

The heat transfer coefficients and top loss coefficients are calculated at intervals of 1 hour using a computer program. The results have been presented in Chapter 5, Table 5. Polynomial approximations are used for property values like thermal diffusivity, α, kinematic viscosity, ν, and thermal conductivity of air, k_a.

APPENDIX D

INDIVIDUAL DATA OF EXPERIMENTAL RESULTS

Data Key for Tables D1 through D3

SFLUX	Insolation (solar flux) W/m^2
TAMB	Ambient Temperature (K)
TGLS1	Cover Temperature Test Unit 1 (K)
TGLS2	Cover Temperature Test Unit 2 (K)
TAIR1	Air Gap Temperature Test Unit 1 (K)
TAIR2	Air Gap Temperature Test Unit 2 (K)
TFRON1	Front Wall Surface Temperature Unit 1 (K)
TFRON2	Front Wall Surface Temperature Unit 2 (K)
TINT1	Interior Wall Surface Temperature Unit 1 (K)
TINT2	Interior Wall Surface Temperature Unit 2 (K)
QFRON1	Front Wall Surface Heat Flux, Unit 1 (W/m^2)
QFRON2	Front Wall Surface Heat Flux, Unit 2 (W/m^2)
QBACK1	Interior Wall Surface Heat Flux, Unit 1 (W/m^2)
QBACK2	Interior Wall Surface Heat Flux, Unit 2 (W/m^2)

Data Key for Table D4

I	Hour number
Z1	Integration of Front Wall Heat Flux, Unit 1 (J/m^2)
Z2	Integration of Front Wall Heat Flux, Unit 2 (J/m^2)

Table D.1 Data for Phase I of Experiment

Unit 1 - Single Cover Unit 2 - Single Cover

DATA FOR PHASE I OF EXPERIMENT (COMPARISION OF TWO IDENTICAL TROMBE WALL TEST UNITS WITH SINGLE COVERS
DAY 113 --> RELATIVE HUMIDITY= 62 % AVERAGE WIND SPEED= 1.80 M/S
DAY 114 --> RELATIVE HUMIDITY= 59 % AVERAGE WIND SPEED= 3.08 M/S

TIME	SFLUX	TAMB	TGLS1	TGLS2	TAIR1	TAIR2	TFRON1	TFRON2	TINT1	TINT2	QFRON1	QFRON2	QBACK1	QBACK2
0.0	0.0	281.0	283.8	284.3	287.3	287.8	291.5	291.5	293.4	293.4	-83.6	-83.9	26.8	26.9
1.0	0.0	280.7	283.6	284.0	287.2	287.6	290.8	290.7	293.3	293.3	-83.7	-84.0	26.8	26.9
2.0	0.0	279.9	283.3	283.9	286.7	287.2	290.1	290.2	293.3	293.2	-84.6	-84.5	26.8	26.9
3.0	0.0	279.5	282.4	283.1	285.9	286.4	289.5	289.6	293.1	293.0	-84.6	-84.5	25.5	25.8
4.0	0.0	279.0	282.0	282.5	285.4	285.8	288.9	288.9	292.9	292.8	-83.4	-83.4	24.9	25.2
5.0	0.0	278.7	281.7	282.2	285.1	285.5	288.5	288.5	292.7	292.7	-83.2	-82.7	23.6	23.8
6.0	1.3	278.0	281.2	281.7	284.8	285.1	288.1	288.1	292.4	292.4	-80.3	-80.4	22.0	21.9
7.0	5.0	279.6	281.3	281.7	285.3	285.6	288.3	288.2	292.1	292.1	-63.5	-64.1	20.4	20.6
8.0	78.7	282.9	284.6	285.8	290.5	291.6	290.8	291.4	291.7	291.7	-5.6	-6.0	16.5	16.5
9.0	224.0	285.3	289.5	290.5	298.2	299.0	296.2	297.1	291.6	291.6	95.0	98.1	12.8	13.2
10.0	326.5	286.0	293.1	294.0	304.2	305.3	301.2	302.0	291.6	291.6	154.5	157.2	11.1	10.9
11.0	466.4	288.5	296.5	297.1	311.0	312.2	308.9	309.7	291.4	291.4	161.2	166.6	8.3	9.0
12.0	316.7	286.7	296.5	297.1	308.3	309.5	309.9	310.3	291.4	291.4	93.6	97.1	8.2	8.9
13.0	443.1	292.5	301.2	301.5	319.1	318.7	315.9	315.9	291.4	291.5	243.2	243.6	8.9	9.3
14.0	284.5	289.3	296.8	297.4	307.4	307.4	311.2	311.0	291.4	291.4	-54.5	-53.7	9.6	9.9
15.0	348.1	294.9	299.5	299.2	312.5	312.0	312.3	312.0	292.1	292.2	104.5	100.4	9.5	10.0
16.0	100.4	293.2	294.8	294.8	304.6	304.5	307.3	307.2	292.6	292.7	-23.6	-22.3	11.9	11.8
17.0	17.5	288.0	292.0	292.1	298.6	298.7	303.0	302.6	293.2	293.3	-78.2	-74.9	14.5	14.4
18.0	7.8	287.0	290.7	290.8	296.2	296.2	300.7	300.3	293.6	293.6	-89.2	-86.6	16.6	16.3
19.0	2.8	285.0	289.0	289.1	293.7	293.7	298.3	297.9	294.2	294.2	-99.3	-93.8	19.7	18.9
20.0	1.7	283.5	287.4	287.4	291.8	291.8	296.2	295.8	294.6	294.6	-99.6	-95.1	22.7	21.6
21.0	0.0	282.4	285.9	286.1	290.3	290.3	294.7	294.2	294.8	294.6	-102.3	-97.5	24.3	23.9
22.0	0.0	281.9	285.5	285.3	289.7	289.3	293.4	293.0	295.2	295.0	-93.8	-91.0	25.8	25.0
23.0	0.0	281.4	284.0	284.3	288.5	288.3	292.3	292.0	295.0	294.8	-95.1	-92.9	25.8	25.2
24.0	0.0	279.6	283.6	283.4	287.8	287.3	291.4	290.9	295.3	295.0	-95.0	-92.3	26.2	25.7
25.0	0.0	280.0	282.9	283.0	287.0	286.8	290.8	290.4	294.7	294.5	-94.1	-90.8	26.7	25.6
26.0	0.0	278.3	281.9	282.0	286.3	285.9	289.9	289.6	294.8	294.6	-95.5	-92.9	27.1	26.0
27.0	0.0	277.7	281.4	281.5	285.6	285.3	289.3	288.9	294.6	294.3	-92.3	-89.7	27.1	25.8
28.0	0.0	276.6	280.6	280.5	284.8	284.4	288.4	288.0	294.2	293.9	-93.7	-91.1	26.5	25.3
29.0	0.0	276.5	280.4	280.5	284.5	284.3	288.0	287.7	293.8	293.6	-90.6	-88.4	24.8	24.0
30.0	0.0	275.2	279.5	279.4	283.9	283.2	287.0	286.7	293.5	293.2	-89.6	-85.8	24.0	23.8
31.0	4.3	278.5	280.7	280.6	284.9	284.3	287.2	286.9	293.2	292.9	-72.0	-68.7	23.8	22.5
32.0	61.8	281.8	284.6	284.9	290.4	290.0	290.4	290.0	292.9	292.6	-12.1	-12.1	19.1	17.9
33.0	219.2	284.5	290.1	290.4	298.8	298.3	296.3	295.8	292.6	292.3	96.1	96.0	15.2	14.3
34.0	358.6	285.6	295.1	295.4	306.9	307.2	303.5	303.3	292.4	292.0	177.7	177.5	12.4	11.7
35.0	454.6	287.3	298.6	298.4	314.1	313.8	311.2	310.9	292.1	291.9	221.4	218.7	11.3	10.2
36.0	538.0	288.9	302.4	302.0	319.6	319.3	316.9	316.6	292.1	291.7	245.2	240.4	10.5	9.0
37.0	555.8	291.2	304.7	304.3	322.1	321.8	319.4	319.3	292.1	291.8	240.4	229.6	9.6	8.8
38.0	431.0	293.9	305.2	304.8	321.0	320.6	320.1	319.7	292.5	292.1	174.1	165.8	11.3	9.9
39.0	303.2	295.9	303.1	302.8	316.0	315.6	316.9	316.4	292.9	292.6	85.7	80.1	11.4	10.4
40.0	154.7	295.9	299.5	299.1	309.1	308.8	311.7	311.3	293.6	293.4	-49.7	-44.0	13.7	11.8
41.0	9.1	289.2	295.0	294.8	301.3	300.9	305.7	305.3	294.1	293.9	-94.0	-90.2	17.8	16.0
42.0	5.6	288.7	293.6	293.5	299.1	298.7	303.3	302.9	294.6	294.4	-93.5	-89.2	20.6	19.0
43.0	2.5	288.0	292.1	291.8	296.6	296.2	300.9	300.3	295.7	295.5	-101.5	-97.7	23.9	22.4
44.0	1.6	286.5	290.5	290.4	294.9	294.5	298.6	298.3	296.1	295.9	-97.0	-93.2	27.8	25.5
45.0	0.0	285.2	289.1	289.0	293.4	293.0	296.6	296.5	296.3	296.3	-100.2	-95.4	30.6	28.2
46.0	0.0	284.6	288.6	288.3	292.0	292.1	295.9	295.6	297.0	296.8	-98.9	-93.9	31.6	29.2
47.0	0.0	283.6	287.5	287.3	291.3	291.0	294.8	294.5	297.0	296.8	-97.5	-92.2	33.3	30.7
48.0	0.0	283.1	286.9	286.4	290.5	290.1	293.7	293.5	297.4	297.1	-99.1	-93.6	34.3	31.0

Table D.2 Data for Phase II of Experiment

Unit 1 - Single Cover Unit 2 - Double Cover

DATA FOR PHASE II OF EXPERIMENT (COMPARISION OF SINGLE COVER TROMBE WALL UNIT WITH DOUBLE COVER UNIT)
DAY 174 --> RELATIVE HUMIDITY= 78 % AVERAGE WIND SPEED= 2.86 M/S
DAY 175 --> RELATIVE HUMIDITY= 63 % AVERAGE WIND SPEED= 3.08 M/S

TIME	SFLUX	TAMB	TGLS1	TGLS2	TAIR1	TAIR2	TFRON1	TFRON2	TINT1	TINT2	QFRON1	QFRON2	QBACK1	QBACK2
0.0	0.0	292.3	296.2	299.5	299.2	301.4	301.7	304.9	299.1	298.7	-49.7	-43.1	34.1	39.6
1.0	0.0	291.3	295.3	298.7	298.3	300.8	300.8	304.3	299.2	298.9	-49.6	-43.7	33.9	40.1
2.0	0.0	291.0	295.0	298.4	298.1	300.2	300.3	303.6	299.5	299.1	-50.0	-44.0	31.7	37.9
3.0	0.0	290.5	294.3	297.6	297.4	299.5	299.6	302.8	299.1	298.8	-50.7	-44.3	28.4	34.6
4.0	0.0	290.1	293.4	296.8	296.5	298.9	298.9	302.2	298.3	298.5	-62.3	-55.7	26.0	32.2
5.0	0.0	289.2	292.5	296.0	295.7	298.2	297.8	301.5	297.4	297.7	-49.3	-42.7	22.9	28.9
6.0	0.0	288.4	291.7	295.4	295.0	297.6	297.5	301.0	297.0	297.3	-49.4	-42.4	20.4	26.5
7.0	5.6	288.6	291.6	295.3	295.2	297.8	297.4	301.0	296.4	296.8	-31.8	-25.5	20.6	25.4
8.0	8.8	290.7	292.8	296.1	297.0	299.0	298.4	301.5	295.3	295.9	-7.8	-1.9	17.9	24.0
9.0	95.3	292.0	294.3	298.6	300.8	302.8	300.0	303.0	295.0	295.6	12.6	18.7	17.6	22.9
10.0	182.1	294.0	298.7	301.7	304.8	305.8	303.2	305.6	294.6	295.4	39.7	45.8	17.1	22.6
11.0	237.3	296.6	300.8	304.3	308.7	309.2	305.8	307.5	294.5	295.3	67.9	73.6	15.2	21.8
12.0	333.3	300.2	304.8	308.6	315.4	315.3	311.8	312.4	294.3	295.1	128.0	130.3	16.5	23.2
13.0	384.8	300.5	307.7	311.3	319.4	318.3	315.2	315.1	294.4	295.2	138.3	135.7	17.0	25.0
14.0	294.4	304.4	308.3	311.2	320.6	319.7	317.1	316.6	294.5	295.2	152.9	149.4	18.2	25.6
15.0	335.6	306.2	308.6	312.0	320.6	319.2	317.1	317.4	295.0	295.6	95.7	95.8	19.6	26.2
16.0	231.9	306.0	307.2	310.8	314.9	315.3	315.3	316.0	295.2	295.8	4.3	4.4	20.7	26.5
17.0	29.3	299.4	303.5	307.3	309.5	310.8	311.6	313.4	295.8	296.2	-26.6	-13.4	23.0	27.6
18.0	15.6	297.7	302.2	305.6	307.2	308.6	309.4	311.3	296.2	296.6	-32.9	-26.9	25.3	30.2
19.0	6.0	295.7	300.2	303.7	304.6	306.2	307.2	309.4	296.3	296.7	-36.4	-42.4	26.3	31.5
20.0	3.3	294.9	299.0	302.2	303.0	304.5	305.7	308.1	296.6	296.9	-57.3	-49.7	27.0	35.1
21.0	1.4	294.1	298.0	301.0	301.5	303.1	304.1	306.6	297.1	297.3	-71.3	-56.1	28.3	36.3
22.0	0.0	293.8	296.9	300.0	300.3	302.1	302.7	305.5	297.7	297.6	-74.0	-57.9	30.0	37.0
23.0	0.0	292.4	295.8	299.0	299.2	301.0	301.7	304.4	297.8	297.6	-71.7	-56.6	29.4	36.1
24.0	0.0	291.3	295.1	298.0	298.4	300.0	300.8	303.5	297.6	297.4	-72.0	-57.2	27.7	34.7
25.0	0.0	290.6	294.1	297.1	297.5	299.2	300.1	302.7	297.0	297.1	-73.4	-58.2	26.7	31.9
26.0	0.0	289.5	292.8	296.3	296.3	298.4	299.1	301.9	296.5	296.8	-76.1	-60.3	24.6	31.4
27.0	0.0	288.4	292.2	295.3	295.6	297.5	298.6	301.2	295.8	296.2	-72.8	-57.5	22.7	28.9
28.0	0.0	287.9	291.6	294.8	295.0	297.1	297.7	300.6	295.5	296.0	-78.7	-65.0	20.8	26.2
29.0	0.0	287.1	290.9	294.1	294.5	296.3	297.1	299.8	294.7	295.3	-80.1	-65.9	18.4	24.8
30.0	1.2	287.1	290.8	293.7	294.1	295.9	296.7	299.4	294.5	295.2	-80.6	-66.8	17.4	23.8
31.0	2.9	288.4	290.6	293.5	294.3	295.9	296.4	299.1	293.9	294.6	-73.9	-58.9	16.4	22.8
32.0	9.4	289.8	292.7	295.3	296.7	297.9	297.7	300.1	293.5	294.2	-36.7	-29.5	15.4	22.5
33.0	26.7	291.5	294.9	297.6	299.8	300.8	299.7	301.8	293.3	294.0	-2.1	-5.4	14.2	20.9
34.0	174.5	294.3	298.3	300.4	304.0	304.3	302.5	303.9	293.1	293.8	17.7	22.1	13.2	20.1
35.0	248.9	294.4	300.7	303.1	308.3	307.9	305.4	306.2	293.4	293.9	53.2	54.7	14.1	19.2
36.0	326.1	296.9	304.3	307.0	314.2	313.1	310.0	309.9	293.7	294.2	98.6	92.9	14.9	20.6
37.0	366.6	298.1	307.1	310.1	317.9	317.4	314.4	313.5	294.0	294.5	121.4	115.4	15.9	22.3
38.0	347.3	300.0	308.0	311.4	321.2	319.3	316.7	315.5	295.0	295.4	114.9	109.0	18.5	24.1
39.0	322.1	300.5	308.6	311.9	320.3	318.3	317.0	316.5	295.8	296.1	85.5	81.3	20.6	26.1
40.0	233.9	306.3	307.6	310.4	316.0	315.4	315.6	315.1	296.0	296.3	26.6	25.6	21.6	28.3
41.0	64.2	304.9	306.2	308.9	312.6	313.1	313.6	313.8	296.2	296.5	5.3	9.0	22.8	30.0
42.0	13.8	298.0	303.1	305.5	307.9	308.4	310.1	311.0	296.6	296.8	-31.5	-37.5	25.3	32.0
43.0	5.7	296.6	300.9	303.9	305.2	306.4	307.6	309.2	297.2	297.2	-54.4	-47.8	30.5	34.1
44.0	2.9	297.0	299.9	303.6	303.6	305.8	306.8	308.8	298.2	297.7	-70.9	-56.4	29.4	36.2
45.0	0.0	295.0	298.4	301.3	301.9	303.2	304.3	306.2	298.1	297.6	-76.0	-61.0	29.0	34.5
46.0	0.0	294.2	297.1	300.2	300.5	302.1	302.9	305.3	298.0	297.6	-77.9	-63.6	27.2	35.3
47.0	0.0	293.4	296.2	299.3	299.5	301.1	301.8	304.3	297.8	297.5	-76.8	-62.6	26.9	31.7
48.0	0.0	291.8	295.5	297.6	298.7	299.4	301.0	302.8	297.5	297.3	-76.9	-62.7	27.5	30.4

Table D.3 Data for Phase III of Experiment

Unit 1 - Single Cover, Fiber-Batt Absorber
Unit 2 - Double Cover

DATA FOR PHASE III OF EXPERIMENT (COMPARISION OF DOUBLE COVER TROMBE WALL UNIT WITH FIBER ABSORBER UNIT)
DAY 196 --> RELATIVE HUMIDITY= 68 % AVERAGE WIND SPEED= 3.34 M/S
DAY 197 --> RELATIVE HUMIDITY= 76 % AVERAGE WIND SPEED= 3.66 M/S

TIME	SFLUX	TAMB	TGLS1	TGLS2	TAIR1	TAIR2	TFRON1	TFRON2	TINT1	TINT2	QFRON1	QFRON2	QBACK1	QBACK2
0.0	0.0	296.7	297.8	301.8	301.9	303.2	305.6	304.9	299.9	300.6	-22.8	-33.1	29.5	33.5
1.0	0.0	296.3	297.1	301.2	301.3	302.7	305.1	304.3	299.8	300.5	-23.3	-33.5	29.4	32.8
2.0	0.0	295.8	296.4	300.9	300.8	302.4	304.7	304.0	299.8	300.4	-23.6	-33.6	29.4	33.4
3.0	0.0	295.0	295.9	300.1	300.3	301.6	304.3	303.2	299.7	300.1	-23.9	-35.2	29.4	32.7
4.0	0.0	294.9	295.6	299.6	299.9	302.0	304.0	302.7	299.6	299.9	-23.7	-35.3	29.4	32.5
5.0	0.0	294.2	295.5	299.4	299.7	300.8	303.8	302.3	299.5	299.7	-23.1	-34.5	29.3	32.3
6.0	1.2	294.0	295.2	298.8	299.5	300.2	303.5	301.7	299.3	299.4	-23.1	-34.6	29.1	31.2
7.0	3.1	294.5	295.6	299.0	300.4	300.6	303.4	301.7	299.2	299.2	-15.0	-24.8	28.5	29.6
8.0	31.0	296.4	298.4	300.2	303.6	302.3	304.1	302.6	299.0	298.9	4.4	-1.4	28.4	28.6
9.0	104.4	297.9	301.4	302.1	308.4	305.1	305.3	304.4	299.0	298.7	29.7	30.5	28.4	28.3
10.0	183.3	300.9	305.8	305.4	313.4	309.2	307.0	307.2	298.9	298.6	54.2	60.9	28.3	27.8
11.0	256.1	303.1	309.9	308.6	318.5	312.9	308.8	309.9	298.9	298.5	79.9	96.4	28.0	26.0
12.0	221.8	302.6	309.1	310.5	315.5	313.4	310.4	312.0	298.8	298.4	48.3	69.1	26.8	24.7
13.0	411.9	303.9	317.8	314.5	329.9	321.9	313.7	317.1	298.8	298.4	140.1	169.9	25.3	22.7
14.0	215.3	306.3	313.4	315.2	324.6	322.0	314.7	318.8	298.8	298.5	97.6	130.3	25.7	22.9
15.0	342.9	308.0	316.1	316.1	327.9	323.2	315.8	319.6	298.9	298.7	103.5	131.9	25.8	23.3
16.0	275.6	308.7	315.1	315.6	324.7	320.9	315.8	318.9	299.0	298.9	72.3	83.9	25.8	24.5
17.0	167.1	308.9	310.7	313.6	319.3	318.0	314.7	317.3	299.1	299.2	38.4	42.4	26.2	25.7
18.0	81.2	304.1	306.7	311.0	312.7	313.7	313.0	314.6	299.2	299.4	2.7	-3.3	28.2	28.4
19.0	44.1	302.7	304.5	308.6	309.7	310.9	311.4	312.2	299.3	299.7	-8.8	-15.7	29.5	30.4
20.0	22.2	301.8	302.7	307.2	307.3	309.1	310.1	310.6	299.4	300.1	-17.9	-25.4	30.4	31.2
21.0	5.9	300.5	301.4	306.0	305.7	307.6	309.3	309.3	299.5	300.4	-23.3	-31.4	31.2	32.6
22.0	1.0	299.2	300.2	304.7	304.5	306.3	308.3	308.0	299.6	300.5	-24.4	-32.1	32.5	34.8
23.0	0.0	298.4	299.1	303.6	303.6	305.2	307.6	307.0	299.8	300.6	-25.1	-33.4	34.4	36.3
24.0	0.0	297.8	298.6	302.8	303.1	304.3	307.1	306.0	299.9	300.6	-24.8	-33.5	34.2	35.9
25.0	0.0	297.3	298.2	302.5	302.6	304.0	306.4	305.7	300.1	300.8	-24.9	-33.8	34.0	35.9
26.0	0.0	296.3	297.4	301.3	302.0	302.9	306.2	304.6	299.8	300.2	-25.6	-34.2	33.9	36.2
27.0	0.0	295.9	296.8	301.1	301.5	302.6	305.8	304.4	299.7	300.2	-25.6	-35.1	33.7	36.5
28.0	0.0	295.4	296.4	300.5	301.2	302.0	305.4	303.7	299.6	300.1	-25.4	-35.2	33.6	36.8
29.0	0.0	295.0	296.3	299.9	300.8	301.4	305.0	303.0	299.5	299.9	-24.7	-35.6	33.4	35.8
30.0	1.0	295.1	296.3	299.9	300.6	301.1	304.8	302.7	299.5	299.9	-24.2	-34.7	33.3	35.5
31.0	2.4	294.1	295.8	299.3	300.9	301.0	304.6	302.3	299.4	299.5	-20.2	-28.9	33.1	34.8
32.0	9.8	296.1	298.0	300.2	304.0	302.5	305.1	303.1	299.4	299.2	-0.2	-5.1	32.9	34.2
33.0	104.2	299.7	302.3	302.6	309.0	305.4	306.5	304.8	299.3	298.7	26.2	27.4	32.9	32.1
34.0	166.2	301.5	305.2	305.1	313.1	308.7	307.8	307.1	299.3	298.6	47.2	53.3	32.8	32.2
35.0	257.5	303.6	310.5	309.3	319.7	313.6	310.3	310.9	299.2	298.5	80.7	98.0	31.3	30.7
36.0	331.2	305.9	313.9	313.3	325.9	319.2	313.3	315.6	299.2	298.5	111.6	140.5	29.4	29.4
37.0	318.9	307.2	314.3	315.5	323.1	319.4	315.0	317.8	299.3	298.6	64.6	70.9	28.5	25.8
38.0	379.0	308.9	316.9	316.1	327.3	321.6	315.9	319.0	299.3	298.7	80.7	73.1	28.4	25.1
39.0	224.4	310.2	314.9	315.2	326.7	321.8	316.3	318.9	299.4	298.8	91.0	114.6	28.5	25.2
40.0	159.0	307.4	311.1	313.4	317.5	316.6	314.4	316.3	299.4	299.1	29.1	29.2	28.6	25.7
41.0	18.4	301.4	304.1	309.2	309.0	311.3	312.1	312.8	299.5	299.4	-20.7	-28.3	30.6	28.3
42.0	3.0	297.9	299.9	306.3	306.8	308.7	310.9	310.9	299.6	299.7	-23.2	-29.3	30.7	29.4
43.0	15.2	298.8	302.5	306.4	309.0	309.1	310.6	310.4	299.6	299.8	-4.8	-9.9	31.3	30.1
44.0	3.3	298.2	300.7	305.1	305.8	307.0	309.4	308.8	299.7	300.0	-21.7	-29.6	32.5	32.4
45.0	1.3	297.1	299.1	303.7	304.1	305.3	308.4	307.2	299.7	300.1	-27.1	-36.5	33.5	34.3
46.0	0.0	297.2	298.9	302.9	303.6	304.5	308.0	306.3	299.7	300.3	-26.3	-35.8	35.5	36.5
47.0	0.0	297.3	298.4	302.2	303.1	303.8	307.3	305.5	299.8	300.3	-26.0	-35.5	35.7	38.4
48.0	0.0	296.4	297.9	301.4	302.4	302.9	306.7	304.4	299.7	300.3	-26.0	-35.7	36.9	39.8

Table D.4 Comparison of Energy Gain for Phase III of Experiment

PHASE III OF EXPERIMENT

I	QERON1	QERON2	Z1	Z2
1	-22.8000	-33.1000	0.0000	0.0000
2	-23.3000	-33.5000	-23.0500	-33.3000
3	-23.6000	-33.6000	-46.5000	-66.8500
4	-23.9000	-35.2000	-70.2500	-101.2500
5	-23.7000	-35.3000	-94.0500	-136.5000
6	-23.1000	-34.5000	-117.4500	-171.4000
7	-23.1000	-34.6000	-140.5500	-205.9500
8	-15.0000	-24.8000	-159.6000	-235.6500
9	4.4000	-1.4000	-164.9000	-248.7500
10	29.7000	30.5000	-147.8500	-234.2000
11	54.2000	60.9000	-105.9000	-188.5000
12	79.9000	96.4000	-38.8500	-109.8500
13	48.3000	69.1000	25.2500	-27.1000
14	140.1000	169.9000	119.4500	92.4000
15	97.6000	130.3000	238.3000	242.5000
16	103.5000	131.9000	338.8499	373.5999
17	72.3000	83.9000	426.7498	481.4998
18	38.4000	42.4000	482.0996	544.6497
19	2.7000	-3.3000	502.6496	564.1995
20	-8.8000	-15.7000	499.5994	554.6995
21	-17.9000	-25.4000	486.2493	536.1494
22	-23.3000	-31.4000	465.6492	505.7493
23	-24.4000	-32.1000	441.7991	473.9993
24	-25.1000	-33.4000	417.0491	441.2493
25	-24.8000	-33.5000	392.0989	407.7991
26	-24.9000	-33.8000	367.2488	374.1489
27	-25.6000	-34.2000	341.9988	340.1489
28	-25.6000	-35.1000	316.3987	305.4988
29	-25.4000	-35.2000	290.8987	270.3486
30	-24.7000	-35.6000	265.8486	234.9486
31	-24.2000	-34.7000	241.3986	199.7986
32	-20.2000	-28.9000	219.1986	167.9987
33	-0.2000	-5.1000	208.9986	150.9987
34	26.2000	27.4000	221.9986	162.1487
35	47.2000	53.3000	258.6985	202.4987
36	80.7000	98.0000	322.6484	278.1484
37	111.6000	140.5000	418.7983	397.3984
38	64.6000	70.9000	506.8982	503.0984
39	80.7000	73.1000	579.5481	575.0984
40	91.0000	114.6000	665.3979	668.9482
41	29.1000	29.2000	725.4478	740.8481
42	-20.7000	-28.3000	729.6477	741.2981
43	-23.2000	-29.3000	707.6975	712.4980
44	-4.8000	-9.9000	693.6975	692.8979
45	-21.7000	-29.6000	680.4475	673.1479
46	-27.1000	-36.5000	656.0474	640.0979
47	-26.3000	-35.8000	629.3472	603.9478
48	-26.0000	-35.5000	603.1970	568.2976
49	-26.0000	-35.7000	577.1970	532.6975

Table D.5

TEMPERATURE PROFILE DATA FOR DOUBLE COVER WALL

XAXS	TP0500	TP0900	TP1200	TP1500	TP1800	TP2400
0.00	301.81	301.80	313.61	319.66	313.08	304.87
2.54	302.99	302.64	309.29	315.91	314.06	305.85
5.08	303.33	302.58	306.62	312.26	312.54	306.24
8.10	303.70	302.43	304.81	309.51	311.04	306.41
10.95	303.96	302.43	303.84	307.73	309.77	306.45
13.73	304.04	302.36	302.92	305.87	308.12	306.19
18.81	303.89	302.21	301.85	303.50	305.58	305.46
27.15	303.19	301.41	300.65	301.24	302.72	303.96
32.23	302.14	300.75	299.72	300.14	301.17	302.63
34.93	301.56	300.15	299.23	299.77	300.65	302.09
39.69	299.94	299.00	298.60	298.74	299.70	300.22

Data Key:

XAXS	Distance of thermocouple from front of wall.
TP0500	Temperature at 0500 hours (K)
TP0900	Temperature at 0900 hours (K)
TP1200	Temperature at 1200 hours (K)
TP1800	Temperature at 1800 hours (K)
TP2400	Temperature at 2400 hours (K)

BIBLIOGRAPHY

Akbari, H., Borgers, T.R., "Free Convective Laminar Flow within the Trombe Wall Channel", Solar Energy, Vol. 22, pp. 165-174, 1979.

Arumi, F., "A Model for the DEROB/PASOLE System", Proceedings of the 2nd National Passive Solar Conference, Vol. 2.2, Philadelphia, PA, March 16-18, 1978.

Bahadori, M.H., "Passive Cooling Systems in Iranian Architecture", Scientific American, Vol. 238, p. 144, 1978.

Balcomb, J.D., "Passive Solar Energy Systems for Buildings", Chapter 16 in "Solar Energy Handbook" eds. Kreider, J.F., Kreith, F., McGraw-Hill Book Co., 1979.

Balcomb, J.D., McFarland, R.D., Moore, S.W., "Passive Testing at Los Alamos", Proceedings of the 2nd National Passive Solar Conference, Vol. 2.2, Philadelphia, PA, March 16-18, 1978.

Balcomb, J.D., McFarland, R.D., Moore, S.W., "Simulation Analysis of Passive Solar Heated Buildings - Comparison with Test Room Results", Proceedings of the 1977 Annual Meeting of the American Section of the International Solar Energy Society, Vol. 1, Orlando, FL, June 6-10, 1977.

Balcomb, J.D., McFarland, R.D., "A Simple Empirical Method for Estimating the Performance of a Passive Solar Heated Building of the Thermal Storage Wall Type", Proceedings of the 2nd National Passive Solar Conference, Vol. 2.2, Philadelphia, PA, March 16-18, 1978.

Balcomb, J.D., Hedstrom, J.C., McFarland, R.D., "Simulation Analysis of Passive Solar Heated Buildings - Preliminary Results", Solar Energy, Vol. 19, No. 3, pp. 277-82, 1977.

Benedict, R.P., "Fundamentals of Temperature, Pressure and Flow Measurements", 2nd Edition, John Wiley and Sons, 1977.

Bilgen, E., Jeldres, R., "On the Optimization of Trombe Wall Solar Collectors", ASME Paper No. 78-WA/Sol-13, 1978.

Birkebak, R.C., Enoch, I.E., Ozil, E., "Experimental Study of Heat Transfer in Fiberglass Material", A paper presented at the Joint AIAA/ASME Heat Transfer, Fluids and Thermophysics Conference, St. Louis, MO, June 7-10, 1982.

Birkebak, R.C., Ozil, E., Enoch, I., "Energy Transfer in Fibrous Materials with One Free Surface", submitted to Journal of Heat Transfer, ASME, 1982.

Casperson, R.L., Hocevar, C.J., "Experimental Investigation of the Trombe Wall", Report No. DOE/CS/34145-1, DOE Grant No. EG-77-G-04-4145, Energy Engineering Group, Inc., May 15, 1979.

Casperson, R.L., Hocevar, C.J., "Experimental Investigation of the Trombe Wall Solar Energy System", Proceedings of the 3rd National Passive Solar Conference, San Jose, CA, Jan. 11-13, 1979.

Chen, F., "Energy Transfer in Fibrous Insulating Materials", Master's Thesis, Department of Mechanical Engineering, University of Kentucky, 1979.

Davis, Jr., L.B., "Energy Transfer in Fur", Ph.D. Thesis, University of Kentucky, Mechanical Engineering, 1972.

Davis, L.B. and Birkebak, R.C., "One-Dimensional Radiative Energy Transfer in Thin Layer of Fibrous Materials", J. Applied Physics, Vol. 44, No. 10, pp. 4585-4587, 1972.

Davis, L.B., Jr. and Birkebak, R.C., "On the Transfer of Energy in Layers of Fur", Biophysical Journal, 14, pp. 249-268, 1974.

Duffie, J.A., Beckman, W.A., "Solar Engineering of Thermal Processes", John Wiley and Sons, Inc., 1980.

Enoch, I.E., Ozil, E. and Birkebak, R.C., "Polynomial Approximation Solution of Heat Transfer by Conduction and Radiation in a One-Dimensional Absorbing, Emitting and Scattering Medium", submitted to Journal of Numerical Heat Transfer, 1982.

Grimmer, D.P., "Theoretical Considerations in the Use of Small Passive-Solar Test-Boxes to Model the Thermal Performance of Passively Solar-Heated Building Designs", Solar Energy, Vol. 22, pp. 343-350, 1979.

Grimmer, D.P., McFarland, R.D., Balcomb, J.D., "Initial Experiments on the Use of Small Passive-Solar Test-Boxes to Model the Thermal Performance of Passively Solar-Heated Building Designs", Solar Energy, Vol. 22, pp. 351-354, 1979.

Hewlett-Packard Co., "HP-2240A Measurement and Control Processor Users Manual", 2nd Edition, 1978.

Hollands, K.G.T., Unny, T.E., Raithby, G.D. and Konicek, L., "Free Convection Heat Transfer Across Inclined Air Layers", Transactions of the American Society of Mechanical Engineers, Journal of Heat Transfer, Vol. 98, pp. 189-193, 1976.

McMordie, R.K., Kidd, J.H., "The Use of Generalized Thermal Network Analysis for Passive Solar Analysis", Proceedings of the 2nd National Passive Solar Conference, Philadelphia, PA, March 16-18, 1978.

Norris, D.J., "Calibration of Pyranometers in Inclined Inverted Positions", Solar Energy, Vol. 16, pp. 53-55, 1974.

Ohanessian, P. and Charters, W.W.S., "Thermal Simulation of a Passive Solar House Using a Trombe-Michel Wall Structure", Solar Energy, Vol. 20, pp. 275-281, 1978.

Omega Engineering, Inc., "Temperature Measurement Handbook", Omega Engineering, Inc., 1982.

Özil, E. and Birkebak, R.C., "Experimental Study of a Solar Collector with a Fiber Bed as an Absorbing Medium", A paper presented at Izmir International Symposium-II on Solar Energy Fundamentals and Applications, Turkey, 1979.

Özil, E., "Experimental and Theoretical Study of Combined Heat Transfer in Biological Insulating Materials", Ph.D. Dissertation, Department of Mechanical Engineering, University of Kentucky, 1976.

Özil. E. and Birkebak, R.C., "Effects of Environmental Thermal Radiation on the Insulative Property of a Fibrous Material", Proceedings of the Seventh Symposium on Thermophysical Properties, ASME, ed. by Cezairliyan, pp. 319-323, 1977.

Özil, E. and Birkebak, R.C., "Radiative Energy Transfer Effects on Fibrous Insulating Materials", Energy Conservation in Heating, Cooling and Ventilating Buildings, ed. by Hoogendorm and Afgan, Vol. 1, pp. 115-124, Hemisphere Publishing Co., 1978.

Palmiter, L., Wheeling, T., Corbett, B., "Performance of Passive Test Units in Butte, Montana", Proceedings of the 2nd National Passive Solar Conference, Vol. 2.2, Philadelphia, PA, March 16-18, 1978.

Palmiter, L., Wheeling, T., Corbett, B., "Measured and Modeled Passive Performance in Montana", Proceedings of the 1978 Annual Meeting of the American Section of the International Solar Energy Society, Vol. 2.2, Denver, CO, August 28-31, 1978.

Shurchliffe, W.A., "Solar Heated Buildings: A Brief Survey", 9th Ed., Cambridge, Massachusetts, 1975.

Trombe, F., Robert, J.F., Cabanat, M. and Sesolis, B., "Some Performance Characteristics of the CNRS Solar House Collectors", Passive Solar Heating and Cooling, Conference and Workshop Proceedings, Albuquerque, New Mexico, LA-6637-C, pp. 201-222, May 18-19, 1976.